ASL-CR-81-0072-2

LEVEL

ANALYSIS AND MODELING OF BATTLEFIELD
FIRE PLUMES

FEBRUARY 1981

By

James H. Thompson
John G. Devore

General Electric Company TEMPO
Center of Advanced Studies
Santa Barbara, CA 93102

Under Contract Number DAAD007-80-C-0072

CONTRACT MONITOR: Roberto Rubio

US Army Electronics Research and Development Command
ATMOSPHERIC SCIENCES LABORATORY
White Sands Missile Range, NM 88002

81 7 09 036

NOTICES

(19) REPORT DOCUMENTATION PAGE		READ INSTRUCTIONS BEFORE COMPLETING FORM
1. REPORT NUMBER ASL-CR-81-0072-2	2. GOVT ACCESSION NO. AD-A101164	3. RECIPIENT'S CATALOG NUMBER
4. TITLE (and Subtitle) ANALYSIS AND MODELING OF BATTLEFIELD FIRE PLUMES		5. TYPE OF REPORT & PERIOD COVERED Final Report
		6. PERFORMING ORG. REPORT NUMBER
7. AUTHOR(s) (10) James H. Thompson and John G. Devore	(15)	8. CONTRACT OR GRANT NUMBER(s) DAAD007-80-C-0072
9. PERFORMING ORGANIZATION NAME AND ADDRESS General Electric Company TEMPO Center for Advanced Studies Santa Barbara, CA 93102		10. PROGRAM ELEMENT, PROJECT, TASK AREA & WORK UNIT NUMBERS (11)
11. CONTROLLING OFFICE NAME AND ADDRESS US Army Electronics Research and Development Command Adelphi, MD 20783		12. REPORT DATE February 1981
		13. NUMBER OF PAGES 109
14. MONITORING AGENCY NAME & ADDRESS(if different from Controlling Office) US Army Atmospheric Sciences Laboratory White Sands Missile Range, NM 88002 (12) 110		15. SECURITY CLASS. (of this report) UNCLASSIFIED
		15a. DECLASSIFICATION/DOWNGRADING SCHEDULE

16. DISTRIBUTION STATEMENT (of this Report)

Approved for public release; distribution unlimited

17. DISTRIBUTION STATEMENT (of the abstract entered in Block 20, if different from Report)

18. SUPPLEMENTARY NOTES

Contract Monitor: Roberto Rubio

19. KEY WORDS (Continue on reverse side if necessary and identify by block number)

Plumes
Electro-optical sensors
Thermal effects

20. ABSTRACT (Continue on reverse side if necessary and identify by block number)

This report presents models for the hot turbulent plumes above tactical
battlefield fires. Models are developed for the plume radius, temperature,
and rise velocity as a function of altitude given the initial fire
conditions. The strength of the hot air turbulence is related to the plume
parameters for several assumed flow conditions. The turbulent propagation
effects are evaluated for optical beams whose paths intersect the plume.
Sample results are presented for coherence length, short- and long-term beam
spreading, and beam jitter.

DD FORM 1473 EDITION OF 1 NOV 65 IS OBSOLETE

1

46420

CONTENTS

3

LIST OF FIGURES

TABLES

SECTION 1
INTRODUCTION

There are a wide variety of electro-optical sensors employed in the modern tactical battlefield environment. The environment in which the sensors must operate is often extremely adverse. The two categories of degradation sources which can significantly affect sensor performance are the natural and the man-made. The natural sources include the adverse weather effects such as rain and fog, the effects of naturally occurring aerosols such as wind driven dust, and the natural thermal environment. The man-made sources include all anthropogenic gases, particles, and thermal effects produced by human activity. These include countermeasures smoke, vehicular exhaust and dust, muzzle blast emissions, explosion produced products such as gases, combustion particles, and thrown-up dust and vegetation, and smoke from burning vehicles, structures, and vegetation. In addition to the gases and particles introduced, explosions and fires are a source of heat and atmospheric convection. The resulting thermal environment can severely degrade sensor performance.

The propagation effects due to the natural environment have been studied and modeled for many years; in the last few years most of the man-made effects have received extensive attention. Experimental test programs have been run for countermeasures smoke and explosion produced dust clouds. Models have been or are in the process of being developed for most effects. In this report we begin the study of the thermal effects of battlefield fire plumes.

Fires in a battlefield can be localized, such as burning vehicles and structures, or area fires, such as a burning field. Both the active flame and the rising heated air plume above the flames are regions which

can produce signal propagation degradation. Here we are concerned with the rising heated air plume. Turbulence in the hot rising plume can cause signal amplitude and phase fluctuations, defocusing, beam wandering (jitter) and spreading, time delay, and pulse distortion. In addition the gases and particulate combustion products in the plume can cause absorption and scattering. In this report we derive estimates of the magnitudes of the potential propagation effects of turbulence. In Section 2 we develop models for the size, temperature, and velocity of the rising plume as a function of altitude. In section 3 we relate the plume parameters to the strength of the plume turbulence and also develop models for optical signal propagation through this turbulence. Sample calculations and results are presented. The models developed here can be used in designing experimental plume tests. In turn, the future experimental test results will provide the needed data base for verification and improvement of the present models. The plume model development will be an iterative process between the theoretical and experimental phases.

SECTION 2
PLUME MODELS

The turbulent buoyant plume has been an area of research for more than 40 years (References 1 to 6). Various techniques have been used. Zel'dovich, Rouse, and Batchelor used a similarity approach. Schmidt and Taylor made assumptions about the basic turbulent flow processes. Morton, Taylor, and Turner were able to analyze nonsimilar flows by assuming the ambient air entrainment rate is proportional to the local mean velocity. Normally, the loss of energy from the plume by radiation is ignored. In Reference 7 Morton examined the radiation loss and derived approximate formulas for its effect.

Figure 1 shows a sketch of an ideal fire plume. We will solve for the plume radius, temperature, and rise velocity as a function of altitude. In our analysis we will make the following assumptions:

- The plume is in pressure equilibrium with the ambient atmosphere at all altitudes along its length.
- At a given altitude the plume has a radial "top hat" profile. That is, the temperature, density, and velocity are constant across the plume section.
- The entrained ambient air is instantaneously mixed with the plume air.
- The radiation loss from the plume is negligible.

These are typical assumptions of plume analysis. Experimental measurements indicate that in well developed plume flows the temperature and velocity radial distributions are Gaussian, with the maximum values occurring on the plume centerline. But since all plume formulas are in terms of the integral of the profiles over the radial cross section, only the averaged temperature and velocity values are determined.

WEAKLY BUOYANT
REGION

STRONGLY BUOYANT
REGION

FLAMES
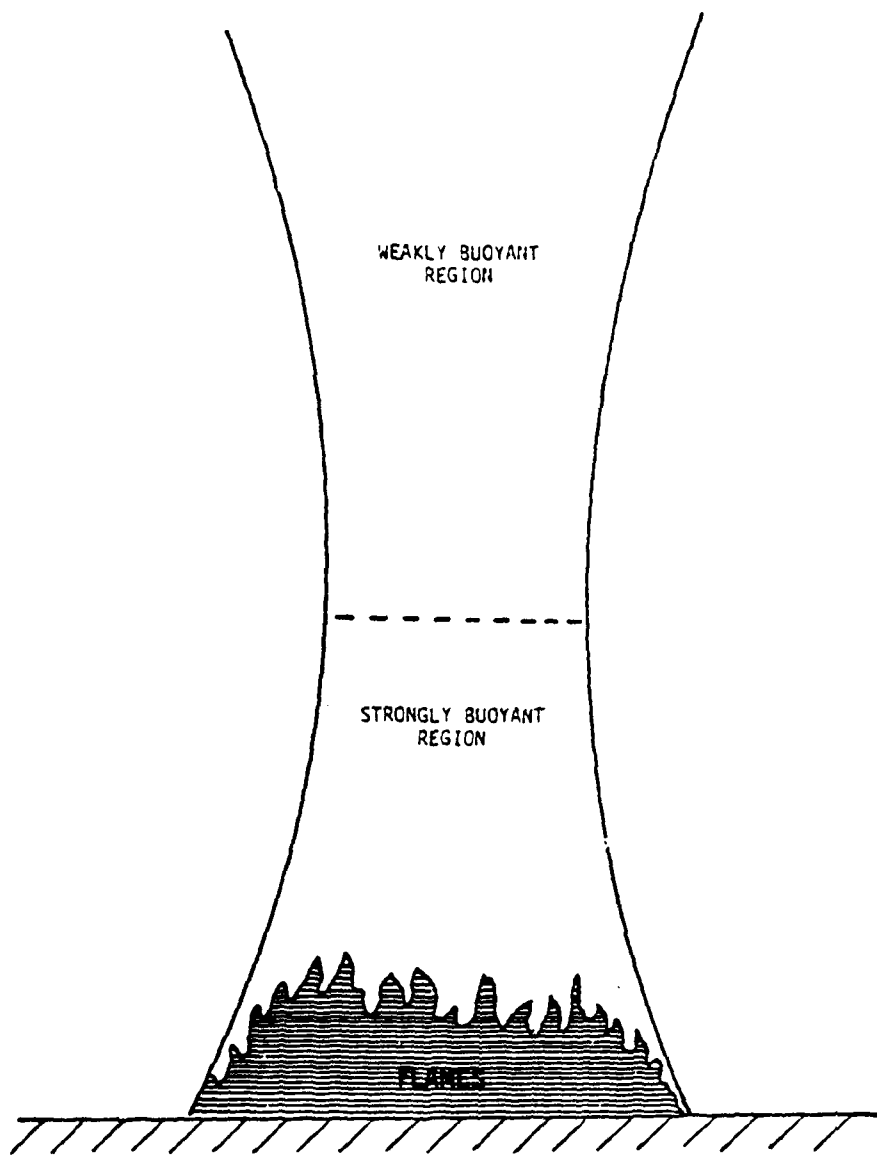
Figure 1.   Ideal fire plumes.

Later we will relate the "top hat" profile values to those of the Gaussian profile.

We adopt the Morton (Reference 7) entrainment hypothesis for buoyant plumes,

$$\alpha = \left(\frac{\rho}{\rho_a}\right)^{1/2} \alpha_o \tag{1}$$

where

α = entrainment constant at a given altitude

ρ = mean plume density at the given altitude (g cm^{-3})

ρ_a = ambient air density at the given altitude (g cm^{-3})

α_o = the well established entrainment constant for weakly buoyant plumes (0.116 for "top hat" profile).

The entrainment rate of ambient air mass per unit plume surface area is $\alpha \rho_a v$, where v is the local plume rise velocity.

For this first model we ignore radiation loss terms. Thus our analysis corresponds to:

- Clean plumes, that is, plumes that are not optically thick due to combustion particulates.
- Dirty plumes with relatively low initial temperatures or with high temperatures accompanied by high rise velocities (in this latter case the cooling due to rapid ambient air mass entrainment dominates the radiation cooling).

At a later date we will add radiation cooling to the plume solution.

Define the following variables:

z = altitude above reference plane (cm)

T = plume temperature at z (K)

ρ = plume density at z (g cm^{-3})

P = plume pressure at z (dynes cm^{-2})

r = plume radius at z (cm)

v = plume rise velocity at z (cm s^{-1})

g = acceleration of gravity (980) (cm s^{-2})

E = internal energy (ergs g^{-1})

M_o = molecular weight of air at standard conditions (28.964) (g)

Z = number of moles of air at temperature T and pressure P per mole of air at standard conditions

γ = effective gas gamma (ratio of specific heats) at temperature T and pressure P

H_p = ambient pressure scale height at altitude z (cm)

R = gas constant (8.317 × 10^7) (ergs K^{-1})

T_a, P_a, Z_a, γ_a are the corresponding quantities for the ambient air.

We take the equation of state of air and the internal energy to be

$$P = \frac{Z\rho RT}{M_o} \quad \text{dynes cm}^{-2} \tag{2}$$

$$E = \frac{P}{\rho(\gamma - 1)} \quad \text{ergs g}^{-1} . \tag{3}$$

The values for Z and γ are given in Tables 1 and 2 (References 8 and 9). For fire plumes, temperatures are generally below 2000 K and density ratios (ratio of plume density to ambient sea level air density) are greater than 0.1. Thus for plumes we can take

Z = 1

and use the following theoretical expression for γ based on the quantization of the vibrational states of diatomic molecules

$$\gamma = \frac{3.5 + S}{2.5 + S}$$

where

$$S = \frac{0.21 \, w}{e^w - 1} + \frac{0.79 \, u}{e^u - 1}$$

$$w = \frac{2.239 \times 10^3}{T}$$

$$u = \frac{3.352 \times 10^3}{T} .$$

The first term in the equation for S is the effect due to oxygen and the second term is due to nitrogen. For plume temperatures and densities the fit to γ is good to three significant figures.

14

Table 1. Equation of state quantity Z.

GILMORE EQUATION OF STATE VALUES FOR AIR

Z - THE NUMBER OF MOLES OF AIR PER MOLE OF COLD AIR

TEMP(DEG. R) PHI/RHMIN =	10**1	10**0	10**-.5	10**-1	10**-1.5	10**-2	10**-2.5	10**-3	10**-4	10**-5	10**-6	10**-7
180	1.0000	1.0000	1.0000	1.0000	1.0000	1.0000	1.0000	1.0000	1.0000	1.0000	1.0000	1.0000
1000	1.0000	1.0100	1.0000	1.0000	1.0000	1.0000	1.0000	1.0000	1.0000	1.0000	1.0000	1.0000
1277	1.0000	1.0000	1.0000	1.0000	1.0000	1.0000	1.0000	1.0000	1.0000	1.0000	1.0000	1.0000
1500	1.0000	1.0000	1.0000	1.0000	1.0000	1.0000	1.0000	1.0000	1.0000	1.0001	1.0004	1.0012
1700	1.0000	1.0000	1.0000	1.0000	1.0000	1.0000	1.0001	1.0001	1.0008	1.0013	1.0040	1.0124
2000	1.0000	1.0000	1.0000	1.0001	1.0004	1.0007	1.0012	1.0017	1.0055	1.0170	1.0487	1.1162
3000	1.0023	1.0072	1.0127	1.0178	1.0373	1.0610	1.0846	1.1341	1.1917	1.2069	1.2109	1.2154
4000	1.0226	1.0682	1.0961	1.1341	1.1670	1.1996	1.2022	1.2107	1.2282	1.2715	1.3883	1.6409
5000	1.0728	1.1448	1.1756	1.1990	1.2171	1.2370	1.2649	1.3081	1.4835	1.7752	1.9542	1.9896
6000	1.1275	1.2298	1.2298	1.2669	1.3196	1.4001	1.4470	1.6603	1.9143	1.9864	2.0051	2.0348
7000	1.1761	1.2699	1.3364	1.4315	1.5623	1.7162	1.8570	1.9384	1.9970	2.0288	2.1105	2.3455
8000	1.2390	1.4001	1.5259	1.6704	1.8261	1.9259	1.9763	2.0010	2.0487	2.1702	2.5007	3.1675
10000	1.4510	1.7570	1.8880	1.9660	2.0080	2.0420	2.0870	2.1600	2.1600	2.1350	3.7730	3.9560
10500	1.5170	1.8270	1.9340	1.9920	2.0310	2.0730	2.1380	2.2450	2.6820	3.4170	3.8800	3.9700
11000	1.5800	1.8840	1.9670	2.0150	2.0570	2.1130	2.2050	2.3540	2.9130	3.6340	3.9320	3.9760
11500	1.6500	1.9240	1.9930	2.0340	2.0880	2.1650	2.2890	2.4770	3.1090	3.7770	3.9560	3.9790
12000	1.7110	1.9570	2.0150	2.0640	2.1270	2.2280	2.3920	2.6420	3.3650	3.8620	3.9670	3.9810
12500	1.7670	1.9830	2.0390	2.0930	2.1740	2.3050	2.5120	2.8110	3.5440	3.9110	3.9730	3.9820
13000	1.8150	2.0070	2.0620	2.1280	2.2310	2.3970	2.6460	2.9860	3.6800	3.9380	3.9770	3.9860
13500	1.8570	2.0290	2.0840	2.1690	2.2960	2.4970	2.7890	3.1570	3.7750	3.9530	3.9770	3.9860
14000	1.8930	2.0500	2.1180	2.2150	2.3710	2.6090	2.9370	3.3150	3.8800	3.9630	3.9820	4.0130
14500	1.9230	2.0730	2.1510	2.2690	2.4540	2.7270	3.0830	3.4530	3.9110	3.9690	3.9860	4.0550
15000	1.9500	2.0990	2.1860	2.3260	2.5610	2.8150	3.2210	3.5680	3.9300	3.9730	3.9960	4.1150
15500	1.9730	2.1250	2.2300	2.3930	2.6390	2.9720	3.3860	3.6600	3.9300	3.9760	4.0190	4.2660
16000	1.9950	2.1540	2.2750	2.4630	2.7340	3.0920	3.4560	3.7310	3.9420	3.9840	4.0580	4.4520
16500	2.0150	2.1860	2.3250	2.5370	2.8180	3.2040	3.5500	3.7850	3.9520	3.9930	4.1230	4.6780
17000	2.0350	2.2200	2.3780	2.6150	2.9380	3.3070	3.6270	3.8260	3.9590	4.0080	4.2230	4.9160
17500	2.0540	2.2570	2.4340	2.6940	3.0350	3.4000	3.6900	3.8560	3.9660	4.0740	4.3600	5.1410
18000	2.0730	2.2960	2.4920	2.7740	3.1280	3.4810	3.7400	3.8800	3.9740	4.0740	4.5310	5.3370
18500	2.0920	2.3370	2.5530	2.8540	3.2150	3.5510	3.7800	3.8900	3.9840	4.1350	4.7220	5.5020
19000	2.1110	2.3800	2.6150	2.9330	3.2950	3.6110	3.8120	3.9120	3.9940	4.2180	4.9190	5.6360
19500	2.1510	2.4250	2.6780	3.0090	3.3680	3.6620	3.8380	3.9240	4.0190	4.3260	5.1080	5.7400
20000	2.1510	2.4710	2.7700	3.0420	3.4330	3.7620	3.8590	3.9350	4.0400	4.4570	5.2890	5.8170
22000	2.2340	2.6600	2.9110	3.3310	3.6270	3.8150	3.9180	3.9900	4.2930	5.0760	5.7450	5.9510
24000	2.3260	2.8450	3.1860	3.5090	3.7810	3.8830	3.9350	4.1180	4.7740	5.5680	5.9170	6.0230
26000	2.4220	3.0110	3.3480	3.6300	3.8210	3.9570	4.1130	4.3740	5.2250	5.8220	5.9940	6.2610
28000	2.5130	3.1540	3.4710	3.7200	3.8980	4.0750	4.3380	4.7340	5.5790	5.9340	6.1380	6.8020
30000	2.6000	3.3760	3.5720	3.8020	3.9630	4.2610	4.6010	5.1080	5.7440	6.0280	6.4860	7.1690
32000	2.6820	3.3760	3.6590	3.8050	4.1510	4.5070	4.9630	5.5700	6.0050	6.5260	6.9880	7.7260
34000	2.7580	3.4670	3.7840	4.0100	4.3480	4.7770	5.2500	5.6240	6.1560	6.9370	7.4310	7.8960
36000	2.8200	3.5550	3.9470	4.1610	4.5640	5.0400	5.4740	5.7700	6.4930	7.3160	7.7160	8.0020
38000	2.8970	3.6430	4.0620	4.3350	4.7900	5.2650	5.6190	5.8810	6.7080	7.6610	7.9960	8.1740
40000	2.9620	3.7340	4.0910	4.5170	5.0020	5.4460	5.7660	6.6020	7.0310	7.8000	8.1600	8.5000
42000	3.0250	3.8370	4.2340	4.7010	5.1880	5.5910	5.8810	6.1550	7.0310	7.7840	8.1680	8.9600
44000	3.0960	3.9070	4.3850	4.8750	5.3450	5.6090	6.0090	6.3560	7.3230	7.9450	8.4390	9.3720
46000	3.1570	4.5910	4.5910	5.0130	5.4400	5.6300	6.1630	6.5950	7.5510	8.0650	8.8020	9.6710
48000	3.2250	4.1810	4.6780	5.1750	5.6010	5.9570	6.3510	6.8490	7.7240	8.2570	9.1720	9.8400
50000	3.2960	4.4010	4.8110	5.3020	5.7160	6.1010	6.5620	7.0920	7.8910	8.5170	9.4410	10.0700
60000	3.6730	4.8470	5.0620	5.8270	6.4220	7.0020	7.5190	7.9270	8.8020	9.8020	10.5400	11.4900
70000	4.0570	5.1530	5.2210	6.5510	7.1720	7.7170	8.2340	8.6490	9.1720	10.5400	11.6700	11.9700
80000	4.8250	5.8070	6.0910	7.1610	7.7890	8.0180	9.0670	8.6500	10.7300	11.6600	12.0100	12.2700

15

Table 2. Internal energy term (γ - 1).

EFFECTIVE GAS GAMMA MINUS ONE (PRESSURE DIVIDED BY DENSITY TIMES INTERNAL ENERGY PER UNIT MASS)

RHO/RHOM =	10**1	10**0	10**-.5	10**-1	10**-1.5	10**-2	10**-2.5	10**-3	10**-4	10**-5	10**-6	10**-7
TEMP(DEG K)												
100												

We first develop the plume equations as a function of time and then as a function of altitude. At some initial time t_o, consider a cross section of the plume at altitude z_o, with plume radius r_o, rise velocity v_o, and of thickness δz_o. At a later time this volume element will be at altitude z, have radius r, rise velocity v, and its thickness will be $\delta z = \delta z_o \, v/v_o$. The mass in the volume element at altitude z is

$$M = \pi r^2 \rho \delta z = \pi r^2 \rho \delta z_o \frac{v}{v_o} \quad g \quad .$$

The mass entrainment rate is given by the Morton assumption

$$\frac{dM}{dt} = \alpha \rho_a v \; (2\pi r \delta z)$$
$$= 2\alpha_o \left(\frac{\rho_a}{\rho}\right)^{1/2} \frac{M}{r} v \quad g \; s^{-1}$$

where the quantity $2\pi r \delta z$ is recognized as the surface area of the volume element. The momentum conservation equation is simply

$$\frac{d(M \, v)}{dt} = M\left(\frac{\rho_a}{\rho} - 1\right) g \quad g \; cm \; s^{-2}$$

where the quantity on the right-hand side of the equation is the buoyant force on the volume element. The temperature equation, accounting for the internal energy of the entrained mass, the expansion, and the changing state of the plume air, is

$$\frac{dT}{dt} = T \left\{ \left(\frac{\gamma-1}{\gamma}\right)\frac{1}{P} \frac{dP}{dt} + \left[\frac{\gamma-1}{\gamma_a-1} \frac{\gamma_a}{\gamma} \frac{Z_a}{Z} \frac{T_a}{T} - 1\right]\frac{1}{M} \frac{dM}{dt} \right.$$
$$\left. + \frac{1}{\gamma(\gamma-1)} \frac{d(\gamma-1)}{dt} - \frac{1}{Z} \frac{dZ}{dt} \right\} \quad K \; s^{-1} \quad .$$

At plume temperatures the dZ/dt term is negligible and the $d(\gamma-1)/dt$ term is minor.

Naturally, the properties of the plume, T, ρ, r, and v do not depend on the volume element considered, but are only functions of altitude. Define the scaled mass parameter

$$m = \rho r^2 v \quad g \; s^{-1} \tag{4}$$

then the equations can be rewritten in terms of m, without reference to a volume element. Thus in the time domain the set of equations to be solved are

17

$$\frac{dm}{dt} = 2\alpha_o \left(\frac{\rho_a}{\rho}\right)^{1/2} \frac{mv}{r}$$

$$\frac{dv}{dt} = \left(\frac{\rho_a}{\rho} - 1\right) g - 2\alpha_o \frac{v^2}{r}\left(\frac{\rho_a}{\rho}\right)^{1/2}$$

$$\frac{dT}{dt} = T\left\{\left(\frac{\gamma-1}{\gamma}\right) \frac{1}{P} \frac{dP}{dt} + \left[\frac{\gamma-1}{\gamma_a-1} \frac{\gamma_a}{\gamma} \frac{Z_a}{Z} \frac{T_a}{T} - 1\right]\frac{1}{m} \frac{dm}{dt} \right.$$
$$\left. + \frac{1}{\gamma(\gamma-1)} \frac{d(\gamma-1)}{dt} - \frac{1}{Z}\frac{dZ}{dt}\right\}$$

with

$$\frac{dz}{dt} = v$$

$$\rho = \rho_a \frac{Z_a}{Z} \frac{T_a}{T}$$

$$\frac{1}{P} \frac{dP}{dt} = - \frac{v}{H_p} \quad .$$

The last auxiliary equation comes from assuming that over the altitude range of the plume the ambient pressure is given by

$$P_a = P_{ao} \, e^{-(z-z_o)/H_p} \quad \text{dynes cm}^{-2}$$

and by the pressure equilibrium assumption

$$P = P_a \quad .$$

In an established plume with constant heat injection rate the plume parameters are only a function of altitude, independent oi time. We rewrite the equations eliminating the time variable by the substitution

$$dt = \frac{dz}{v} \quad .$$

The set of plume equations then becomes

$$\frac{dm}{dz} = 2\alpha_o \left(\frac{\rho_a}{\rho}\right)^{1/2} \frac{m}{r} \tag{5}$$

$$\frac{dv}{dz} = \left(\frac{\rho_a}{\rho} - 1\right)\frac{g}{v} - \frac{2\alpha_o v}{r} \left(\frac{\rho_a}{\rho}\right)^{1/2} \tag{6}$$

$$\frac{dT}{dz} = T\left\{\left(\frac{\gamma-1}{\gamma}\right)\frac{1}{P}\frac{dP}{dz} + \left[\frac{\gamma-1}{\gamma_z-1}\frac{\gamma_a}{\gamma}\frac{Z_a}{Z}\frac{T_a}{T} - 1\right]\frac{1}{m}\frac{dm}{dz}\right.$$

$$\left. - + \frac{1}{\gamma(\gamma-1)}\frac{d(\gamma-1)}{dz} - \frac{1}{Z}\frac{dZ}{dz}\right\} \tag{7}$$

with

$$\frac{1}{P}\frac{dP}{dz} = -\frac{1}{H_p} \tag{8}$$

$$\rho = \rho_a \frac{Z_a}{Z}\frac{T_a}{T} \quad . \tag{9}$$

Given the initial plume parameters T_o (or equivalently ρ_o), r_o and v_o at z_o, the equations can be solved for the plume parameters at all altitudes. The initial radius of the plume is determined by the size of the fire. The initial temperature and velocity are related to the burning rate (energy release) of the fire. Consider the following ideal process. Let air be at temperature T_1, have density ρ_1, and be at pressure P. Add heat of amount q (ergs/g) and let the air expand at constant pressure. The energy equation for this process is

$$E_2 = E_1 + q - P\int_{V_1}^{V_2} dV$$

$$= E_1 + q - P\left(\frac{1}{\rho_2} - \frac{1}{\rho_1}\right) \quad \text{ergs } g^{-1} \quad .$$

Using Equations 2 and 3 and solving for T_2 we have

$$T_2 = \frac{Z_1}{Z_2}\frac{\gamma_1}{\gamma_2}\frac{\gamma_2-1}{\gamma_1-1}T_1 + \frac{\gamma_2-1}{\gamma_2}\frac{qM_o}{Z_2 R} \quad K \quad . \tag{10}$$

Given T_1, Z_1, γ_1, q, and P, Equation 10 can be solved for T_2, Z_2, and γ_2 by iteration using the γ, Z tables. If we make the simplifying assumptions that at plume temperatures

$$Z_1 = Z_2 = 1$$

$$\gamma_1 \approx \gamma_2 = \gamma_a = 1.4 \text{ for air}$$

then the equation reduces to the usual constant pressure equation

$$T_2 = T_1 + \frac{q}{C_p} \tag{11}$$

where

$$C_p = \frac{\gamma R}{(\gamma - 1) M_o} = 10^7 \text{ ergs g}^{-1} \text{ K}^{-1} = 0.24 \text{ cal g}^{-1} \text{ K}^{-1}$$

is the specific heat at constant pressure for air.

For a fire let the burning rate be specified either by the total energy release rate Q (ergs s^{-1}) or by the energy release rate per unit area Q_A (ergs cm^{-2} s^{-1}), where naturally for a fire of radius r_o

$$Q_A = \frac{Q}{\pi r_o^2} \quad \text{ergs cm}^{-2} \text{ s}^{-1} \quad .$$

The air mass flow per unit area across the initial plane is

$$\frac{dm_A}{dt} = \dot{m}_A = \rho_o v_o \quad \text{g cm}^{-2} \text{ s}^{-1} \quad .$$

The heat added per unit mass of air is

$$q = \frac{Q_A}{\dot{m}_A} \quad \text{ergs g}^{-1} \quad .$$

Using the simplified temperature Equation 11, the relation between T_o and v_o is

$$T_o = \frac{T_a}{1 - \dfrac{Q_A}{C_p \rho_a T_a v_o}} \quad K \tag{12}$$

or

$$v_o = \frac{Q_A T_o}{C_p \rho_a T_a (T_o - T_a)} \quad \text{cm s}^{-1} \quad . \tag{13}$$

We have written a computer routine which solves the set of plume Equations 5 through 9. The inputs to the routine are the initial plume parameters T_o, r_o, v_o and the ambient atmospheric profile. The atmospheric profile is specified by giving the ambient air density at the ground and the ambient temperature as a function of altitude (either as a set of tabular values or as a constant lapse rate). The ambient air density and pressure at any point can then be calculated assuming hydrostatic equilibrium.

The outputs of the plume routine are the "top hat" profile values of plume radius, temperature, velocity, and density as a function of altitude. These "top hat" values represent the radially averaged values of the actual profile. The initial (just above the flame tips) radial profiles are determined by the fire configuration. As the plume rises and mixes with ambient air, the plume temperature and velocity rapidly approach Gaussian distributions. We now consider the relationship between the "top hat" and Gaussian profiles.

Let the "top hat" parameters calculated by the computer program at a given altitude be

$\bar{T}$ = plume temperature (K)

$\bar{v}$ = plume rise velocity (m s^{-1})

$\bar{\rho}$ = plume density (g cm^{-3})

R = plume radius (m) .

Take the radial distribution of the temperature and velocity as

$$T(r) - T_a = (T_c - T_a)\, e^{-\frac{1}{2}\left(\frac{r}{\sigma_T}\right)^2} \quad K \tag{14}$$

$$v(r) = v_c\, e^{-\frac{1}{2}\left(\frac{r}{\sigma_v}\right)^2} \quad m\ s^{-1} \tag{15}$$

where

r = radial distance from the plume centerline (m)

$T(r)$ = plume temperature at r (K)

21

T_a = ambient temperature (K)

T_c = plume centerline temperature (K)

σ_T = standard deviation of radial temperature distribution (m)

$v(r)$ = plume rise velocity at r (m s^{-1})

v_c = plume centerline rise velocity (m s^{-1})

σ_v = standard deviation of radial velocity distribution (m) .

Note that it is the excess temperature (temperature above ambient) that is Gaussian distributed. Using the assumption of pressure equilibrium, the density relationship is simply

$$\rho(r)T(r) = \overline{\rho}\,\overline{T} = \rho_a T_a \tag{16}$$

where

$\rho(r)$ = plume density at r (g cm^{-3})

ρ_a = ambient air density (g cm^{-3}) .

The experimental measurements of George, Alpert and Tamanini, Reference 10, indicate that the relation between the "top hat" radius R and the Gaussian radial standard deviation in temperature is

$$\sigma_T = \frac{R}{2} \quad m \quad . \tag{17}$$

The measurements of Reference 10 found that the velocity profile was wider than the temperature profile by about 10 percent. The best previous experimental measurements were those of Rouse, et al, Reference 4, which found the velocity profile to be narrower than the temperature profile by 30 percent. The conclusion in Reference 10 after analysis of the various experimental measurement techniques is that to within experimental error the velocity and temperature profiles can be assumed to be equal in width. Thus we set

$$\sigma_v = \sigma_T = \frac{R}{2} \quad m \quad . \tag{18}$$

In terms of R, the profiles become

$$T(r) - T_a = (T_c - T_a) \, e^{-2\left(\frac{r}{R}\right)^2} \qquad K \tag{19}$$

$$v(r) = v_c \, e^{-2\left(\frac{r}{R}\right)^2} \qquad m \, s^{-1} \quad . \tag{20}$$

For the "top hat" parameters to correspond to the averaged Gaussian parameters requires that the mass, momentum and buoyancy of the plume cross section be the same for both profiles.

mass:
$$\pi R^2 \, \overline{\rho} = \int_0^R 2\pi r \rho(r) \, dr \tag{21}$$

momentum:
$$\pi R^2 \, \overline{\rho}\,\overline{v} = \int_0^R 2\pi r \rho(r) v(r) \, dr \tag{22}$$

buoyancy:
$$\pi R^2 (\overline{\rho} - \rho_a) = \int_0^R 2\pi r \left(\rho(r) - \rho_a\right) dr \tag{23}$$

The buoyancy Equation 23 reduces to the mass Equation 21 and thus contains no additional information. Substituting Equations 16 and 19 into the mass Equation 21 and integrating we have

$$\overline{T} = \frac{T_a}{1 + \frac{1}{2} \ln\left[\frac{T_a}{T_c} + \left(1 - \frac{T_a}{T_c}\right) e^{-2}\right]} \qquad K \tag{24}$$

and inverting,

$$T_c = \frac{T_a(e^2 - 1)}{\exp\left[2 \, \frac{T_a}{\overline{T}}\right] - 1} \qquad K \quad . \tag{25}$$

23

The excess centerline temperature, $T_c - T_a$, is a factor of 2.31 times the excess "top hat" average temperature, $\overline{T} - T_a$, at low excess temperatures and rises to a factor of 2.97 when $\overline{T} - T_a$ reaches 1000 K.

Substituting Equations 16 and 20 into the momentum Equation 22 and solving we have

$$v_c = \overline{v}\left(\frac{T_c - T_a}{\overline{T} - T_a}\right) \quad m\ s^{-1} \quad . \tag{26}$$

Hence the ratio of v_c to $\overline{v}$ is the same as the excess temperature ratio, ranging from 2.31 to 2.97 as $\overline{T} - T_a$ ranges from 0 to 1000 K.

We have used the plume computer routine to solve for the "top hat" profile parameters for a variety of initial conditions. Then assuming that the actual profile is Gaussian at all altitudes, we have used Equations 25 and 26 to convert from "top hat" to Gaussian parameters. Figures 2 through 28 show the results. Plotted are the plume center-line excess temperature, $T_c - T_a$, the centerline velocity, v_c , and the "top hat" radius R as a function of altitude. The radius R represents the 2-sigma point of the Gaussian temperature and veloc-ity distribution. Thus the temperature and velocity decreases from the centerline values at $r = 0$ to values a factor of $e^{-2} = 0.135$ of the centerline values at $r = R$. The altitude in the figures is the altitude above the reference plane where the initial plume param-eters are specified; it can be thought of as the altitude above the tips of the flames. The ambient atmosphere was assumed to have a ground level temperature of 288 K, and have a constant neutral stability lapse rate $(dT_a/dz = -0.0098\ K\ m^{-1})$. Until the plume temperature ap-proaches ambient temperature, the plume parameters are relatively in-sensitive to the lapse rate. For the short range of altitudes shown in the figures, the plume parameters would be essentially the same for any reasonable lapse rate. As the plume approaches ambient conditions, the plume parameters become highly dependent upon the temperature pro-file (lapse rate).

The initial plume radii for the sample cases are taken as 1, 5, and 10 meters. These are chosen to cover the likely range of individual battlefield fires. A 1-m fire corresponds approximately to a piece of equipment or small vehicle such as a jeep; a 5-m fire represents large vehicles such as trucks or tanks; and a 10-m fire is representative of structures such as houses. Area fires such as burning fields cannot be represented by a single fire plume. The initial plume centerline temperatures are taken as 500, 1000, and 1500 K above ambient temperature. These temperatures correspond to cool, normal, and hot fires. For each initial radius and temperature combination, three initial centerline velocities are chosen, corresponding to strong, medium, and weak acceleration of the heated air at the base of the plume.

We have specified the initial ambient and plume temperatures rather than the initial air densities. By specifying the temperatures, the results for the mean plume parameters are essentially independent of the elevation of the ground surface. The mean results apply equally well to sea level as to, say, the 4000-foot elevation at the White Sands Missile Range. The independence of ground elevation (initial ambient density) is readily apparent upon examination of the plume equations 5 through 9. At plume temperatures and densities

$$z = 1$$

$$\frac{\rho_a}{\rho} = \frac{T}{T_a} \quad .$$

The plume density enters only weakly in the determination of γ; and at plume temperatures and densities, γ differs only slightly from the ambient value of 1.4.
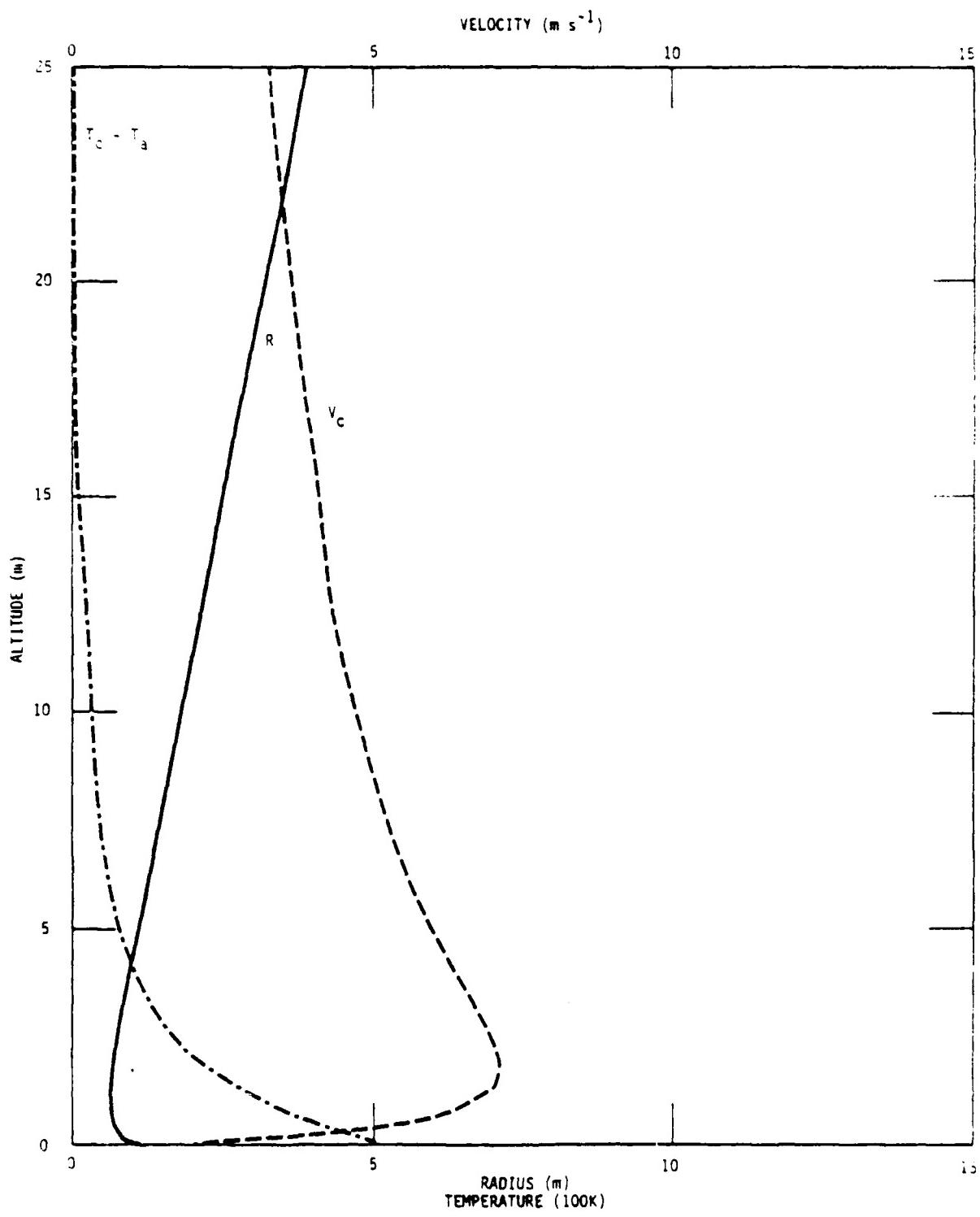
Figure 2. Plume parameters for initial conditions $T_c - T_a = 500$ K, $V_c = 2$ m s^{-1}, $R = 1$ m.

26
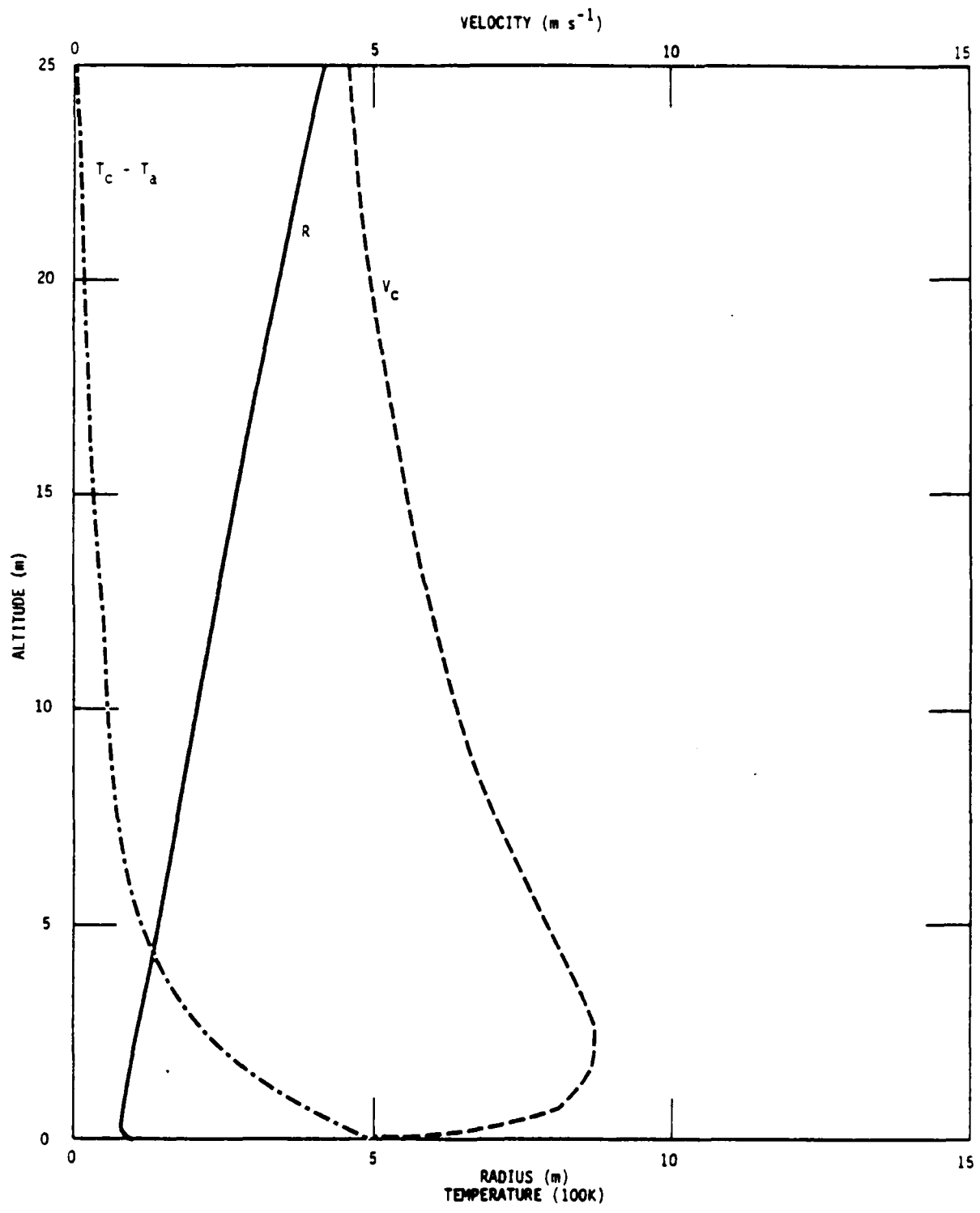
Figure 3. Plume parameters for initial conditions $T_c - T_a = 500$ K, $V_c = 5$ m s^{-1}, $R = 1$ m.

27
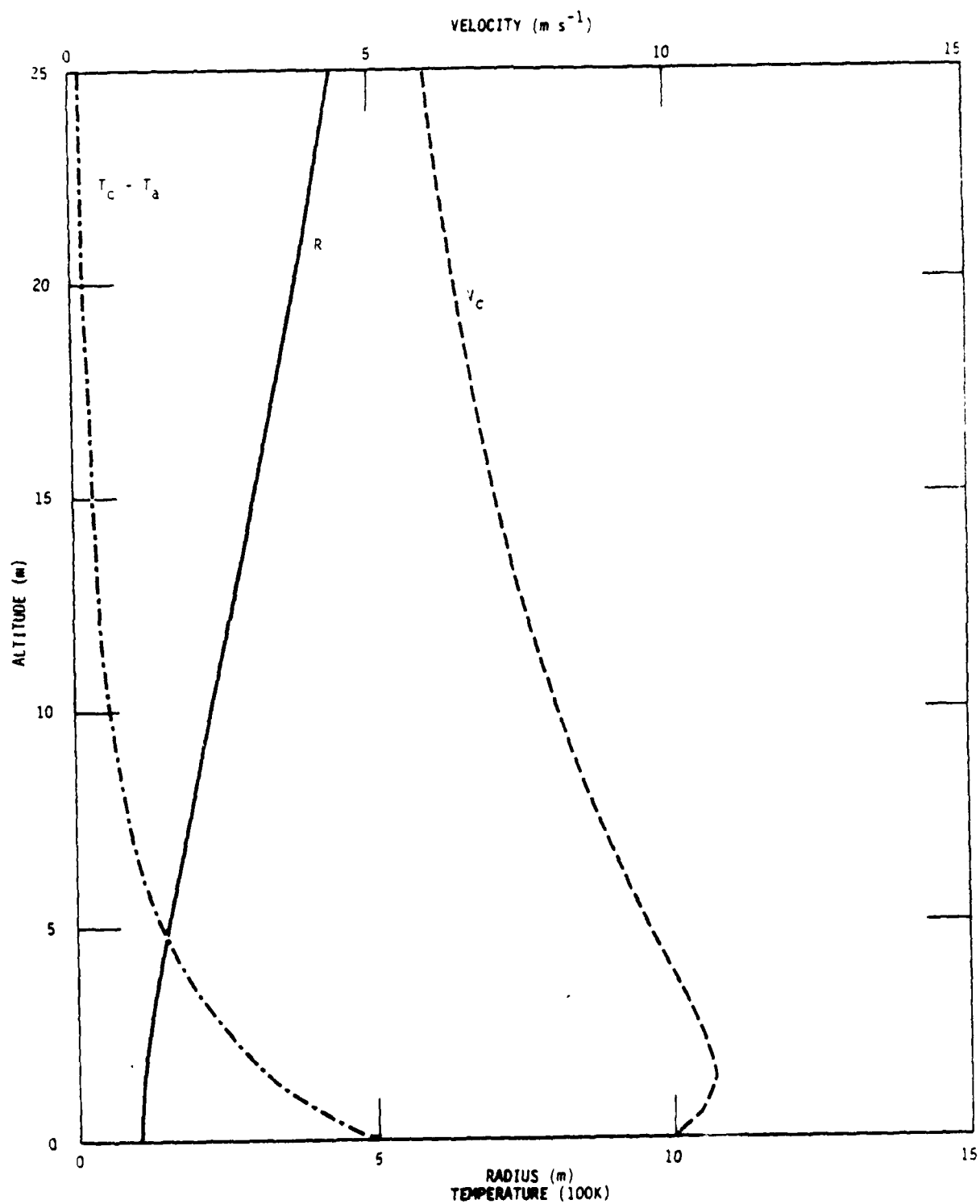
Figure 4.   Plume parameters for initial conditions $T_c-T_a = 500$ K, $V_c = 10$ m s^{-1}, $R = 1$ m.
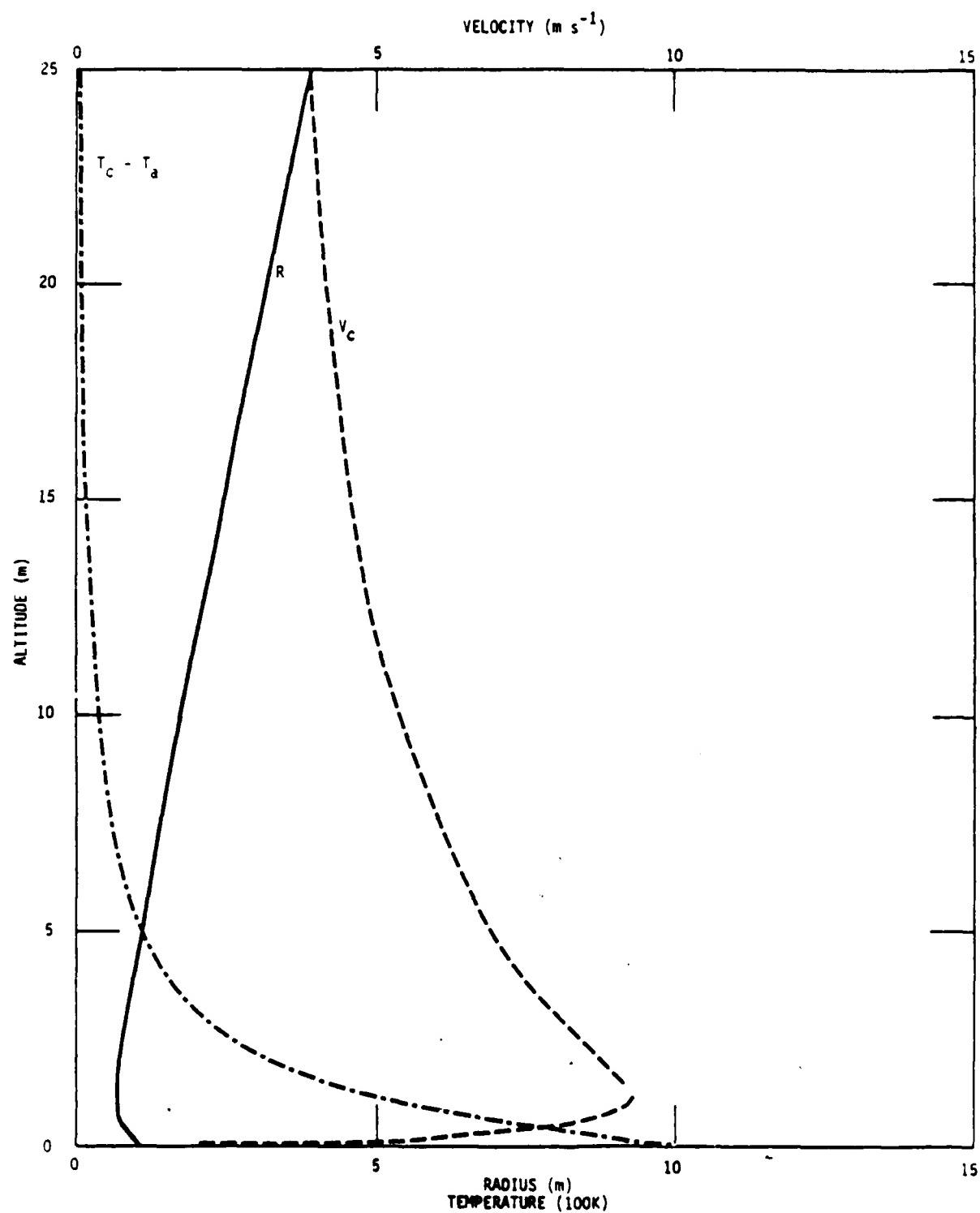
Figure 5. Plume parameters for initial conditions $T_c - T_a = 1000$ K, $V_c = 2$ m s^{-1}, $R = 1$ m.
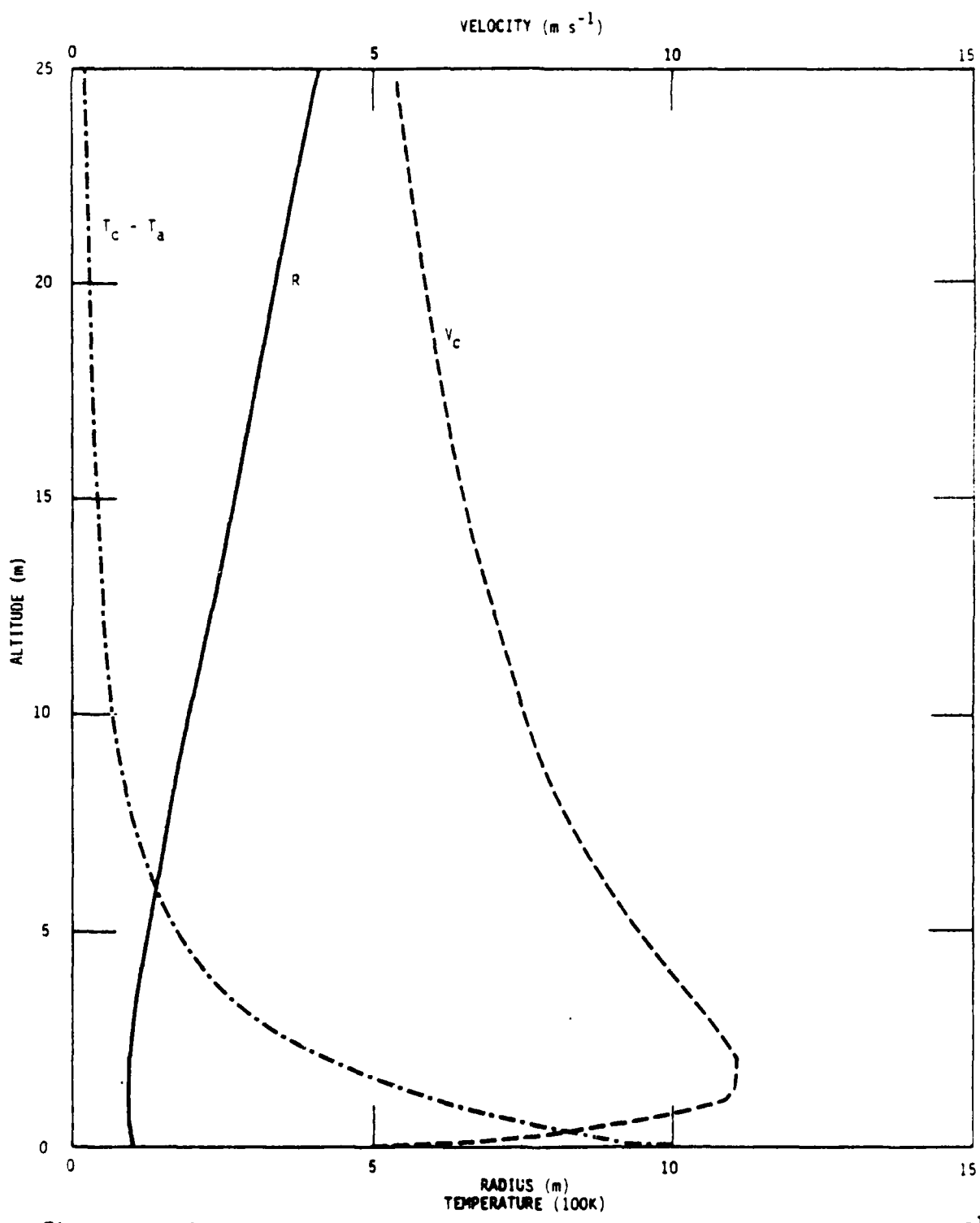
Figure 6. Plume parameters for initial conditions $T_c - T_a = 1000$ K, $V_c = 5$ m s^{-1}, $R = 1$ m.
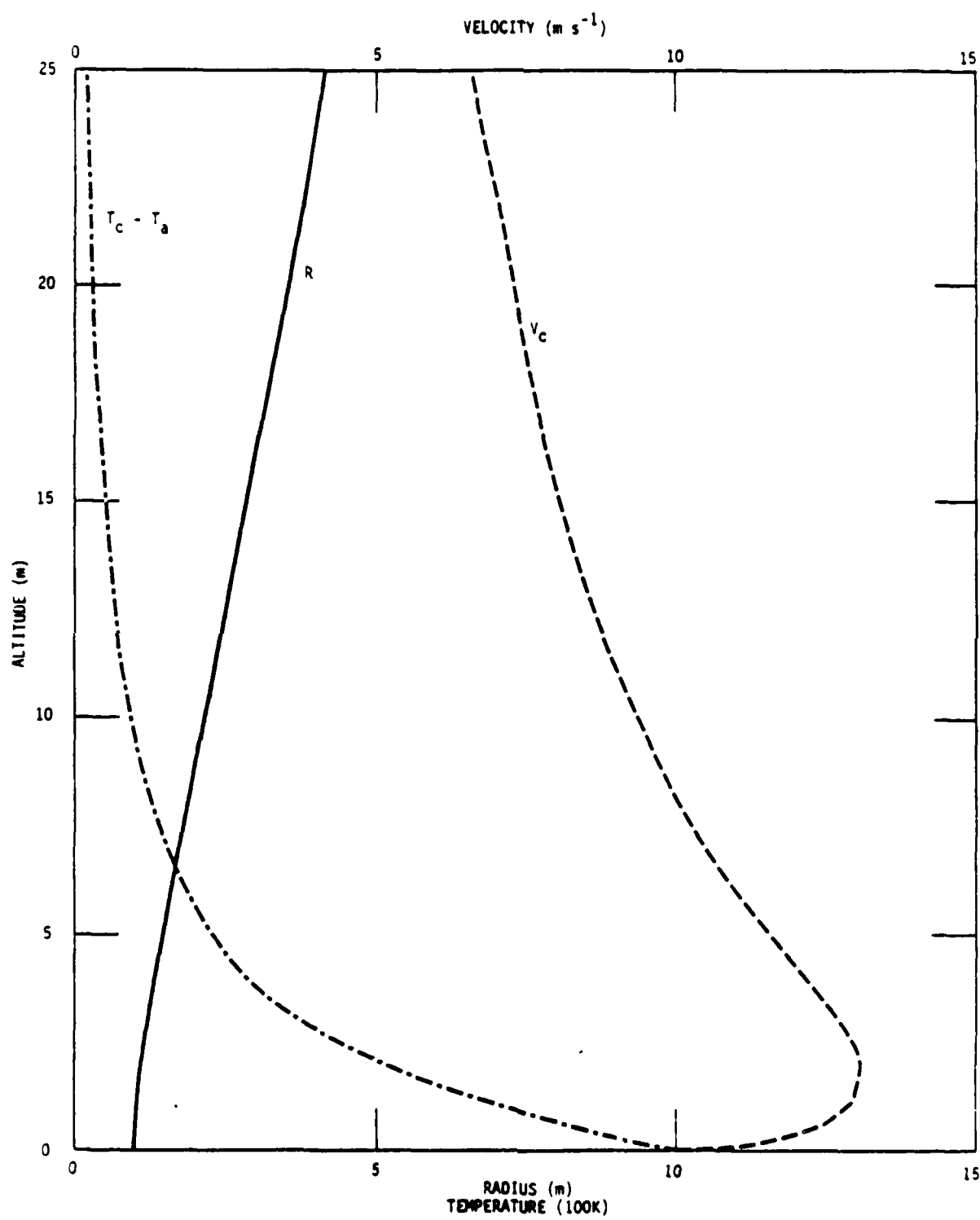
Figure 7. Plume parameters for initial conditions $T_c - T_a$ = 1000 K, V_c = 10 m s^{-1}, R = 1 m.
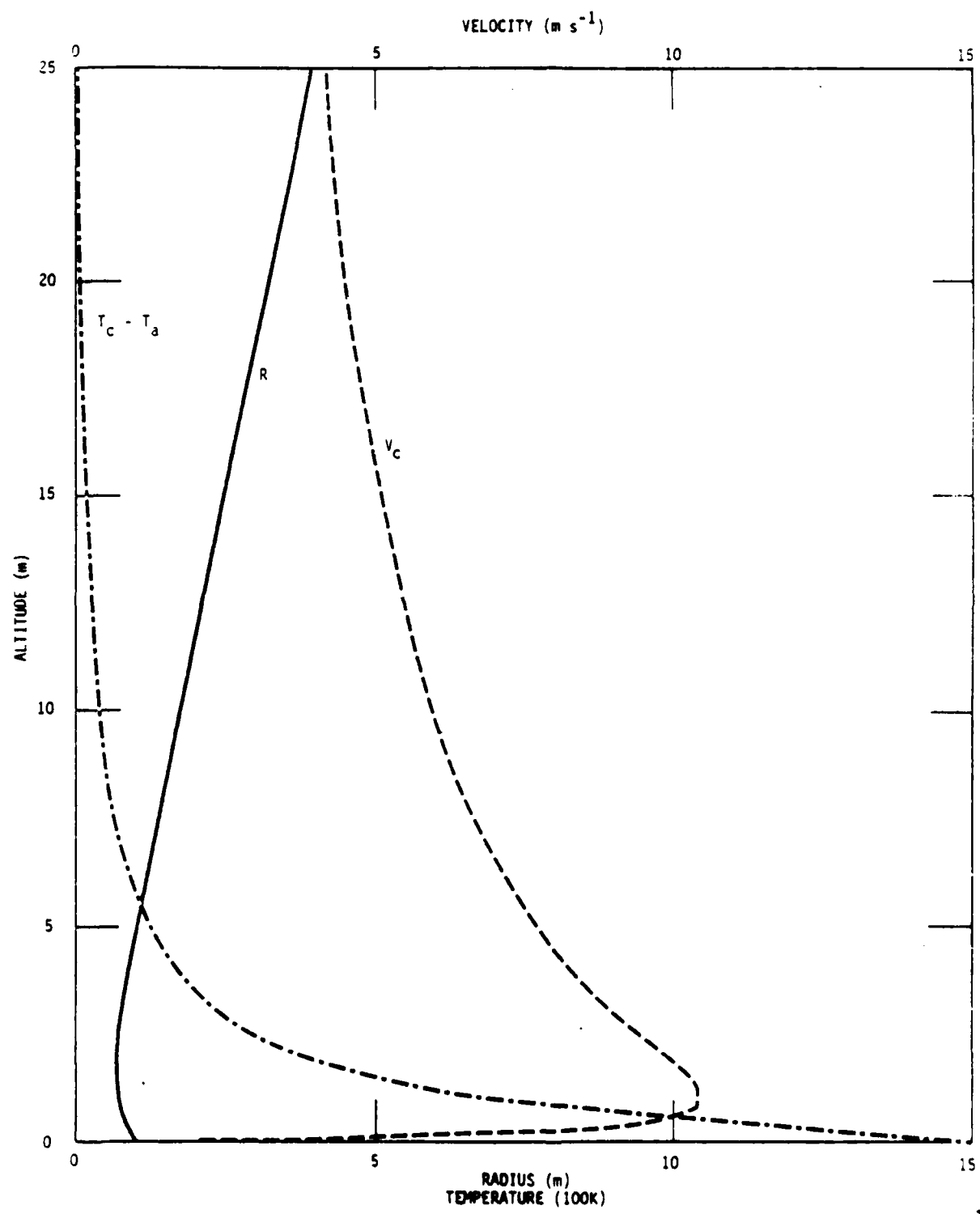
Figure 8. Plume parameters for initial conditions $T_c - T_a = 1500$ K, $V_c = 2$ m s^{-1}, $R = 1$ m.
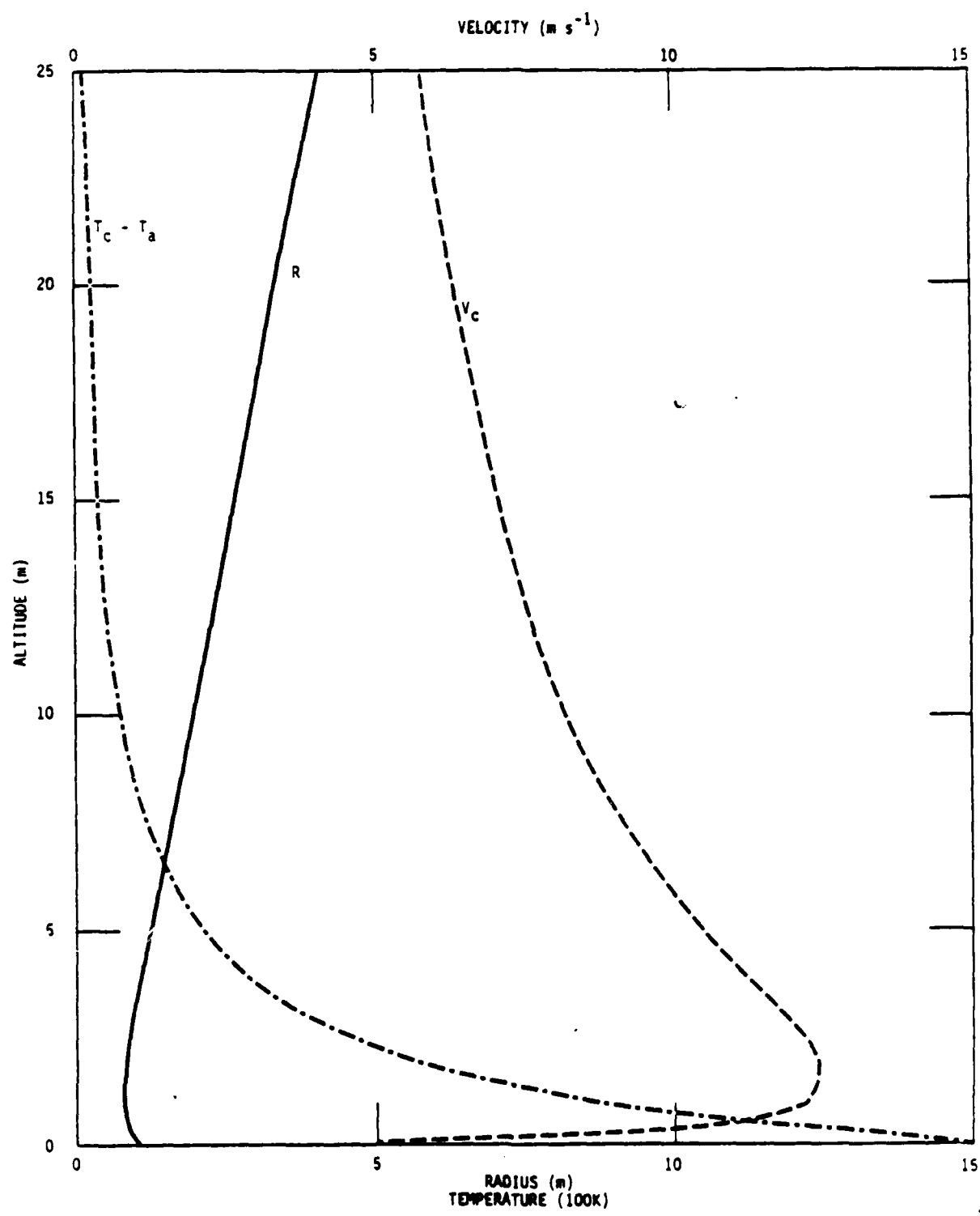
Figure 9. Plume parameters for initial conditions T_c-T_a=1500 K, V_c= 5 m s^{-1}, R=1 m.
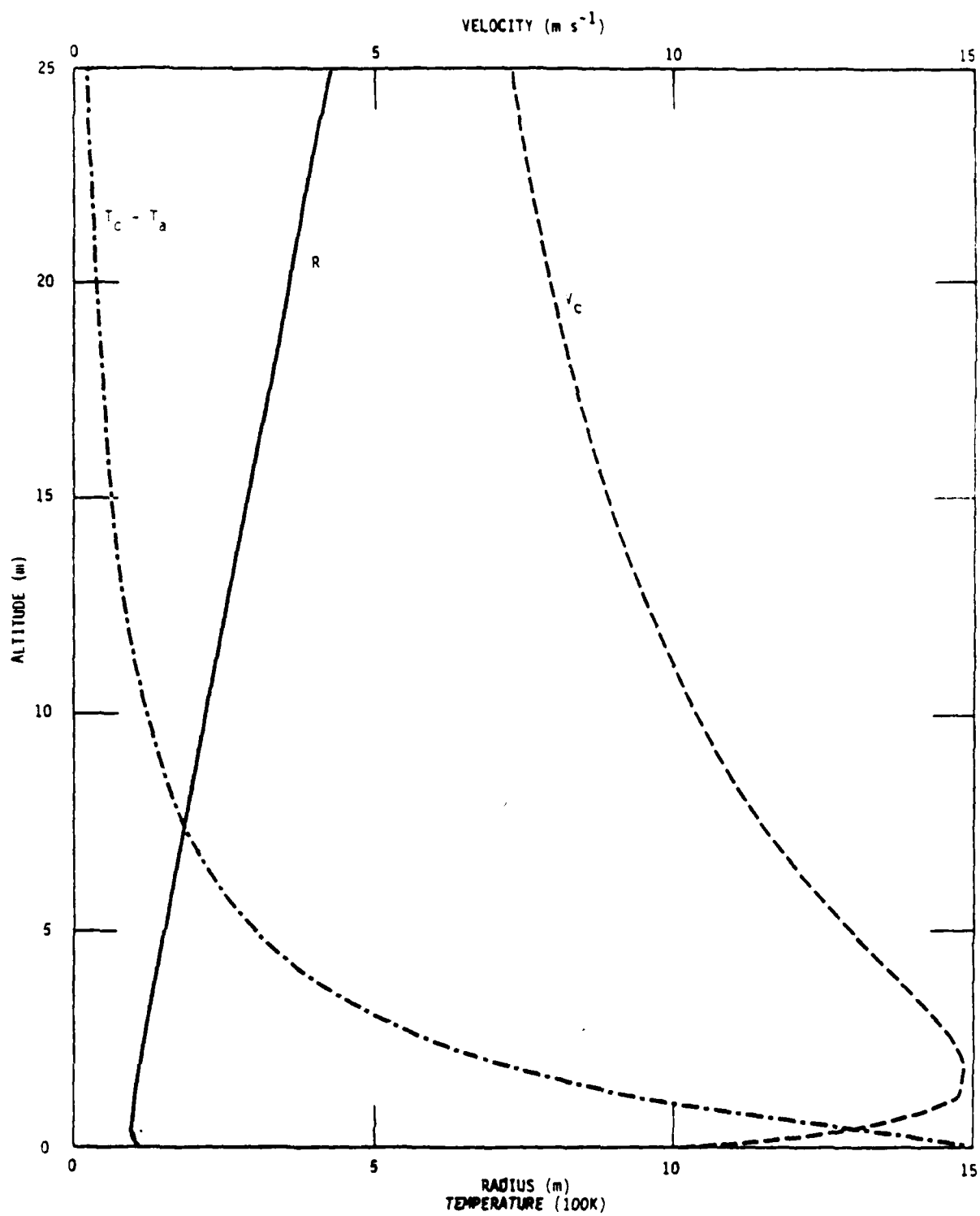
Figure 10. Plume parameters for initial conditions $T_c - T_a = 1500$ K, $V_c = 10$ m s^{-1}, R=1 m.
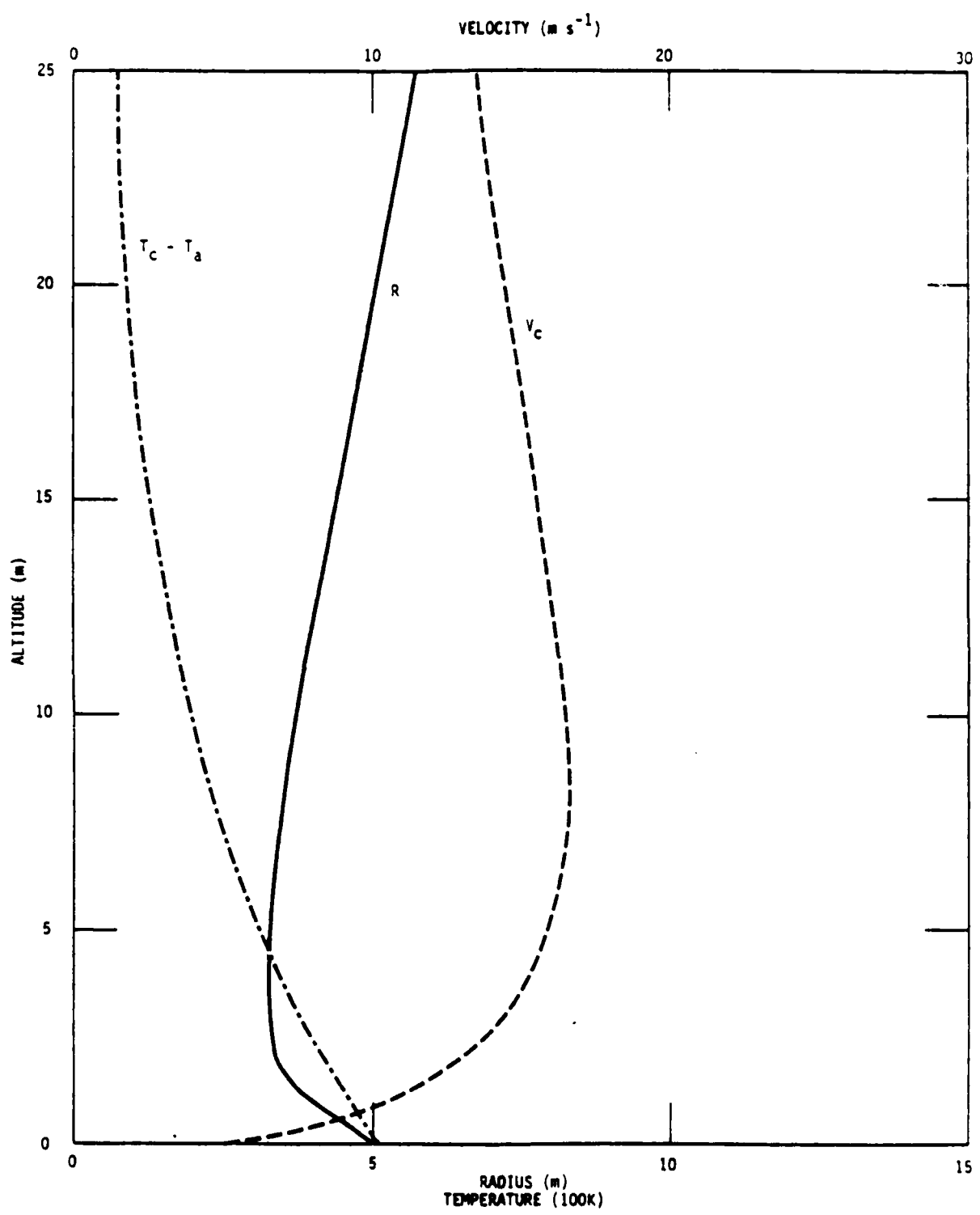
Figure 11.   Plume parameters for initial conditions T_c-T_a=500 K, V_c=5 m s^{-1}, R=5 m.
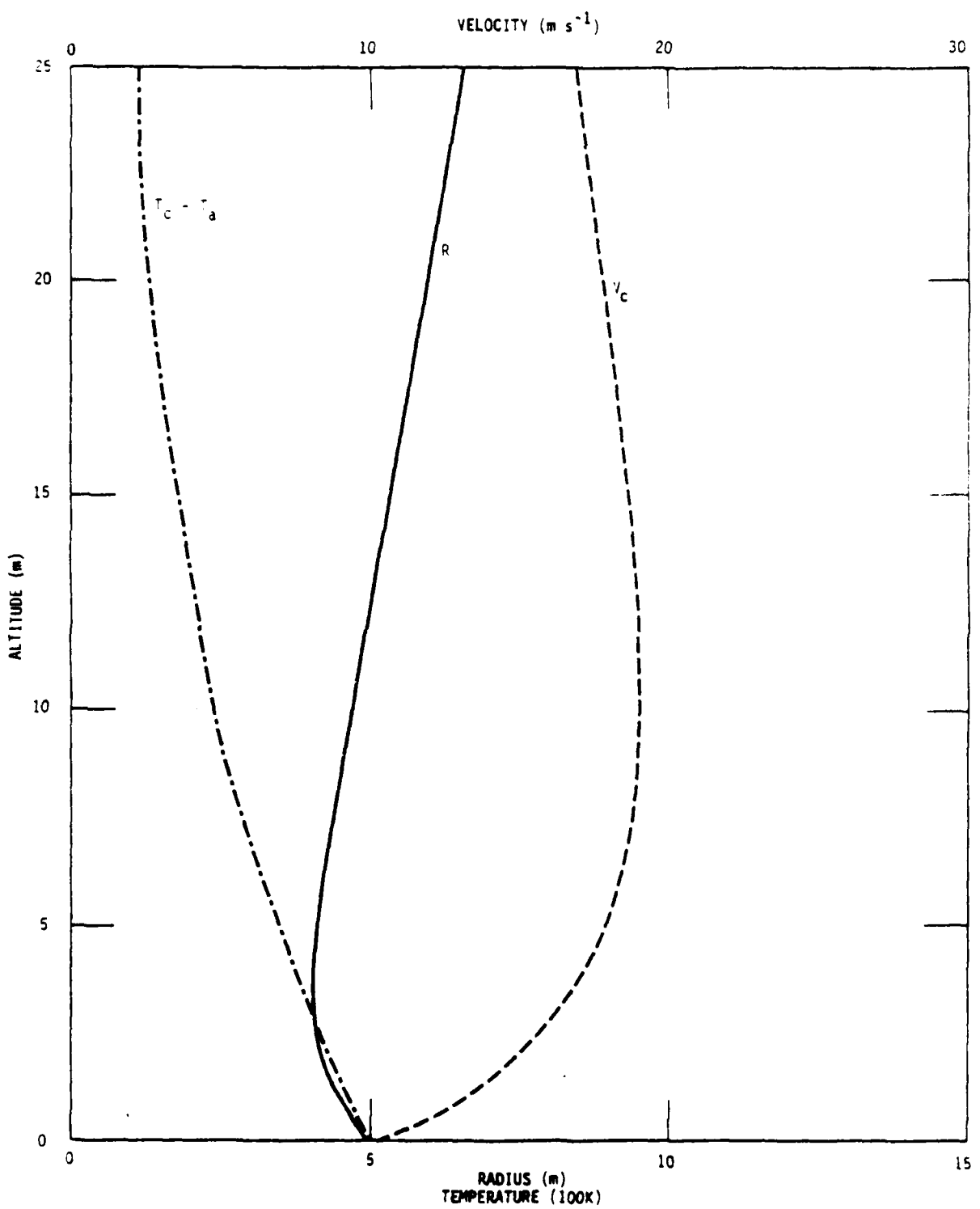
Figure 12. Plume parameters for initial conditions $T_c - T_a = 500$ K, $V_c = 10$ m s^{-1}, R=5 m.
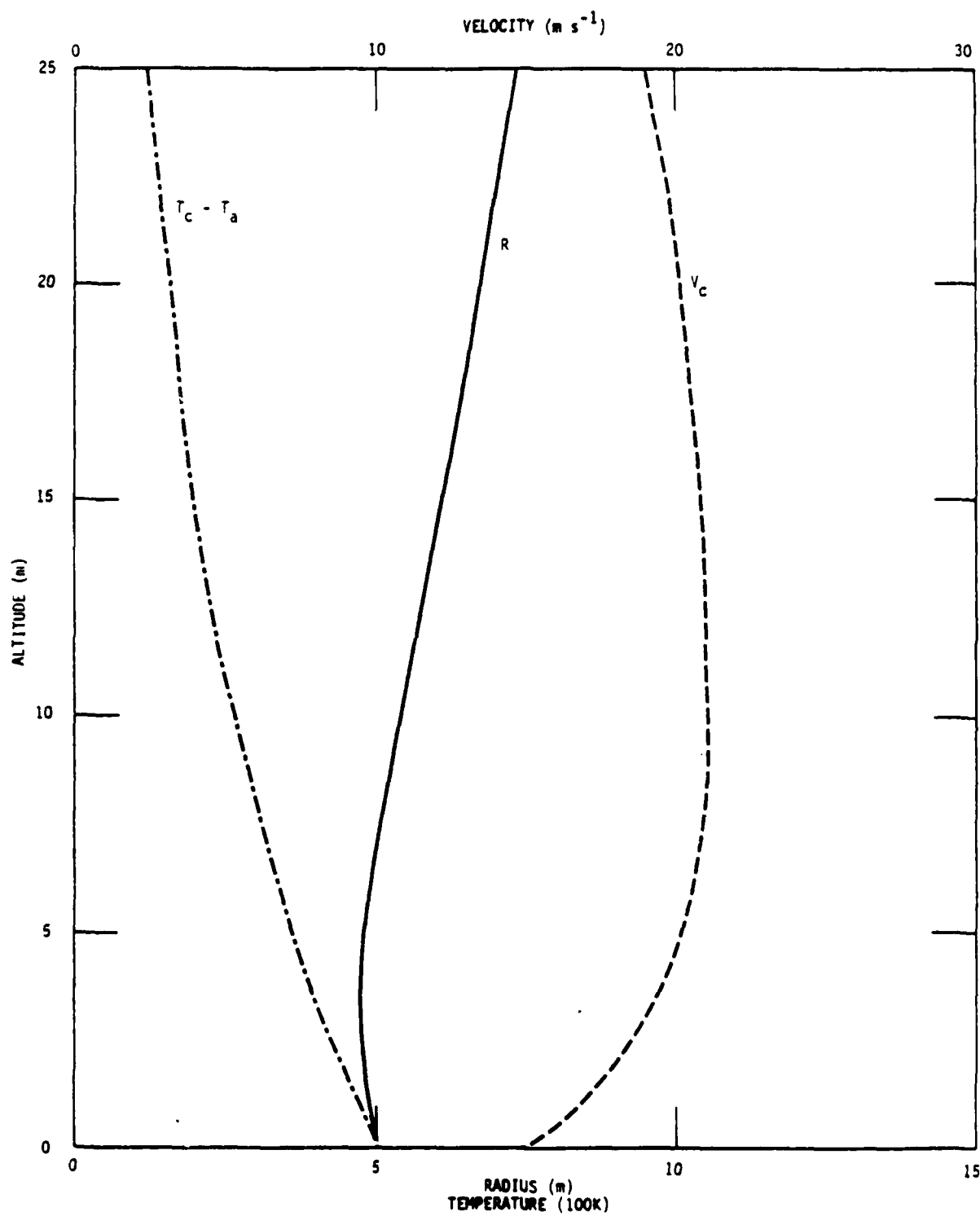
Figure 13. Plume parameters for initial conditions $T_c - T_a = 500$ K, $V_c = 15$ m s^{-1}, R=5 m.

37
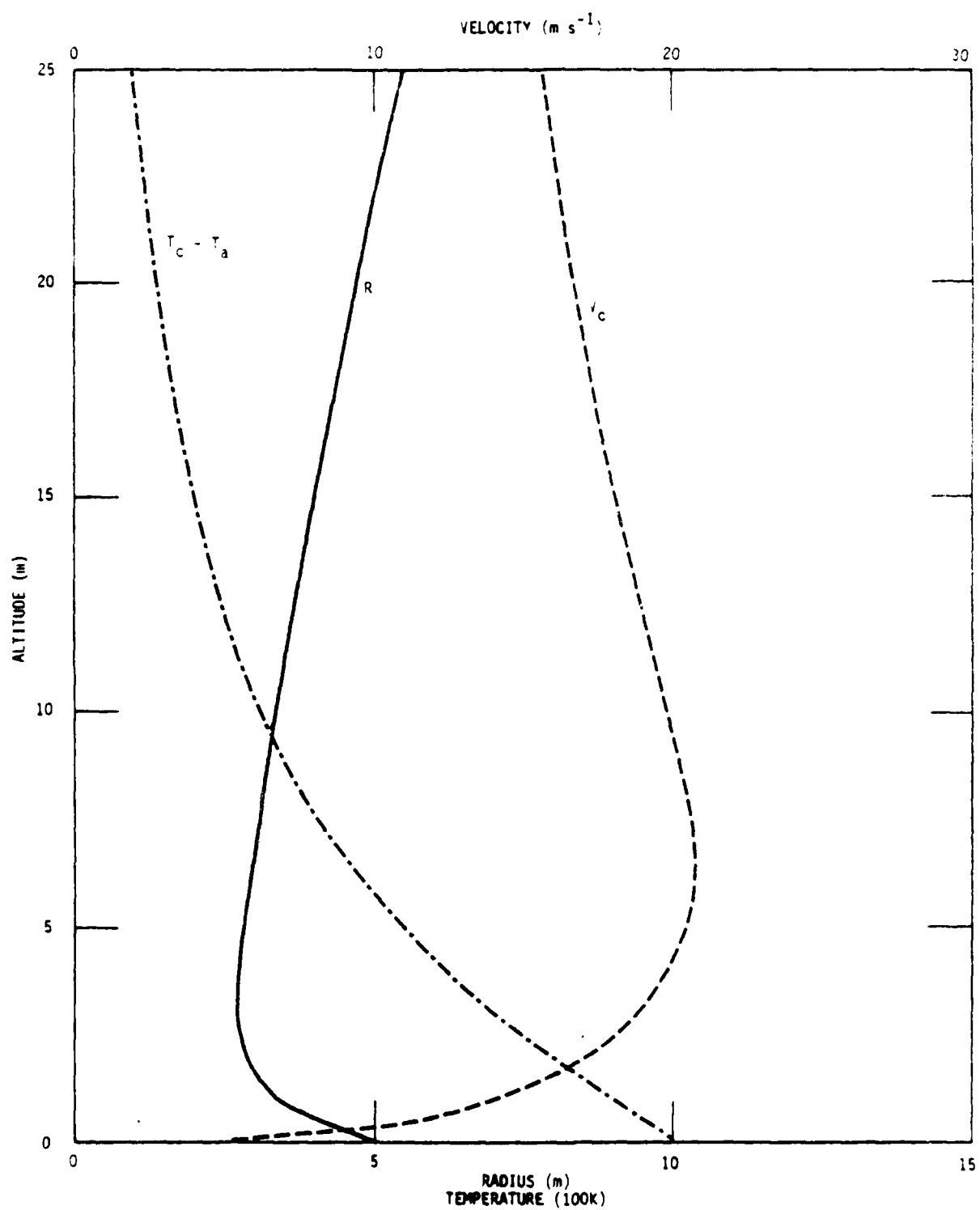
Figure 14. Plume parameters for initial conditions T_c-T_a=1000 K, V_c=5 m s^{-1}, R=5 m.
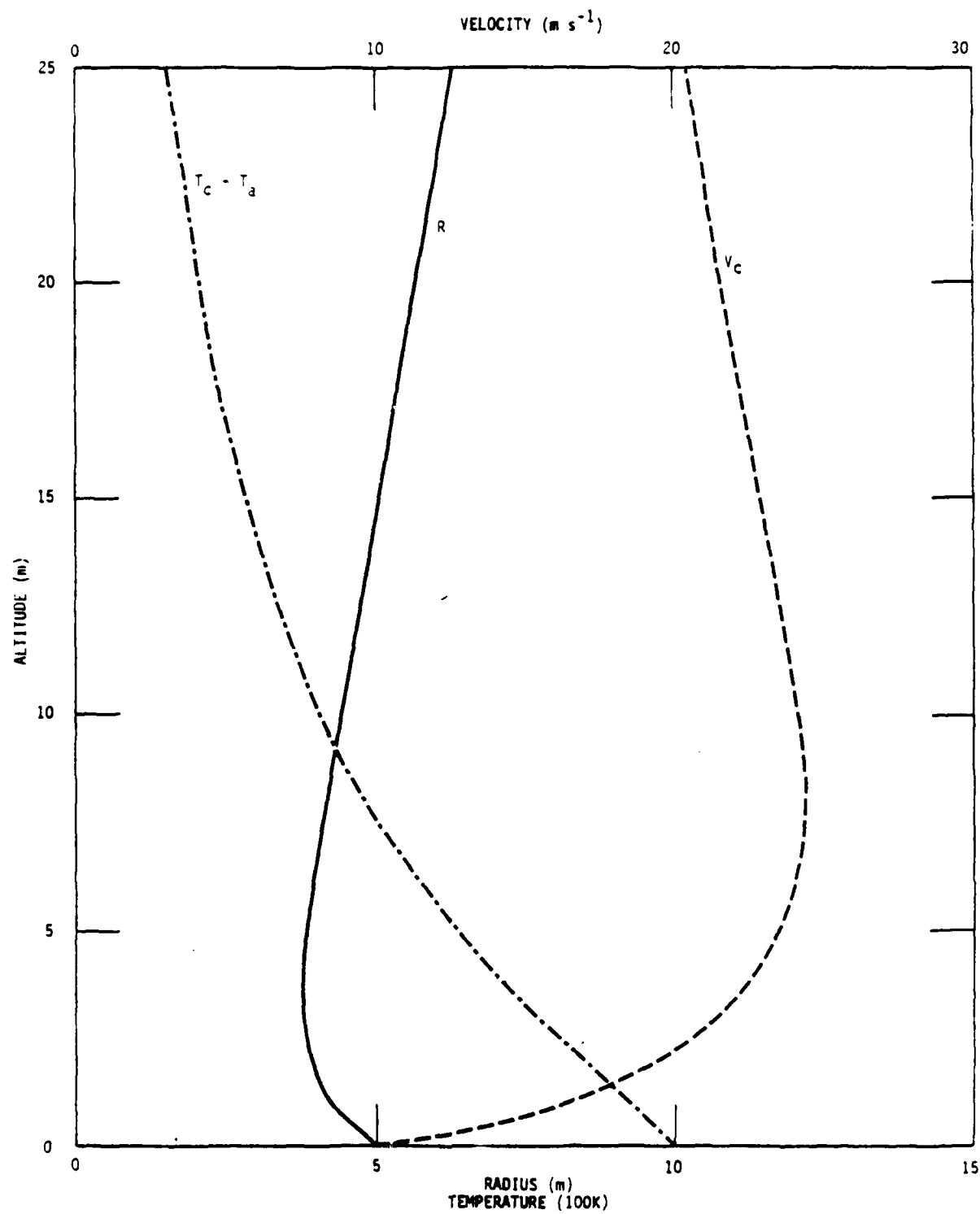
Figure 15. Plume parameters for initial conditions $T_c - T_a = 1000$ K, $V_c = 10$ m s^{-1}, R=5 m.
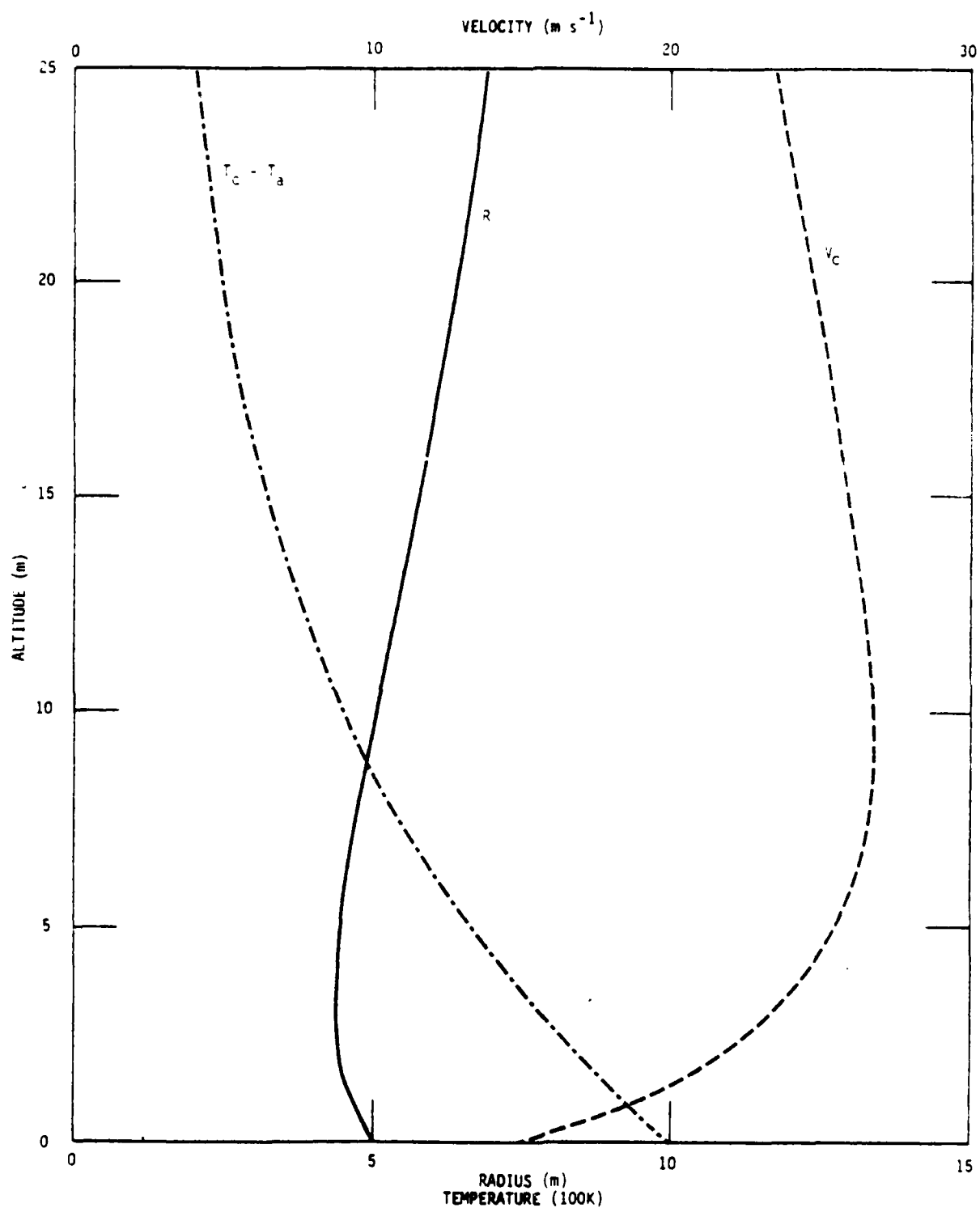
Figure 16.   Plume parameters for initial conditions T_c-T_a=1000 K, V_c=15 m s^{-1}, R=5 m.

40
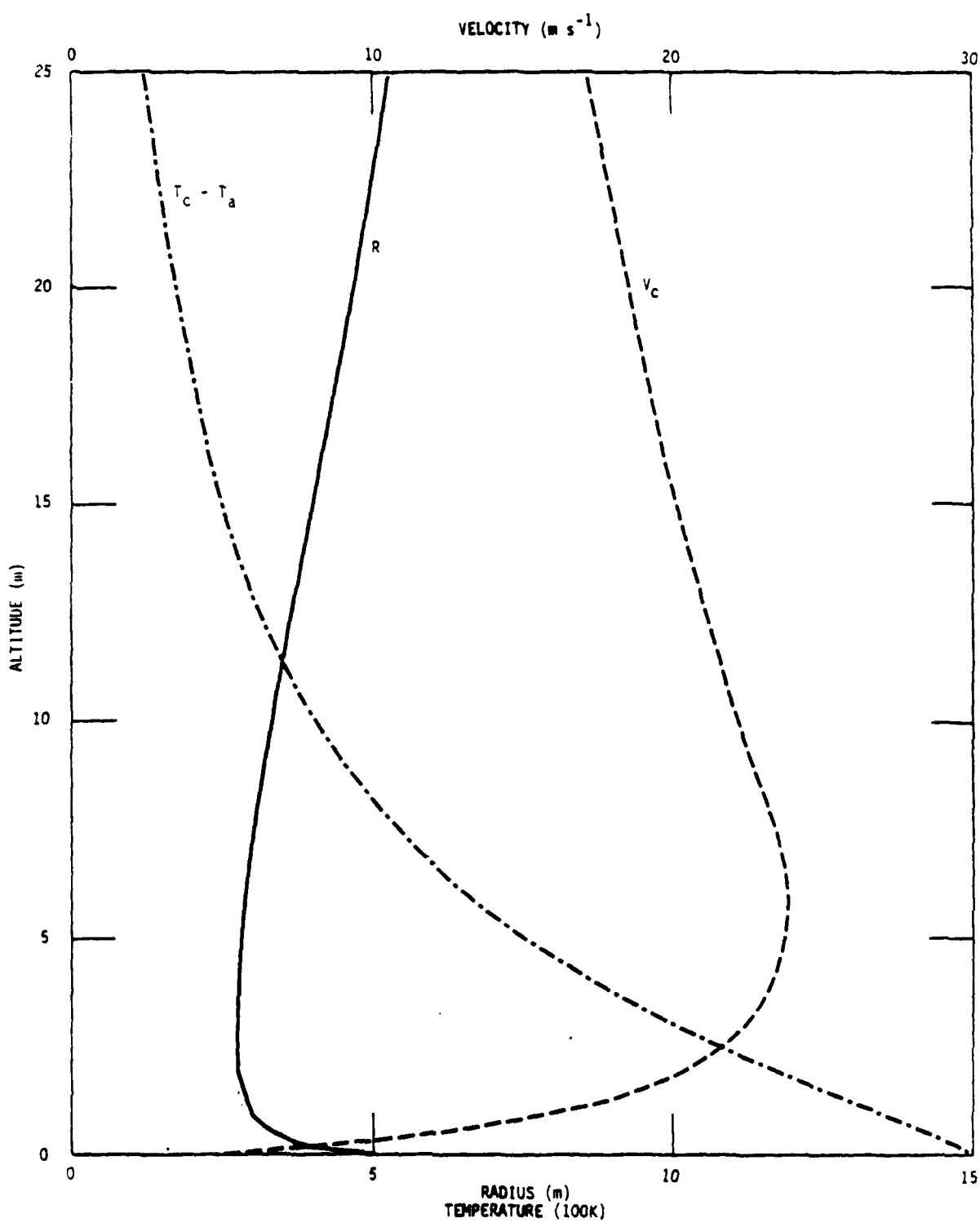
Figure 17. Plume parameters for initial conditions $T_c - T_a = 1500$ K, $V_c = 5$ m s^{-1}, R=5 m.
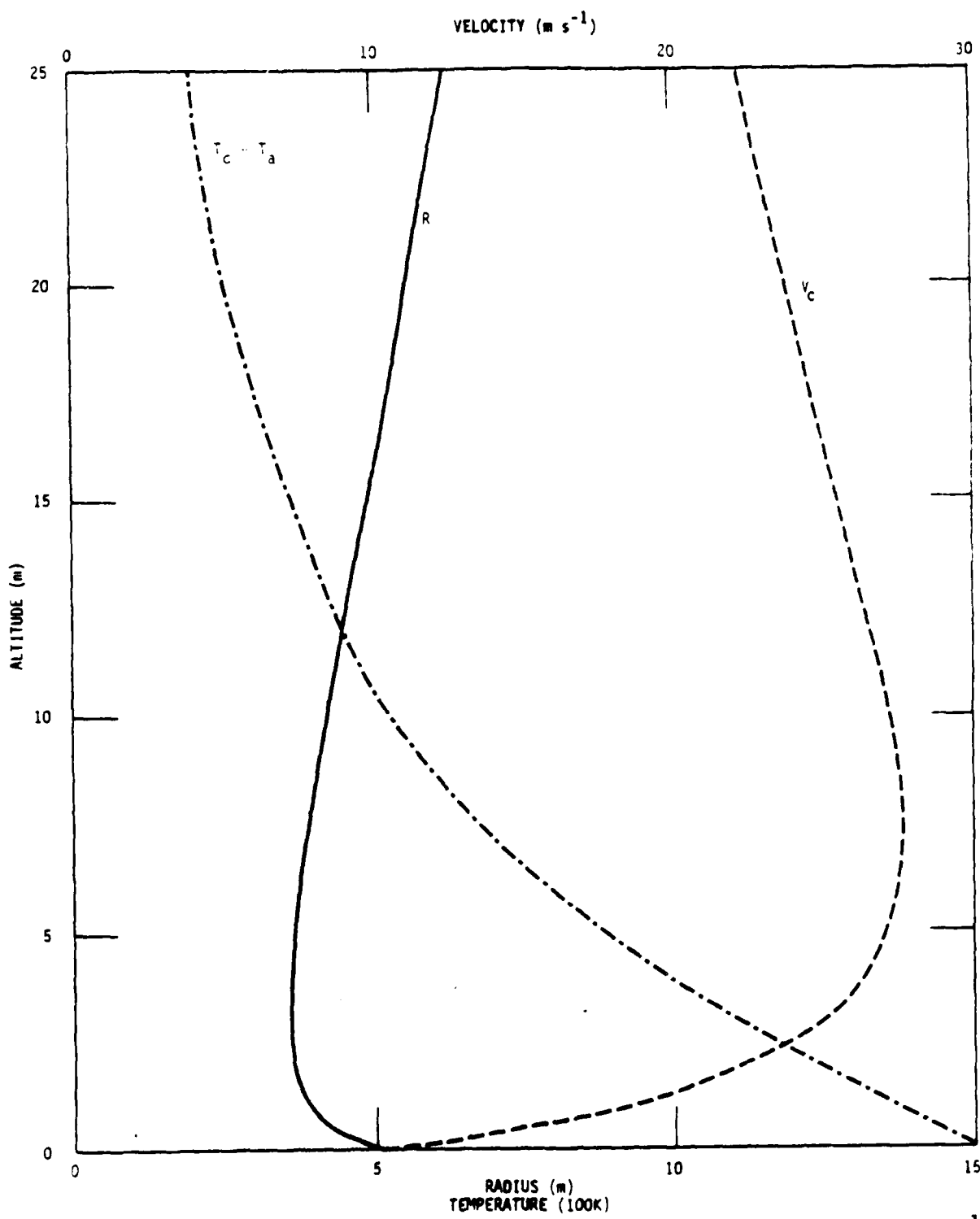
Figure 18. Plume parameters for initial conditions T_c-T_a=1500 K, V_c=10 m s^{-1}, R=5 m.
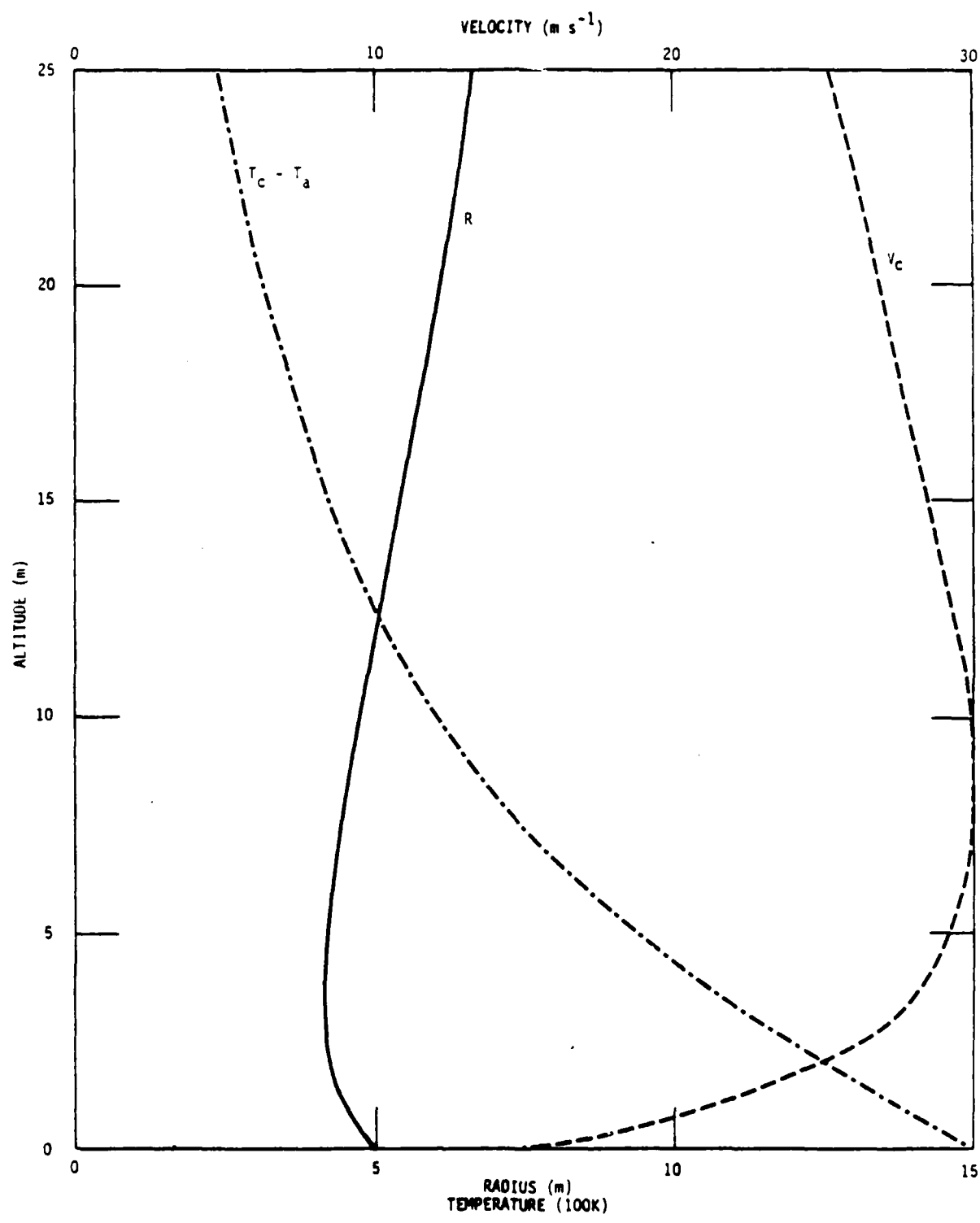
Figure 19. Plume parameters for initial conditions T_c-T_a=1500 K, V_c=15 m s^{-1}, R=5 m.

43
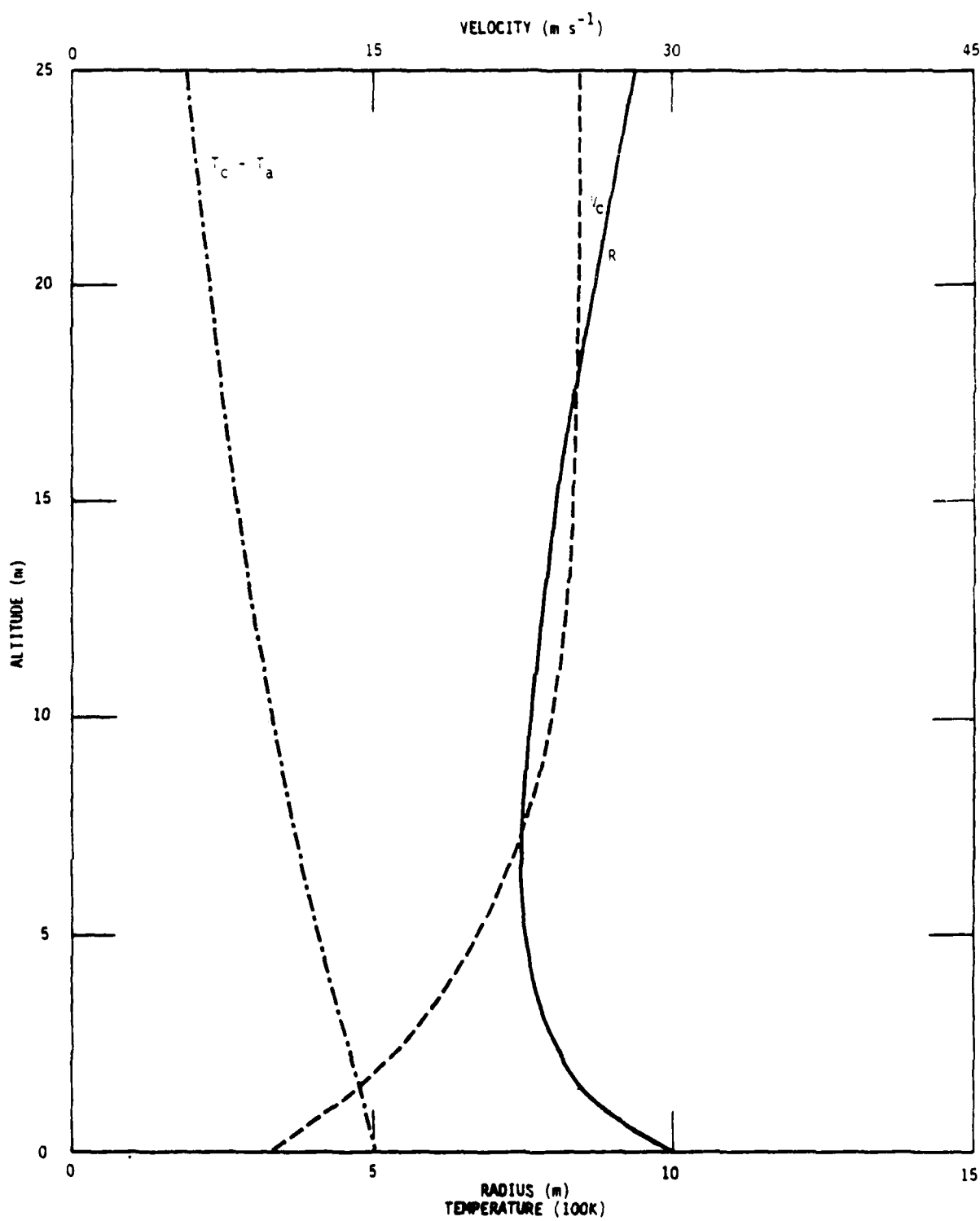
Figure 20. Plume parameters for initial conditions T_c-T_a=500 K, V_c=10 m s^{-1}, R=10 m.
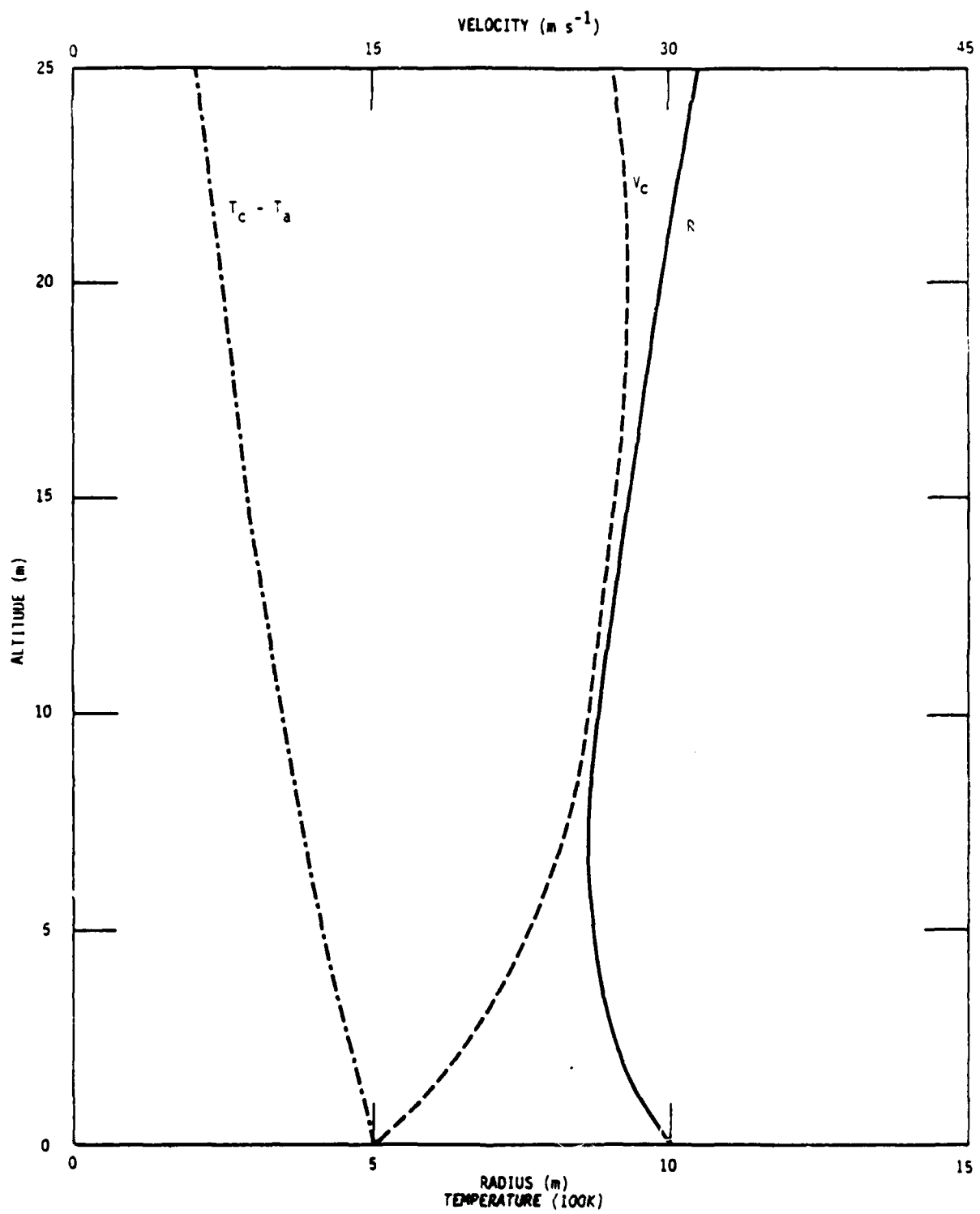
Figure 21. Plume parameters for initial conditions $T_c-T_a=500$ K, $V_c=15$ m s^{-1}, R=10 m.
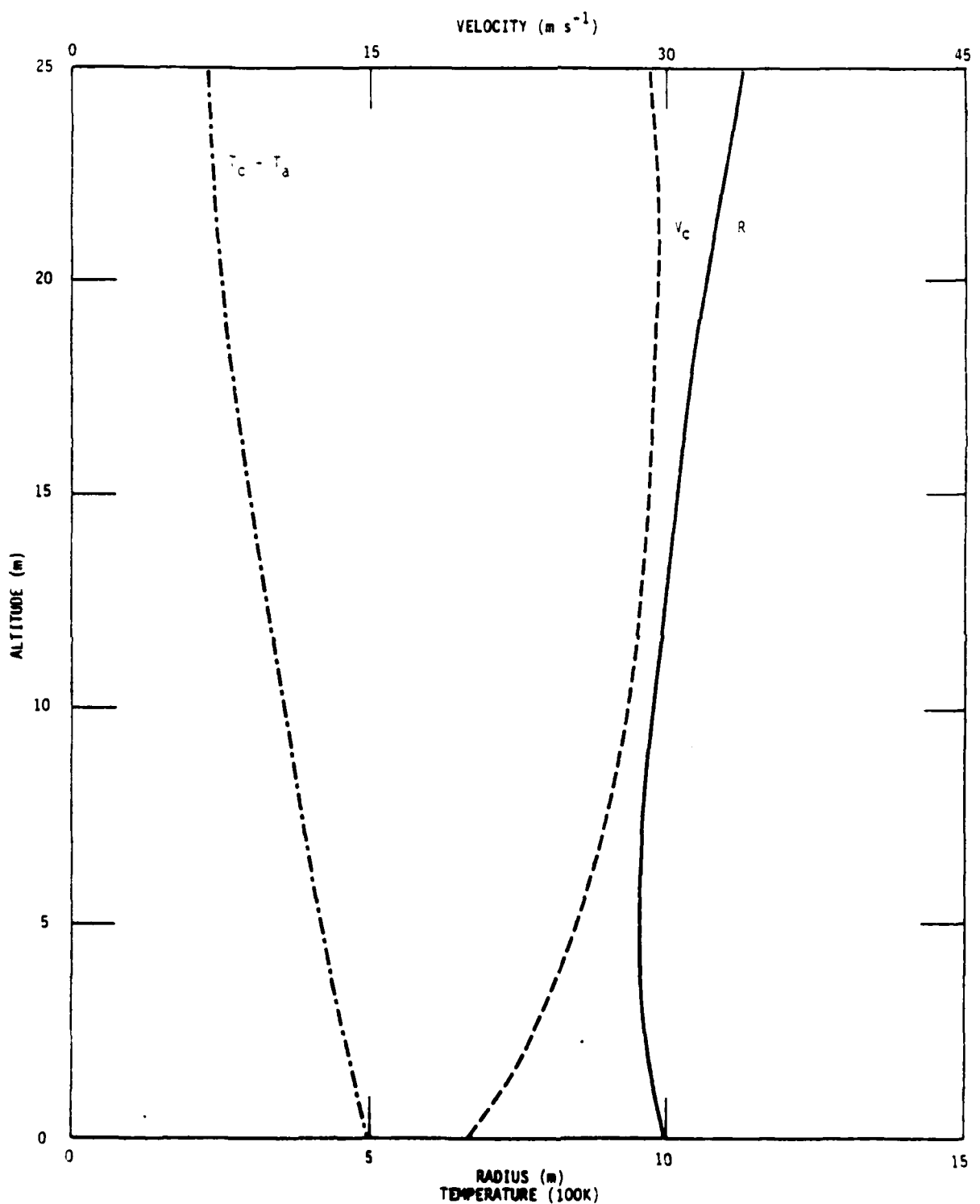
Figure 22. Plume parameters for initial conditions $T_c - T_a = 500$ K, $V_c = 20$ m s^{-1}, R=10 m.

46
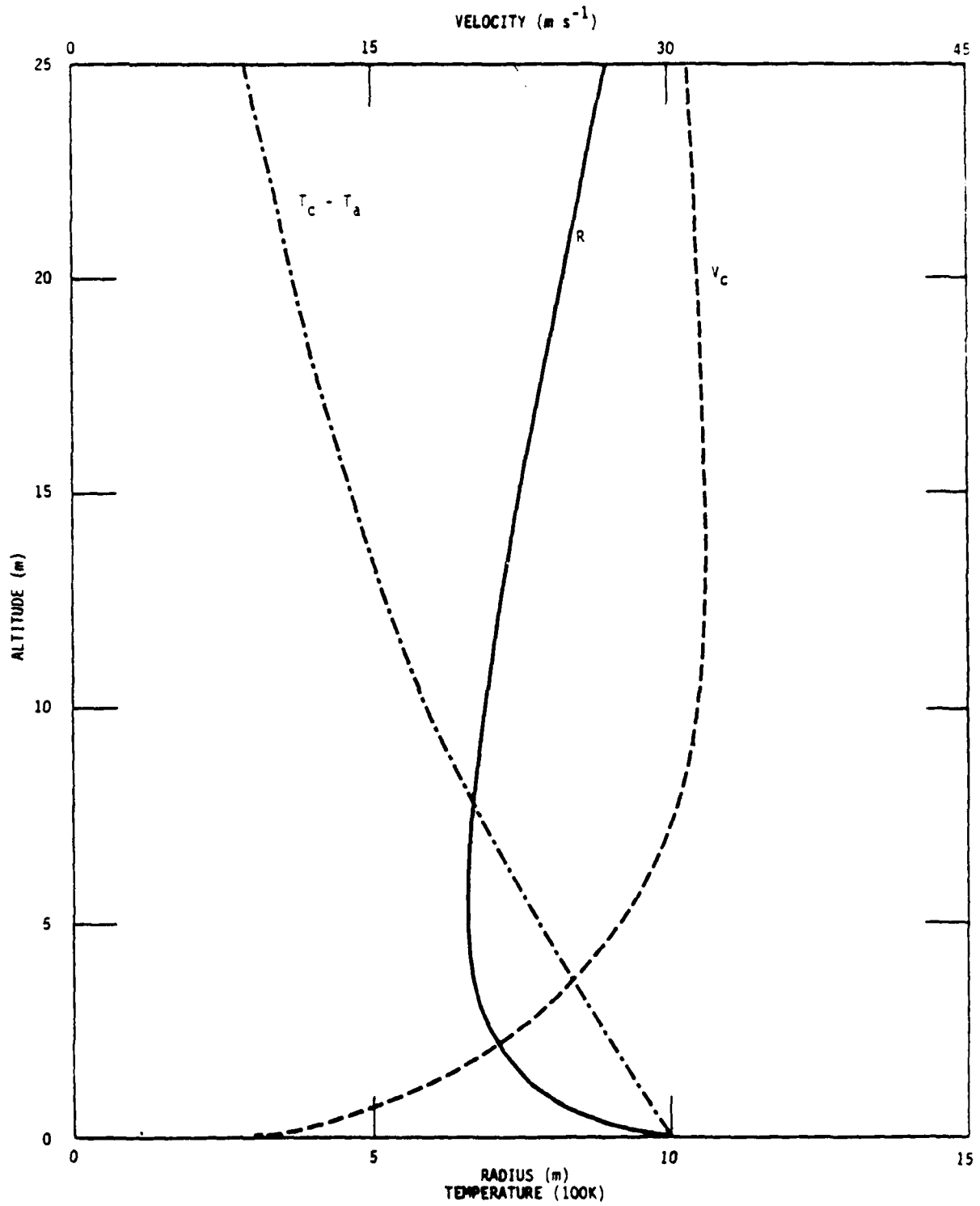
Figure 23. Plume parameters for initial conditions T_c-T_a=1000 K, V_c=10 m s^{-1}, R=10 m.
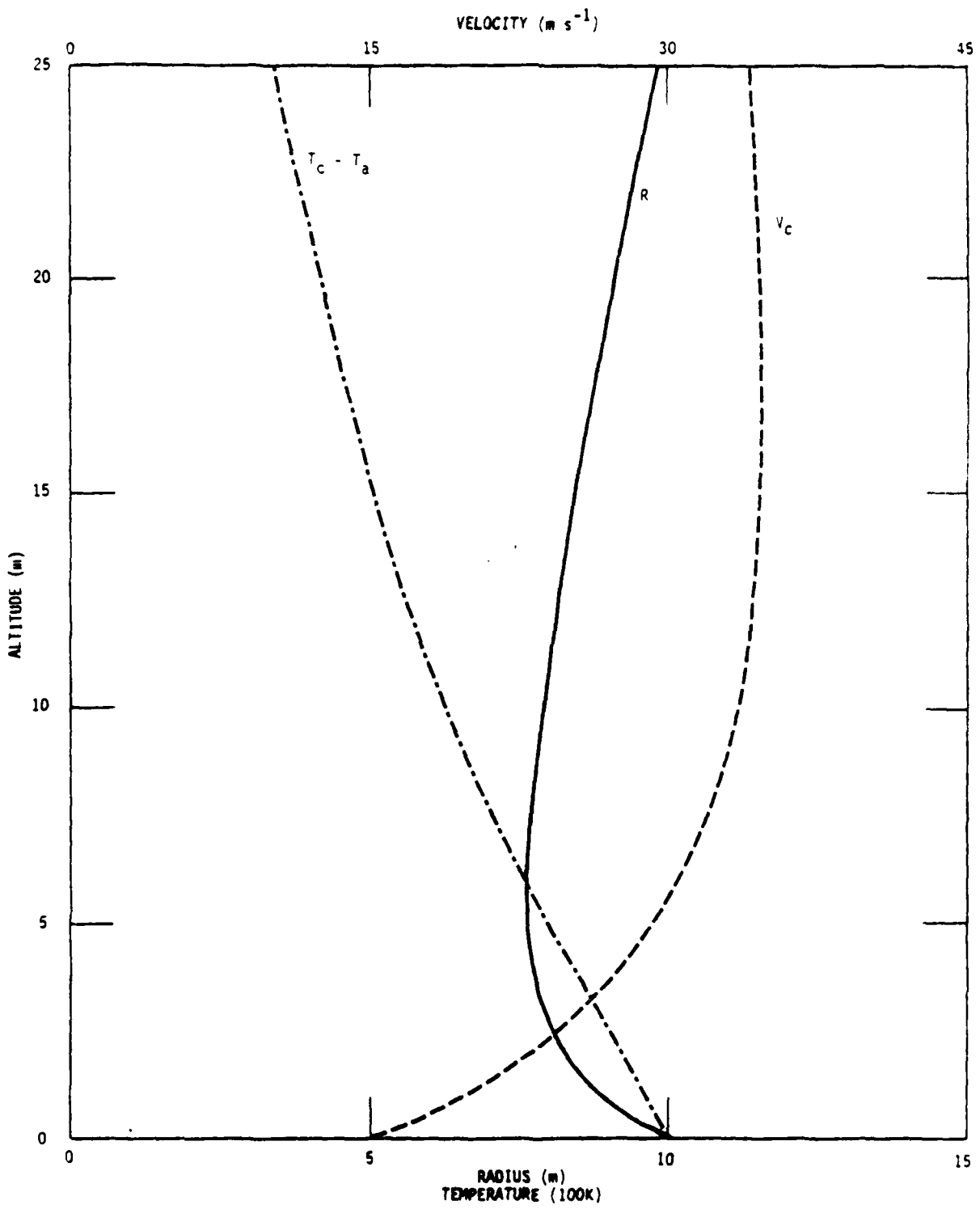
Figure 24. Plume parameters for initial conditions $T_c - T_a = 1000$ K, $V_c = 15$ m s^{-1}, $R = 10$ m.
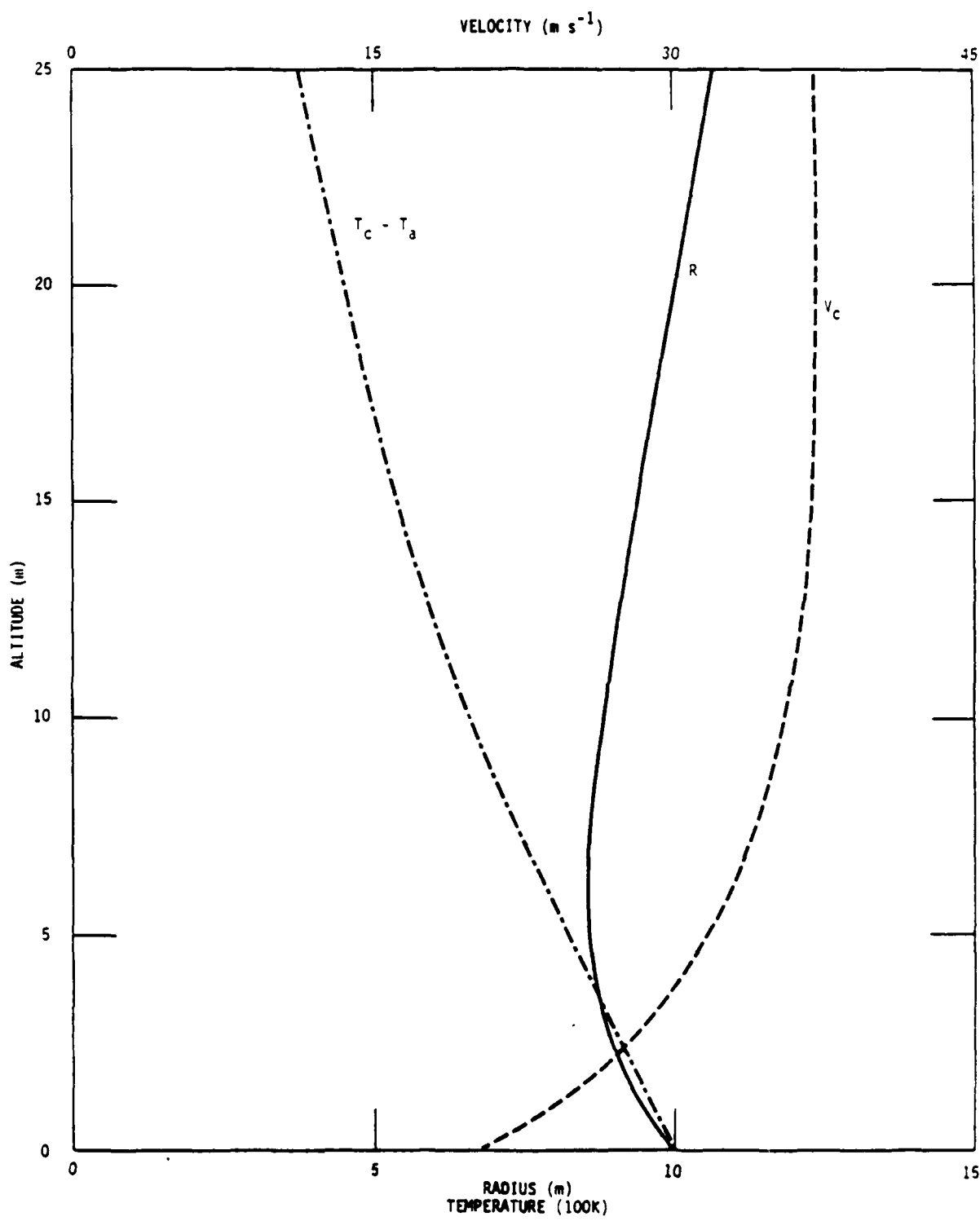
Figure 25. Plume parameters for initial conditions $T_c - T_a = 1000$ K, $V_c = 20$ m s^{-1}, R=10 m.
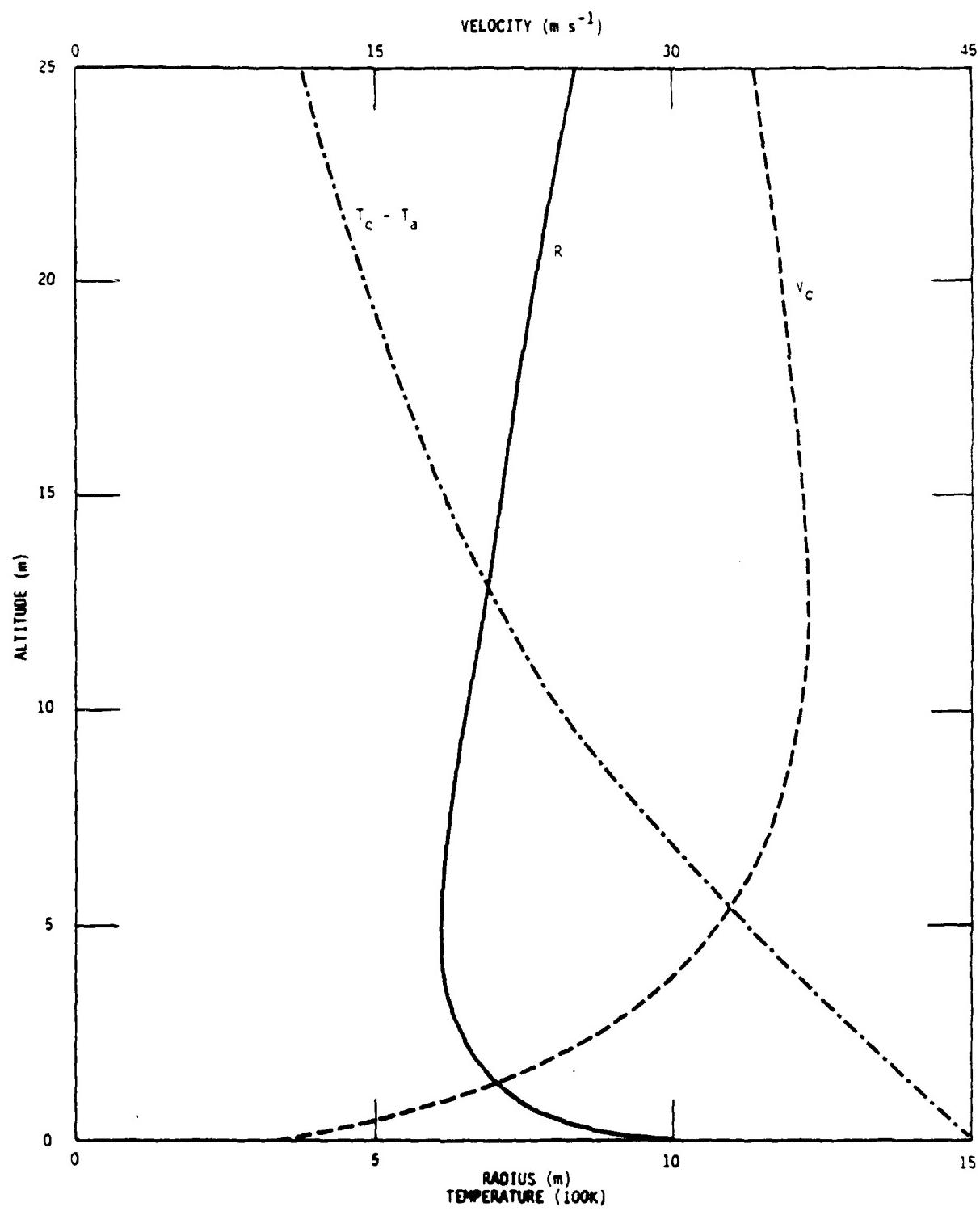
Figure 26. Plume parameters for initial conditions T_c-T_a=1500 K, V_c=10 m s^{-1}, R=10 m.
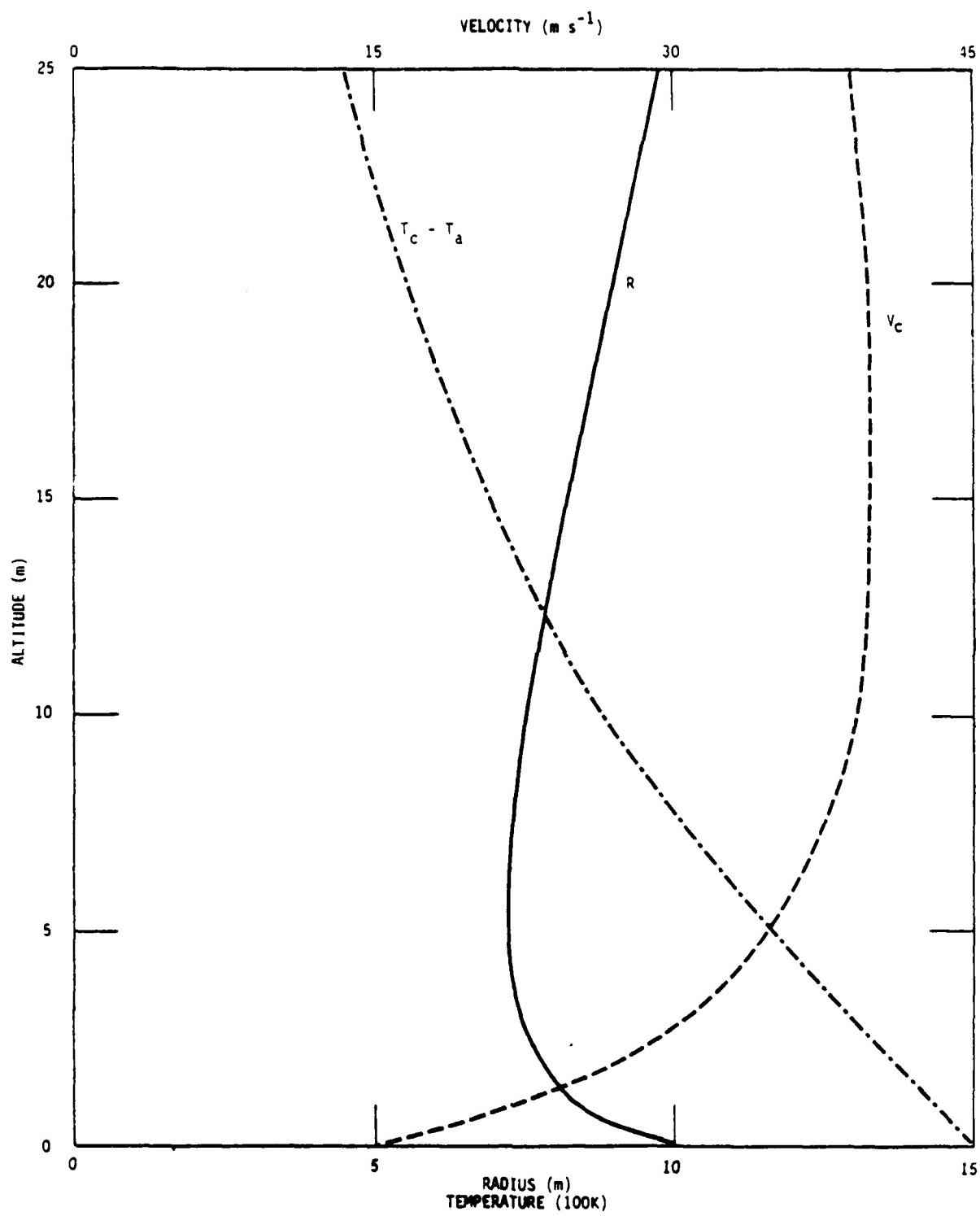
Figure 27. Plume parameters for initial conditions T_c-T_a=1500 K, V_c=15 m s^{-1}, R=10 m.
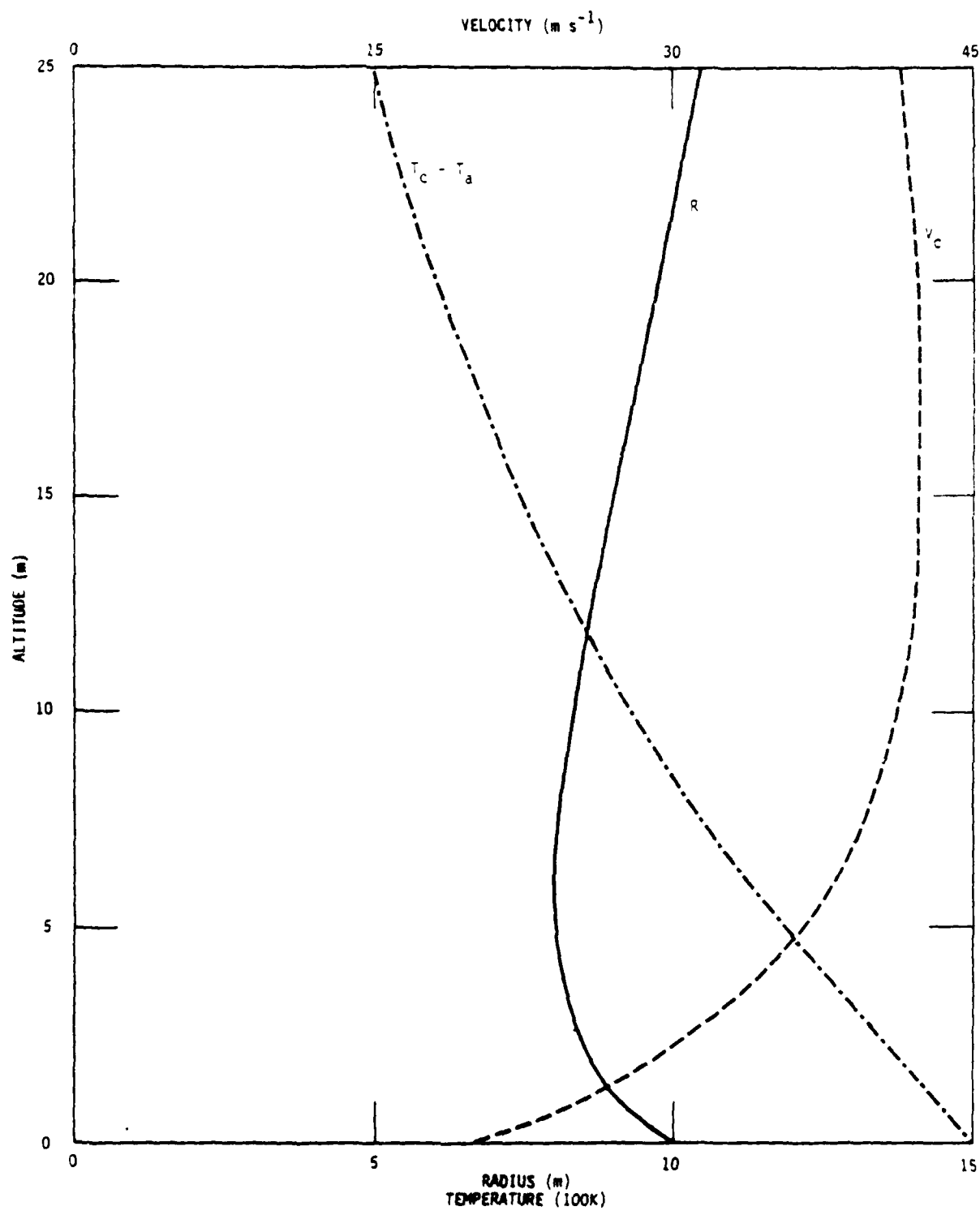
Figure 28. Plume parameters for initial conditions T_c-T_a=1500 K, V_c=20 m s^{-1}, R=10 m.

SECTION 3
PROPAGATION MODELS

INTRODUCTION

The index of refraction gradients and fluctuations within a turbulent hot fire plume can produce significant effects upon the propagation of electro-optical signals. There are two classes of effects; the first is due to the mean properties of the plume and the second is due to the turbulent fluctuations about the mean. The radial and vertical mean temperature gradients in the plume will produce corresponding mean index of refraction gradients. These mean index gradients will cause an electro-optical ray path to bend away from the straight line propagation path towards the regions of higher index. The turbulent fluctuations of the index of refraction about the mean index will cause random propagation effects. These turbulent effects include beam spreading and jitter, signal decorrelation, and phase and amplitude scintillations. First we will examine the mean bending due to the thermal gradients and then the turbulent propagation effects.

It is the spatial and temporal distribution of the index of refraction which determine the electro-optical propagation effects. Clean air is essentially nonabsorbing at visible optical wavelengths and for microwaves at frequencies less than about 72 GHz. The index of refraction is then real and is given by (References 11 and 12)

$$n-1 = \frac{77.6}{T} \left[P \left(1 + \frac{7.52 \times 10^{-3}}{\lambda^2} \right) + \frac{B\varepsilon}{T} \right] \times 10^{-6} \tag{27}$$

where

P = atmospheric pressure measure in millibars
(1 standard atmosphere = 1013.2 millibars)

λ = radiation wavelength (μm)

ϵ = water vapor pressure (millibars)

T = absolute temperature (K)

$$B = \begin{cases} -0.120 \text{ at optical frequencies} \\ 4810 \text{ at microwave frequencies.} \end{cases}$$

At optical frequencies, the humidity dependent term is negligible.

In the infrared and for the higher microwave frequencies, absorption effects enter and anomalous dispersion (varying dependence on wavelength) occurs. Then the index of refraction can be a rapidly changing function of frequency and the simple, nondispersive index of refraction formula no longer applies. Normally, however, the nondispersive formulation is adequate in the normal atmospheric transmission windows, where systems are designed to operate.

MEAN BENDING EFFECTS

Consider the propagation geometry shown in Figure 29. A horizontal ray path passes through a fire plume at altitude h at a distance d from the plume centerline. The cross section of the plume at altitude h is shown in Figure 30. For calculation purposes we place a cartesian coordinate system with origin on the plume centerline at altitude h, with the z axis vertical (coincident with the plume centerline), x axis horizontal and parallel to the ray path, y axis horizontal and perpendicular to the ray path.

The mean radial and vertical index of refraction gradients in the plume will cause the ray path to bend away from the geometrically straight ray path. The radial gradient will cause a bending in the y direction away from the plume centerline and the vertical gradient will cause a vertical bending in the positive z (upward) direction. The total mean angular deviation caused by a single plume is expected to be small, on the order of a milliradian. But the total linear
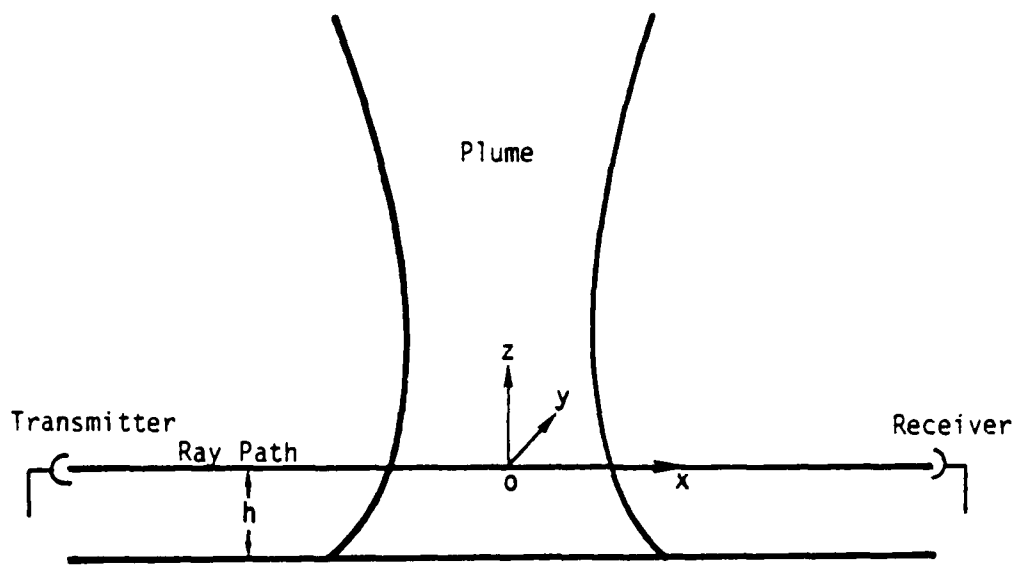
Figure 29 . Ray path geometry.
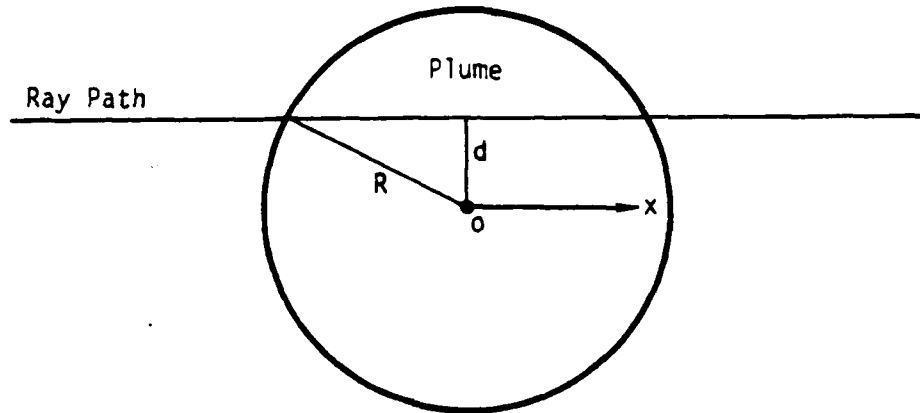
Figure 30. Cross section of ray path through plume.

offset from the straight line path at the receiver depends on the
distance between the plume and the receiver. At 1000 meters beyond
the plume, a one-milliradian angular bending will produce a linear
offset of one meter. Whether this magnitude of angular bending is
significant depends upon the particular electro-optical system.

Define

$$U = \frac{dx}{ds}$$

$$V = \frac{dy}{ds}$$

$$W = \frac{dz}{ds}$$

where s is the distance along the true ray path. Then the equations
for ray tracing are

$$\frac{dU}{ds} = \frac{1}{n} \left[(1 - U^2) \frac{\partial n}{\partial x} - UV \frac{\partial n}{\partial y} - UW \frac{\partial n}{\partial z} \right] \tag{28}$$

$$\frac{dV}{ds} = \frac{1}{n} \left[-UV \frac{\partial n}{\partial x} + (1 - V^2) \frac{\partial n}{\partial y} - VW \frac{\partial n}{\partial z} \right] \tag{29}$$

$$\frac{\partial W}{\partial s} = \frac{1}{n} \left[-UW \frac{\partial n}{\partial x} - VW \frac{\partial n}{\partial y} + (1 - W^2) \frac{\partial n}{\partial z} \right] . \tag{30}$$

In the region of the plume, the deviation of the true ray path from
the straight line path will be extremely small so we can set

$$s = x$$

$$U = 1$$

and drop Equation 28 from consideration. In the nondispersive wave-
length regime,

$$n - 1 \ll 1$$

so we can take

$$\frac{1}{n} = 1 \quad .$$

Since the bending is so slight

$$\frac{\partial n}{\partial x} , \frac{\partial n}{\partial y} , \frac{\partial n}{\partial z} , V , W \ll 1$$

and we neglect all second and third order products in Equations 29 and 30. Our bending equations become simply

$$\frac{dV}{dx} = \frac{\partial n}{\partial y}$$

$$\frac{\partial W}{\partial x} = \frac{\partial n}{\partial z} \quad .$$

For x beyond the plume

$$V(x) = \frac{dy}{dx} = \tan \theta_y \cong \theta_y \qquad \text{since} \qquad \theta_x \ll 1$$

$$W(x) = \frac{dz}{dx} = \tan \theta_z \cong \theta_z$$

where θ_y and θ_z are the total angular bending in the horizontal and vertical planes due to the plume mean thermal gradients. Hence

$$\theta_y = \int_{x_R}^{x_T} \frac{\partial n}{\partial y} \, dx = \int_{-\infty}^{\infty} \frac{\partial n}{\partial y} \, dx \qquad \text{rad} \tag{31}$$

$$\theta_z = \int_{x_R}^{x_T} \frac{\partial n}{\partial z} \, dx = \int_{-\infty}^{\infty} \frac{\partial n}{\partial z} \, dx \qquad \text{rad} \tag{32}$$

where x_R, x_T are the receiver and transmitter x coordinates. Since we are integrating over a Gaussian temperature distribution and the integration limits are well beyond the plume, the finite limits can be replaced by $\pm \infty$, which will simplify the evaluation of the integrals.

Differentiating Equation 27 for the index of refraction we have

$$\frac{\partial n}{\partial y} = \frac{\partial (n-1)}{\partial y} = -\frac{77.6}{T^2}\left[P\left(1 + \frac{7.52 \times 10^{-3}}{\lambda^2}\right)\right] \times 10^{-6}\frac{\partial T}{\partial y} \qquad (33)$$

$$\frac{\partial n}{\partial z} = \frac{\partial (n-1)}{\partial z} = -\frac{77.6}{T^2}\left[P\left(1 + \frac{7.52 \times 10^{-3}}{\lambda^2}\right)\right] \times 10^{-6}\frac{\partial T}{\partial z} \qquad (34)$$

Assuming optical and infrared frequencies, the humidity dependent term has been neglected. The plume is assumed to be in pressure equilibrium so there are no pressure gradients in the horizontal direction. There is a vertical pressure gradient, $\partial P/\partial z$, the hydrostatic pressure lapse rate; but the pressure gradient term is less than one percent of the temperature gradient term and has been neglected.

The plume Gaussian temperature distribution, Equation 19, can be written as

$$T(x,y,z) = T_a(z) + [T_c(z) - T_a(z)]e^{-2\frac{x^2+y^2}{R^2(z)}} \qquad K \qquad (35)$$

where we have explicitly indicated the coordinate dependencies. Along the integration path $y = d$. Thus

$$\frac{\partial T(x,d,t)}{\partial y} = -\frac{4d}{R^2(z)}[T_c(z) - T_a(z)]e^{-2\frac{x^2+d^2}{R^2(z)}} \qquad K\ m^{-1} \qquad (36)$$

$$\frac{\partial T(x,d,z)}{\partial z} = \left\{\frac{\partial T_c(z)}{\partial z} + 4[T_c(z) - T_a(z)]\left[\frac{x^2+d^2}{R^3(z)}\right]\frac{\partial R(z)}{\partial z}\right\}e^{-2\frac{x^2+d^2}{R^2(z)}} \qquad K\ m^{-1}$$

$$(37)$$

In Equation 37 we have neglected the ambient temperature lapse rate, $\partial T_a(z)/\partial z$, in comparison with the other terms.

The integrals defining θ_y and θ_z are obtained by combining Equations 31 through 37. These are non-integrable analytically, except in limiting cases, and must be solved numerically in the general case. We will rearrange the integrals for ease in graphical and numerical solution. Define the following parameters

$$w = \frac{x}{R(z)} = \text{dimensionless path integration parameter}$$

$$F_d = \frac{d}{R(z)} = \text{dimensionless point of closest approach}$$

$$F_T = \frac{T_c(z) - T_a(z)}{T_a(z)} = \begin{array}{l}\text{dimensionless excess temperature}\\\text{on plume centerline}\end{array}$$

$$P_o = 1013.2 \text{ millibars} = \text{standard atmosphere}$$

$$T_o = 288 \text{ K} = \text{typical ground level temperature}$$

$$n_o - 1 = \frac{77.6 \, P_o \times 10^{-6}}{T_o} = 2.73 \times 10^{-4} = \begin{array}{l}\text{typical ambient air index}\\\text{of refraction minus one at sea level.}\end{array}$$

Define the following normalized integrals

$$I_o(F_d) = 8 \times 10^3 \, (n_o - 1) \int_0^\infty e^{-2\left(w^2 + F_d^2\right)} \, dw \qquad (38)$$

$$I_1(F_d, F_T) = 8 \times 10^3 \, (n_o - 1) \int_0^\infty \frac{e^{-2\left(w^2 + F_d^2\right)}}{\left[1 + F_T \, e^{-2\left(w^2 + F_d^2\right)}\right]^2} \, dw \qquad (39)$$

$$I_2(F_d, F_T) = 32 \times 10^3 \, (n_o - 1) \int_0^\infty \frac{w^2 \, e^{-2\left(w^2 + F_d^2\right)}}{\left[1 + F_T \, e^{-2\left(w^2 + F_d^2\right)}\right]^2} \, dw \; . \qquad (40)$$

Then the mean bending formulas with the angles expressed in milli-radians become

$$\theta_y = \left(\frac{P}{P_o}\right)\left(\frac{T_o}{T_a}\right)\left(1 + \frac{7.52 \times 10^{-3}}{\lambda^2}\right) F_d F_T I_1(F_d, F_T) \quad \text{milliradians}$$

(41)

$$\theta_z = \left(\frac{P}{P_o}\right)\left(\frac{T_o}{T_a}\right)\left(1 + \frac{7.52 \times 10^{-3}}{\lambda^2}\right) F_T \left\{\left[-\frac{R}{4(T_c - T_a)}\frac{\partial T_c}{\partial z}\right.\right.$$

$$\left.\left. - F_d^2 \frac{\partial R}{\partial z}\right] I_1(F_d, F_T) - \frac{1}{4}\frac{\partial R}{\partial z} I_2(F_d, F_T)\right\} \quad \text{milliradians} \quad (42)$$

For most wavelengths, the wavelength dependent term, $7.52 \times 10^{-3}/\lambda^2$ can be neglected. Note that the bending does not depend on the physical size of the plumes. Large and small plumes which are similar produce the same bending. The similarity is obvious in the formulation. In the θ_z formula the term

$$\frac{R}{T_c - T_a}\frac{\partial T_c}{\partial z}$$

represents the fractional change in excess centerline temperature per change in height of one plume radius. The $\partial R / \partial z$ term is the same for similar plumes. In fact, in the weakly buoyant rise phase of the plume all model plumes have

$$\frac{\partial R}{\partial z} \approx 0.18 \quad .$$

This 0.18 model value is also confirmed by the experimental measurements of Reference 10.

The plume radius, centerline temperature and gradients are determined by the plume results of Section 2. We evaluate the normalized integrals in the following manner. The I_o integral has the analytic solution

$$I_o(F_d) = 8 \times 10^3 (n_o - 1) \frac{\sqrt{\pi}}{2\sqrt{2}} e^{-2F_d^2} \approx 1.37 e^{-2F_d^2} \quad . \quad (43)$$

The I_1 and I_2 integrals have to be evaluated numerically. They are well behaved integrals and any standard numerical integration technique can be used for evaluation. For user convenience we present the solutions in graphical form. Define the following ratios

$$F_{10}(F_d, F_T) = \frac{I_1(F_d, F_T)}{I_0(F_d, F_T)}$$

$$F_{21}(F_d, F_T) = \frac{I_2(F_d, F_T)}{I_1(F_d, F_T)} \quad .$$

Figures 31 and 32 show the ratios as a function of F_d and F_T. Naturally

$$I_1(F_d, F_T) = I_0(F_d, F_T) \, F_{10}(F_d, F_T) = 1.37 \, e^{-2F_d^2} \, F_{10}(F_d, F_T) \quad (44)$$

$$I_2(F_d, F_T) = I_1(F_d, F_T) \, F_{21}(F_d, F_T) \quad . \qquad\qquad (45)$$

As an example calculation consider a plume with the following parameters

$$\lambda = 1 \ \mu m$$

$$P = P_o$$

$$T = T_o$$

$$F_d = 0.5$$

$$F_T = \frac{1000}{T_o} = 3.47$$

$$\frac{R}{T_c - T_a} \frac{\partial T_c}{\partial z} = -0.5$$

$$\frac{\partial R}{\partial z} = -0.1 \quad \text{(ie, we are in the strongly buoyant accelerating rise phase).}$$

61
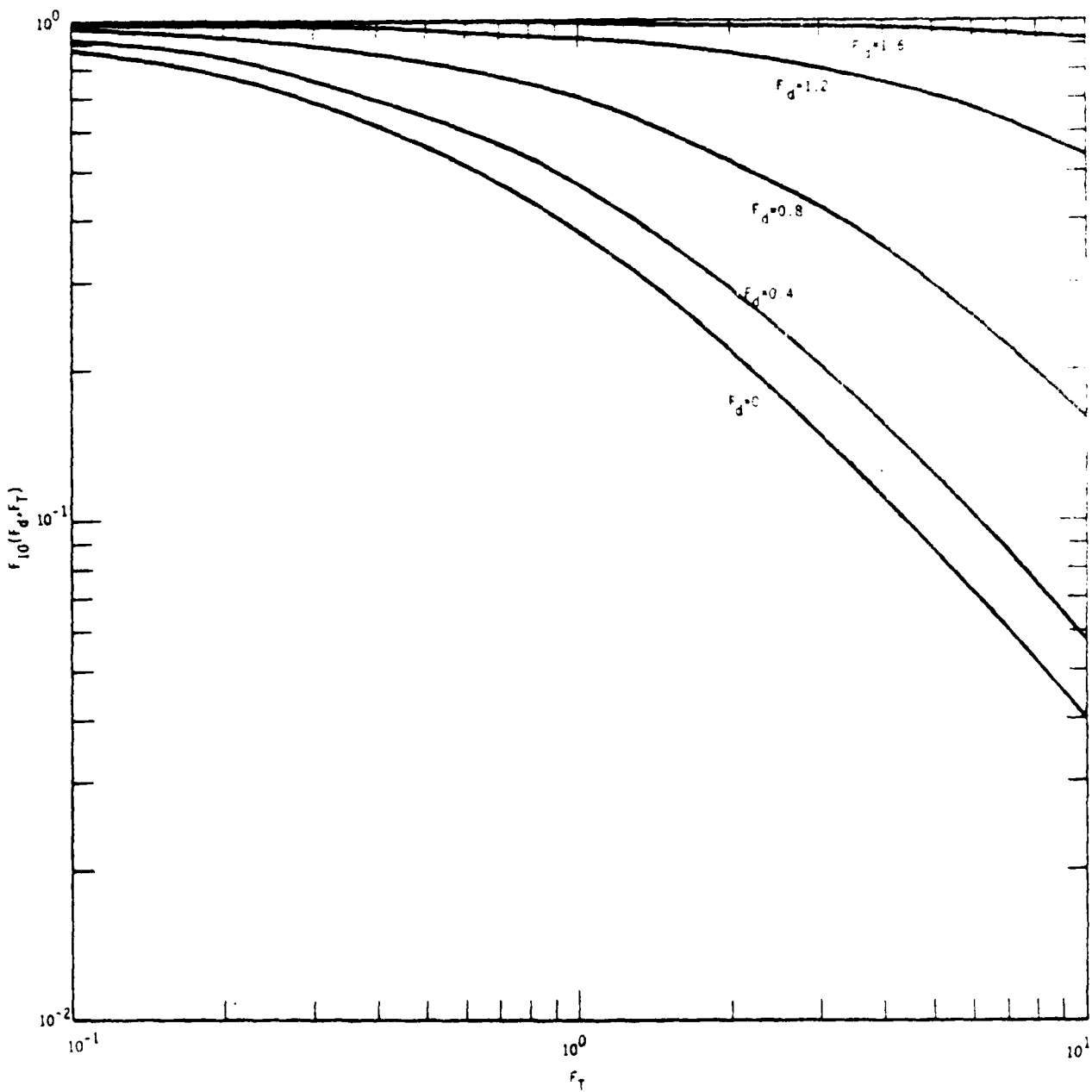
Figure 31. Values of F_{10} (ratio of I_1 to I_0).
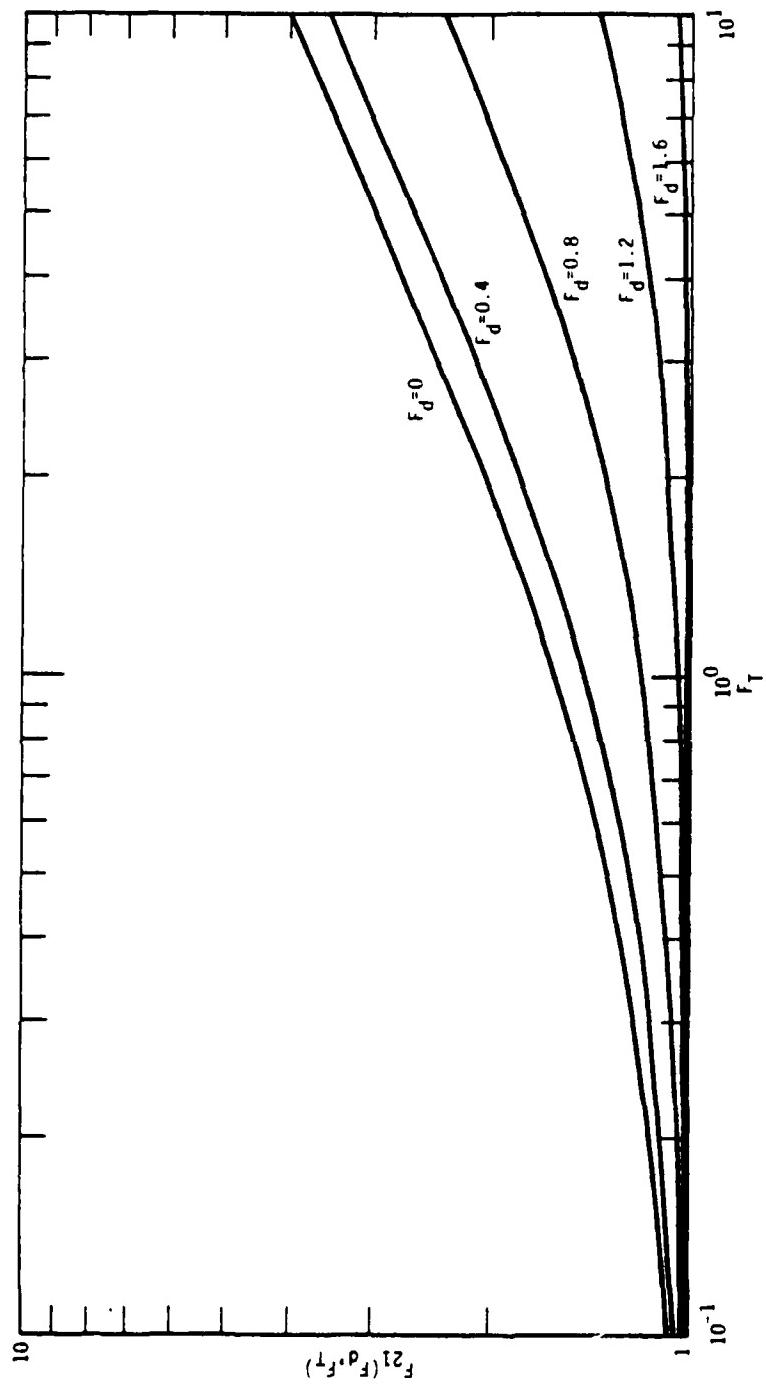
Figure 32. Values of F_{21} (ratio of I_2 to I_1).

63

From Figures 31 and 32 we find

$$F_{10}(0.5, \ 3.47) = 0.21$$

$$F_{21}(0.5, \ 3.47) = 2.20 \quad .$$

Using Equations 44 and 45

$$I_1(0.5, \ 3.47) = 0.17$$

$$I_2(0.5, \ 3.47) = 0.38 \quad .$$

Using Equations 41 and 42

$$\theta_y = 0.30 \quad \text{millirad}$$

$$\theta_z = 0.12 \quad \text{millirad} \quad .$$

TURBULENT PROPAGATION EFFECTS

The turbulence in a hot fire plume causes intense random index of refraction fluctuations which can cause significant effects on the propagation of electro-optical signals. These effects include beam spreading and jitter, loss of coherence, and phase and amplitude scintillations. We first consider the index of refraction fluctuations and then the propagation effects.

Define

$$A = 77.6P \left(1 + \frac{7.52 \times 10^{-3}}{\lambda^2} \right) \times 10^{-6} \quad \text{K} \quad . \tag{46}$$

Then at optical frequencies

$$n-1 = \frac{A}{T} \tag{47}$$

and the variation in the index of refraction

$$dn = d(n-1) = A \left\{ \frac{dP}{PT} + d \left(\frac{1}{T} \right) \right\} \quad . \tag{48}$$

For infinitesimal variations

$$d \left(\frac{1}{T} \right) = -\frac{dT}{T^2} \quad .$$

64

At a point in either the natural atmosphere or a fire plume the pressure fluctuation term is negligible compared to the temperature fluctuation term. The variance of the index of refraction fluctuations is thus

$$\sigma_n^2 = A^2 \, \sigma_{1/T}^2 \tag{49}$$

where $\sigma_{1/T}^2$ is the variance in 1/T fluctuations. For weak (ie, small amplitude) fluctuations

$$\sigma_{1/T}^2 \cong \frac{\sigma_T^2}{T^4} \, K^{-2} \tag{50}$$

where σ_T^2 is the variance of the temperature fluctuations.

First consider a point in the natural atmosphere. Turbulence will cause air parcels originally from both higher and lower altitudes to pass by the point. The temperature of an air parcel at the point depends on the mean temperature of the air at the altitude the parcel originated and the change in temperature due to adiabatic expansion or contraction in moving from one altitude to another. Near sea level the adiabatic lapse rate is -9.8×10^{-3} K per meter. The temperature fluctuations are small so that

$$\sigma_n^2 = \frac{A^2}{T^4} \, \sigma_T^2 \quad . \tag{51}$$

For a sea level pressure of 1013.2 millibars and ambient temperature of 288 K at optical frequencies

$$\sigma_n^2 = 9 \times 10^{-13} \, \sigma_T^2 \quad .$$

In the atmosphere the temperature variance associated with strong turbulence can be of the order of a $(\text{degree})^2$ so that the index of refraction variance can be of the order of 10^{-12}.

Next consider a point in the fire plume. The temperature fluctuations in the hot plume can be several orders of magnitude larger than the ambient temperature fluctuations. Hence the turbulent index of refraction variances can be four orders of magnitude larger than the

ambient variances. Let $\overline{T}$ be the mean temperature of the plume at a point, and σ_T^2 the variance of the temperature fluctuations about the mean. Then for

$$\frac{\overline{T} - T_a}{\overline{T}} \lesssim \frac{1}{4}$$

where T_a is the ambient temperature, we can use the small fluctuation approximation

$$\sigma_n^2 \cong \frac{A^2 \sigma_T^2}{\overline{T}^4} \quad .$$

But for larger temperature variations we cannot use the approximation but must use the full variance equation

$$\sigma_n^2 = A^2 \sigma_{1/T}^2 \quad .$$

The temperature fluctuation probability distribution is required in order to solve the full variance equation. In well developed weakly buoyant plume flows the temperature fluctuations are approximately Gaussian distributed. In the general plume flow the probability distributions are not known. We will consider the Gaussian and several limiting general flow distributions. We first consider the Gaussian. Assume the temperature at a point in the plume has the probability distribution

$$f(T) = \frac{a}{\sqrt{2\pi}\,\sigma_G}\, e^{-\frac{1}{2}\left(\frac{T - \overline{T}}{\sigma_G}\right)^2} \qquad T_a \le T \le 2\overline{T} - T_a \qquad (54)$$

where

a = normalization constant which ensures that

$$\int_{T_a}^{2\overline{T} - T_a} f(T)dT = 1$$

σ_G = truncated Gaussian parameter related to the temperature standard deviation (K).

The temperature distribution chosen is a truncated Gaussian. The lower limit of the temperature range is taken as the natural limit of the

ambient temperature. The upper limit of the temperature range was chosen so as to have a symmetrical probability distribution about the mean. The upper limit is the same number of standard deviations above the mean as the lower limit is below.

The cumulative distribution of the normal random probability function is defined as

$$C_o(x) = \frac{1}{\sqrt{2\pi}} \int_{-\infty}^{x} e^{-\frac{1}{2} t^2} dt \quad . \tag{55}$$

Values of $C_o(x)$ are available in mathematical handbooks; we also have a computer routine for $C_o(x)$. In terms of $C_o(x)$, the normalization constant a is

$$a = \frac{1}{1 - 2 C_o\left(- \dfrac{\overline{T} - T_a}{\sigma_G}\right)} \quad . \tag{56}$$

The temperature variance is by definition

$$\sigma_T^2 = \overline{(T^2)} - (\overline{T})^2$$

$$= \int_{T_a}^{2\,\overline{T} - T_a} T^2 \, f(T)dt - (\overline{T})^2 \, K^2 \quad .$$

Carrying out the integration we have the relationship between the temperature variance and the truncated Gaussian parameter σ_G^2

$$\sigma_T^2 = \sigma_G^2 \left\{ 1 - \frac{2a}{\sqrt{2\pi}} \left(\frac{\overline{T} - T_a}{\sigma_G}\right) e^{-\frac{1}{2}\left(\frac{\overline{T} - T_a}{\sigma_G}\right)^2} \right\} K^2 \quad . \tag{57}$$

The defining equations of $\sigma_{1/T}^2$ are

$$\sigma_{1/T}^2 = \overline{\left(\frac{1}{T^2}\right)} - \left(\overline{\frac{1}{T}}\right)^2 K^{-2} \tag{58}$$

67

where

$$\overline{\left(\frac{1}{T}\right)} = \int_{T_a}^{2\,\overline{T}-T_a} \frac{f(T)}{T}\, dT \quad K^{-1} \tag{59}$$

$$\overline{\left(\frac{1}{T^2}\right)} = \int_{T_a}^{2\,\overline{T}-T_a} \frac{f(T)}{T^2}\, dT \quad K^{-2} \quad . \tag{}$$

Equations 59 and 60 have to be evaluated numerically. We have written a computer routine which for inputs $\overline{T}$, T_a, σ_T computes $\sigma^2_{1/T}$ using Equations 55 through 60. σ^2_n is then found using Equation 43.

In the experimental measurements of Reference 12 of the temperature fluctuations in a well developed, weakly buoyant plume flow it was found that on the plume centerline

$$\sigma_T \approx 0.4(\overline{T} - T_a) \quad . \tag{}$$

Figure 33 shows the index of refraction variance for this assumed temperature variance. Also shown is the variance calculated using the small fluctuation approximation, Equation 52. The simple approximation equation can be used for excess temperatures below about 100 K; at higher temperatures the full equations must be used. We see that the index of refraction variance first increases as the plume temperature increases, reaches a peak, and then declines as the temperature increases still further. The decline with increasing temperature is caused by the inverse temperature dependence of the index of refraction. The peak is some three orders of magnitude above the typical values encountered in strong turbulence in the atmosphere. Note that in a plume, the mean temperature is a maximum at the plume centerline and decreases radially to the ambient temperature. Hence even in a very high temperature plume there will be a portion of the plume at the temperature of the maximum index of refraction variations.
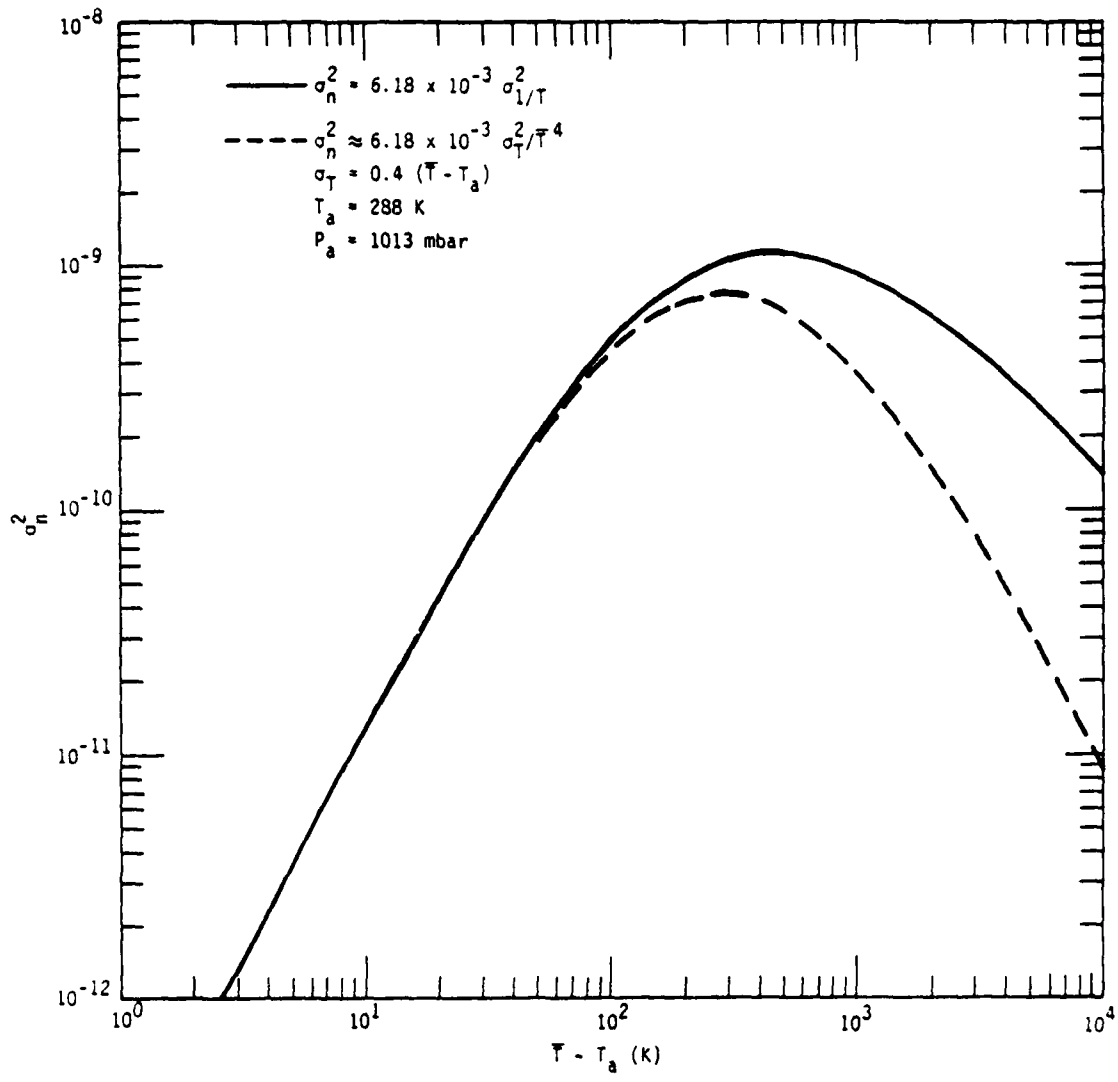
Figure 33. Index of refraction variance as a function of excess plume temperature for Gaussian temperature fluctuations.

The relationship between σ_T and mean excess plume temperature given in Equation 61 is for well developed, weakly buoyant plume flow. We can assume that the initial hot plume air and the subsequently entrained cool ambient air are relatively well mixed. The experimentally measured Gaussian type temperature distributions at a point confirm the well mixed assumption. But there are circumstances where we do not expect well mixed flows. In the weakly buoyant phase the turbulence is expected to be of the dissipative type. In the low-altitude, strongly buoyant regimes the flow is primarily convective. Until the convective flow decays into a dissipative flow, mixing may not be well developed. Also interactions of the ambient turbulent flow fields may disrupt the smooth mean flow fields of our ideal noninteracting plume model. A likely result of the disruptions is the introduction of volumes of ambient air into the plume flow, or the breakup of the plume resulting in volumes of the plume air being introduced into the ambient flow fields. The disruptions will produce volume elements that are not well mixed.

Flows which are not well mixed will have *relatively large temperature fluctuations* about the mean temperature. The temperature fluctuation probability distribution will no longer be of the Gaussian type. Gaussian-like distributions are characteristic of relatively small temperature fluctuations, that is, relatively well mixed flows. For the symmetric truncated Gaussian the maximum standard deviation (square root of the variance) possible is

$$\sigma_T \leq \frac{\overline{T} - T_a}{\sqrt{3}} = 0.58(\overline{T} - T_a) \qquad T_a \leq T \leq 2\overline{T} - T_a \quad .$$

Even if the upper temperature limit is allowed to extend to infinity so we have an asymmetric truncated (one side) Gaussian distribution, the maximum standard deviation is only

$$\sigma_T \leq \sqrt{\frac{\pi}{2} - 1}\ (\overline{T} - T_a) = 0.76(\overline{T} - T_a) \qquad T_a \leq T \leq \infty \quad .$$

70

We begin our study of non-well mixed flows by examining the limiting case of completely nonmixed temperature elements.

Consider the following simple limiting case. In the vicinity of a point let the plume air consist of discrete volumes of air. The discrete volumes are at either the ambient temperature T_a or some higher temperature T_2. Let f_a be the fraction of the total volume which is at temperature T_a. Obviously the fraction of the volume at T_2 is $1 - f_a$. The mean (volumetric) temperature for this simple discrete bimodal temperature distribution is

$$\overline{T} = f_a T_a + (1 - f_a)T_2 \quad K \tag{62}$$

and the variance is

$$\sigma_T^2 = \overline{T^2} - (\overline{T})^2$$

$$= f_a T_a^2 + (1 - f_a)T_2^2 - (\overline{T})^2$$

$$= f_a(1 - f_a)(T_2 - T_a)^2$$

$$= (T_2 - \overline{T})(\overline{T} - T_a) \quad . \tag{63}$$

For discrete volume elements the index of refraction variance becomes

$$\sigma_n^2 = \overline{(n^2)} - [\overline{n}]^2$$

$$= n_a^2 f_a + n_2^2(1 - f_a) - [n_a f_a + n_2(1 - f_a)]^2$$

$$= \frac{A^2(T_2 - \overline{T})(\overline{T} - T_a)}{(T_a T_2)^2} = \frac{A^2 \sigma_T^2}{(T_a T_2)^2} \tag{64}$$

where

n_a = index of refraction of air at temperature T_a

   = A/T_a

n_2 = index of refraction of air at temperature T_2

   = A/T_2.

$\overline{T}$ is the mean temperature for discrete volume elements. If the volume elements were uniformly mixed the mean temperature of the uniformly mixed volume would become

$$T_u = f_{am}T_a + (1 - f_{am})T_a$$

$$= \frac{T_a T_2}{f_a T_2 + (1 - f_a)T_a} \tag{65}$$

where f_{am} is the fraction of the total mass which is at temperature T_a. In deriving the second part of Equation 65, we used the pressure equilibrium assumption

$$\rho_a T_a = \rho_2 T_2 = \rho_u T_u \tag{66}$$

where ρ_a and ρ_2 are the densities in the volume elements before mixing and ρ_u is the density of the uniformly mixed volume.
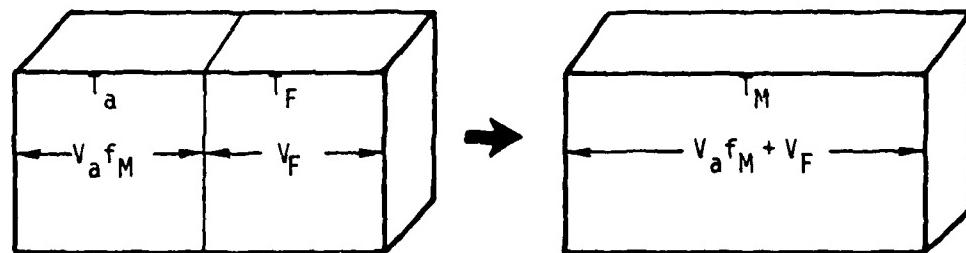
Next let us consider a very simple model for the non-well mixed regions of the fire plume and evaluate the index of refraction fluctuations. We assume that initially at the base of the plume the plume air consists entirely of hot air at temperature T_F. As the initial hot air rises, cold ambient air of temperature T_a is entrained into the plume. We assume that a fraction f_M of the entrained air is uniformly mixed with the initial hot plume air, resulting in a mixture with intermediate temperature T_M. The rest of the entrained air, of fraction $(1 - f_M)$, remains at the ambient temperature T_a. The temperature distribution is thus discrete bimodal, one temperature being T_a, the second T_M. The mixing fraction f_M is a rough measure of how well mixed the flow is. Figure 34 shows a simple diagram of the mixing model.

The volume fractions in this mixing model are
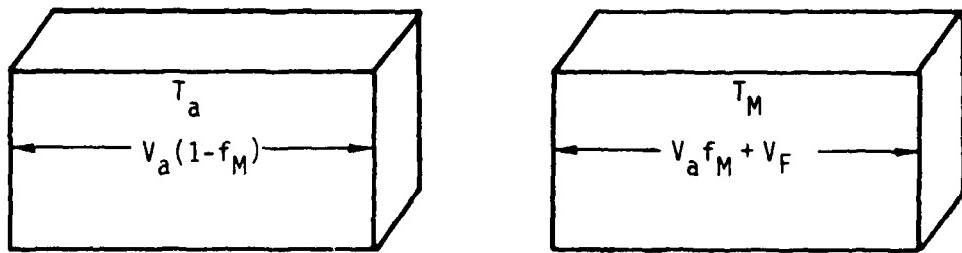
f_{ab} = total volume fraction of ambient air before mixing

$1 - f_{ab}$ = volume fraction of initial hot plume air

$f_{a\ell} = (1 - f_M)f_{ab}$ = volume fraction of air left at ambient temperature after mixing
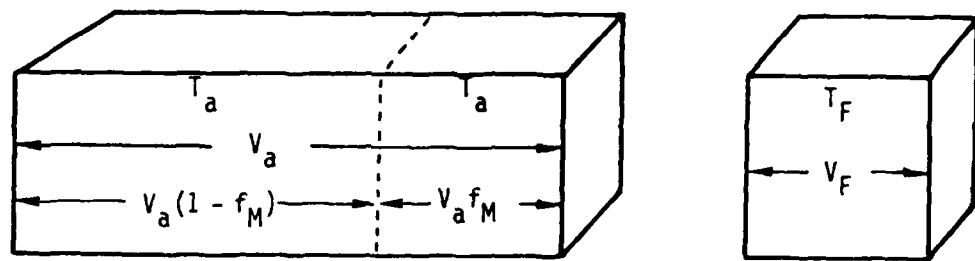
(a) Before mixing $f_{ab} = \dfrac{V_a}{V_a + V_F}$

(b) Mixing of ambient and hot plume air

(c) After mixing $f_{a\ell} = \dfrac{V_a(1 - f_M)}{V_a + V_F}$

Figure 34. Diagram of discrete bimodal mixing model.

73

$$f_{ax} = f_M f_{ab} = \text{volume fraction of ambient air mixed with}$$
$$\text{initial plume air.}$$

The temperature of the uniformly mixed plume and ambient air is found by applying Equation 65 with

$$f_a = \frac{f_{ax}}{f_{ax} + (1 - f_{ab})}$$

$$T_2 = T_F$$

$$T_u = T_M \quad .$$

The result is

$$T_M = \frac{T_a T_F [1 - f_{a\ell}]}{T_F f_{ax} + T_a (1 - f_{ab})} \quad K \qquad (67)$$

The mean temperature of the discrete bimodal volume distribution after mixing is found by applying Equation 62 with

$$f_a = f_{a\ell}$$

$$T_2 = T_M$$

which gives

$$\overline{T} = T_a f_{a\ell} + T_M (1 - f_{a\ell}) \quad . \tag{68}$$

Applying Equations 63 and 64 we have for the temperature and index of refraction variances after mixing

$$\sigma_T^2 = (T_M - \overline{T})(\overline{T} - T_a) \quad K^2 \tag{69}$$

$$\sigma_n^2 = \frac{A^2 (T_M - \overline{T})(\overline{T} - T_a)}{(T_a T_M)^2} = \frac{A^2 \sigma_T^2}{(T_a T_M)^2} \tag{70}$$

Figure 35 shows the index of refraction variances for various values of the mixing fraction f_M. The initial conditions assumed were standard
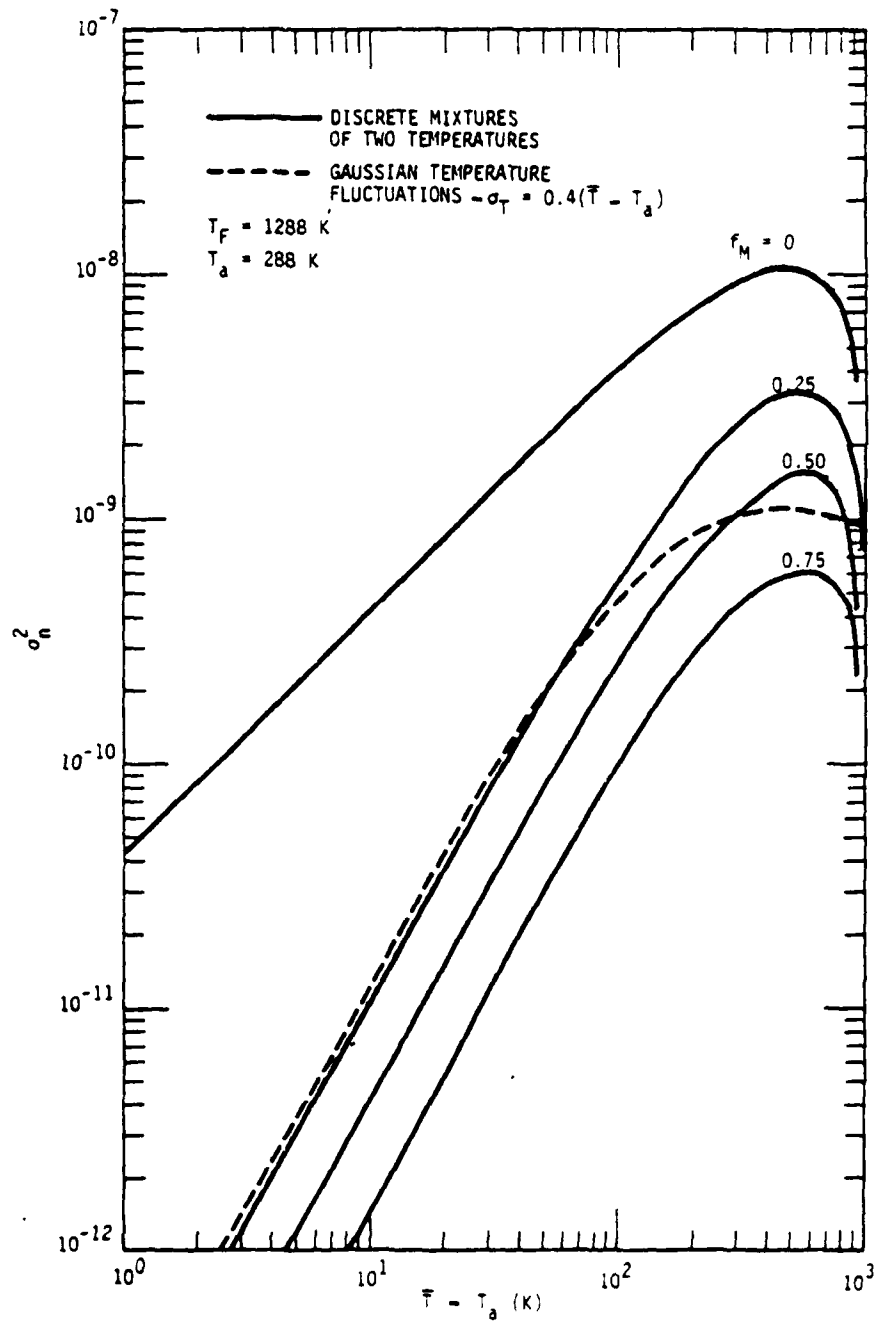
Figure 35.   Index of refraction variances for discrete
bimodal temperature distributions.

75

atmospheric pressure and

$$T_a = 288 \text{ K}$$

$$T_F = 1288 \text{ K} \quad .$$

Also shown for comparison is the index variance for the truncated
Gaussian temperature fluctuation distribution of the well developed
flow with

$$\sigma_T = 0.4(\overline{T} - T_a) \quad .$$

As expected, the variance for the discrete volumes increases as the
mixing of the initial hot plume air decreases. At the peak, the no
mixing case ($f_M = 0$) has a variance an order of magnitude larger than
the well developed flow variance. For excess temperatures below about
100 K, the well developed flow corresponds fairly closely to the $f_M =$
0.25 mixing case. The sharp falloff as the excess temperature approaches
1000 K occurs because in our simple discrete model initially all the
plume air is at temperature T_F with no entrained ambient air. Thus
initially the variance is zero in the discrete model.

PROPAGATION MODELS

We next obtain estimates of the propagation effects on optical
beams due to the turbulence in a fire plume. We consider the propaga-
tion geometry shown in Figure 36. A laser beam of initial diameter D
passes through a plume whose centerline is halfway between the laser
and the screen. As before the propagation path is horizontal and the
point of closest approach of the beam centerline to the plume center-
line is specified by the impact parameter distance d. On that part of
the propagation path outside the plume, the beam is propagating in the
ambient atmospheric turbulence. As shown in the previous subsection
the strength of the index of refraction fluctuations in the ambient
atmosphere is expected to be several orders of magnitude below the
plume fluctuations. For relatively short path lengths ($\sim$ 1000 m or

76
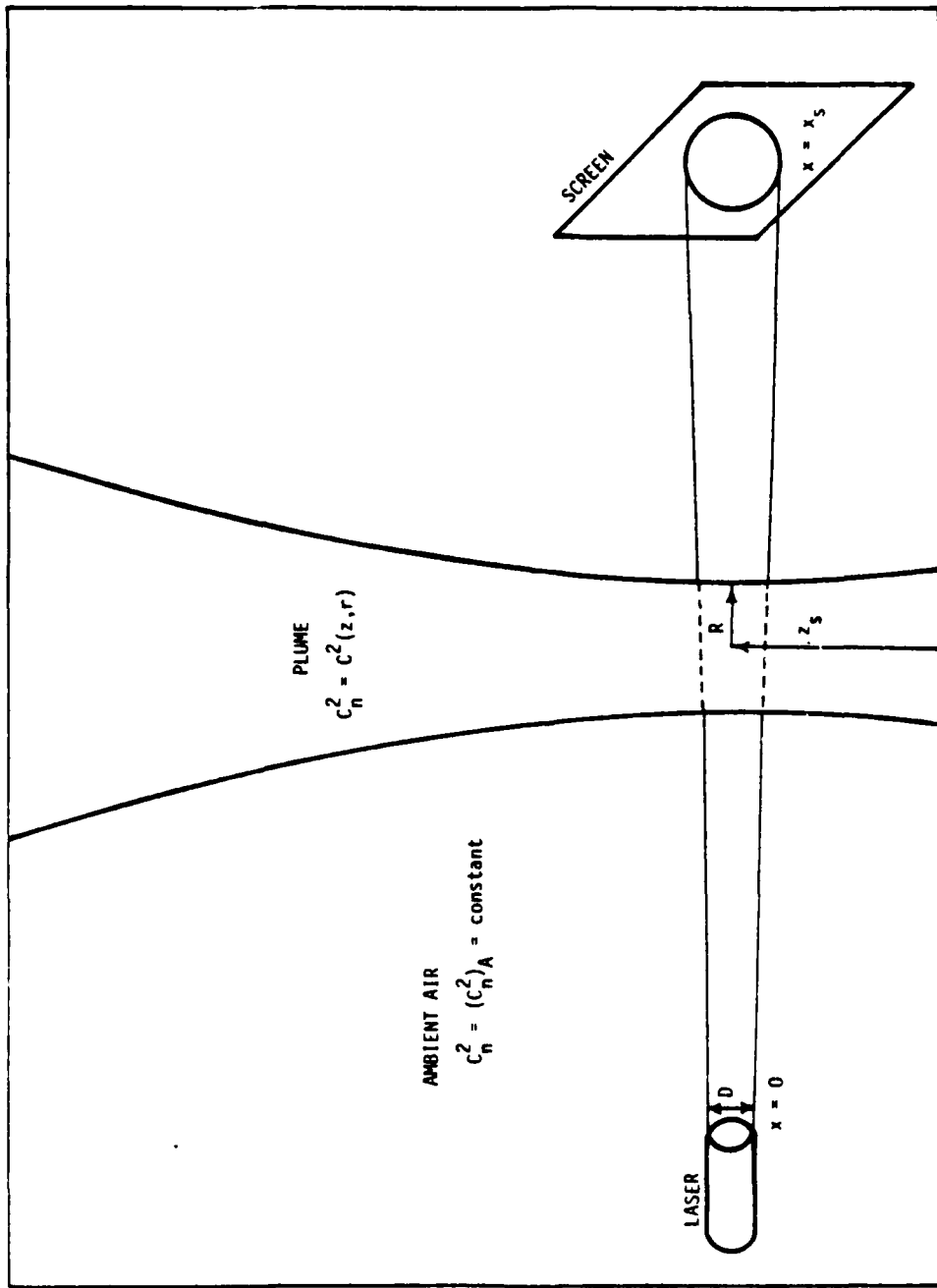
Figure 36. Laser beam propagation geometry.

less) we expect the plume turbulence effects to completely dominate the atmospheric turbulence effects.

The plume turbulent parameters required for propagation calculations are the magnitude and spectrum of the index of refraction fluctuations σ_n^2 is a measure of the magnitude. The spectrum depends upon the char-acteristics of the plume flow. In fully developed turbulence of the dissipative type, the spectrum of the velocity fluctuations is known to be Kolmogorov. The ambient atmospheric turbulence is generally Kolmogorov. A conservative passive additive is a quantity which is carried along by the turbulent velocity flow fields and which does not influence the flow. The additive fluctuations assume the same spectrum as the velocity spectrum. In the ambient atmosphere the potential temperature is a conservative passive additive. Thus the ambient atmospheric temperature fluctuations are also Kolmogorov. Since in the ambient atmosphere the index of refraction fluctuations are pro-portional to the temperature fluctuations (Equation 51), the normal atmospheric index of refraction fluctuations are also Kolmogorov.

In a fire plume the initial flow is convective, decaying into a dissipative flow. The velocity fluctuations in the dissipative regime are expected to be essentially Kolmogorov. Although the plume tempera-ture is not a passive additive since the plume flow is driven by the buoyancy, the temperature fluctuations are also expected to be essentially Kolmogorov in the dissipative regime. As we have seen, the index of refraction fluctuations at high temperatures are not directly propor-tional to the temperature fluctuations (see Equation 53). Thus the index of refraction fluctuation spectrum will be a somewhat modified version of the temperature spectrum. However since we do not know the temperature spectrum, we will make the simplifying assumption that in the dissipative flow regime of the plume the index of refraction fluct-uations have a Kolmogorov spectrum. Since we also do not know the spectrum in the convective region, we will make the further simplifying assumption that the spectrum is Kolmogorov everywhere. This assumption simplifies the propagation calculations. We will make estimates of the

78

magnitude of the fluctuations depending on whether the flow is convective or dissipative, but we will use the same spectral shape (Kolmogorov) in both flow regimes.

There are three characteristic size regimes associated with the turbulent eddies. According to the Kolmogorov theory, these regimes can be characterized by two size scales: the outer scale of turbulence, L_o, and the inner scale (also called microscale) of turbulence, ℓ_o. The first size regime is called the input range and here

$$\text{eddy size} > L_o \quad .$$

It is in this regime that the energy is extracted from the mean flows and converted to turbulent energy. The spectrum in this range depends on the particular flow characteristics and no general formulas exist. The spectrum is normally anisotropic in the input range. The second size regime is called the inertial subrange, and here

$$\ell_o < \text{eddy size} < L_o \quad .$$

This is the eddy cascade range. The large eddies break up into smaller eddies, which in turn further subdivide into still smaller eddies, and so on. As the subdivision continues, any initial anisotropy is lost and the turbulence is essentially isotropic in this range. The inertial subrange is essentially energy conserving; the energy loss due to viscosity dissipation is negligible compared to the kinetic energy of an eddy. Kolmogorov considered the physical characteristics of fully developed turbulence in the inertial subrange and deduced that the spectrum was proportional to $K^{-11/3}$ where

$$K = \text{eddy wavenumber } (m^{-1})$$

$$= \frac{2\pi}{\text{eddy size}} \quad .$$

The third size regime is the dissipation range and here

$$\text{eddy size} < \ell_o \quad .$$

79

When the subdividing eddies reach a size of the smallness of the inner scale, the dissipation of the eddy kinetic energy due to viscosity effects begins to dominate. The eddy no longer subdivides and ceases to exist as an entity as the viscosity converts the eddy kinetic energy into random heat energy. The spectrum rapidly drops to zero in this size range.

For mathematical convenience the three regimes are often combined in one spectral formula, usually called the modified von Karman spectrum

$$\phi_n(K) = 0.033 \ C_n^2 \left(K^2 + \frac{1}{L_o^2}\right)^{-11/6} \exp\left(- \frac{K^2}{K_m^2}\right) \tag{71}$$

where

ϕ_n = spectrum of index of refraction fluctuations

C_n^2 = structure constant of index of refraction fluctuations $(m^{-2/3})$

$K_m = 5.92/\ell_o \ (m^{-1})$.

Figure 37 shows a sketch of the spectrum. The input range is shown dotted; although Equation 71 mathematically covers the input range, the expression must be considered only an approximation since the actual spectrum depends on the flow characteristics and is generally unknown.

The strength of the turbulence is specified by the magnitude of the structure constant, C_n^2. In the ambient atmosphere C_n^2 varies from about $10^{-18} \ m^{-2/3}$ for weak turbulence to $10^{-13} \ m^{-2/3}$ for strong turbulence. For the Kolmogorov spectrum, the relation between the structure constant and the previously considered index of refraction variance, σ_n^2, is (References 13 and 14)

$$C_n^2 = \frac{1.91 \ \sigma_n^2}{L_o^{2/3}} \quad m^{-2/3} \quad . \tag{72}$$

We will use two different methods to compute the structure constant in the fire plume. In the first method we utilize the experimental measurements of Reference 10 and assume

80
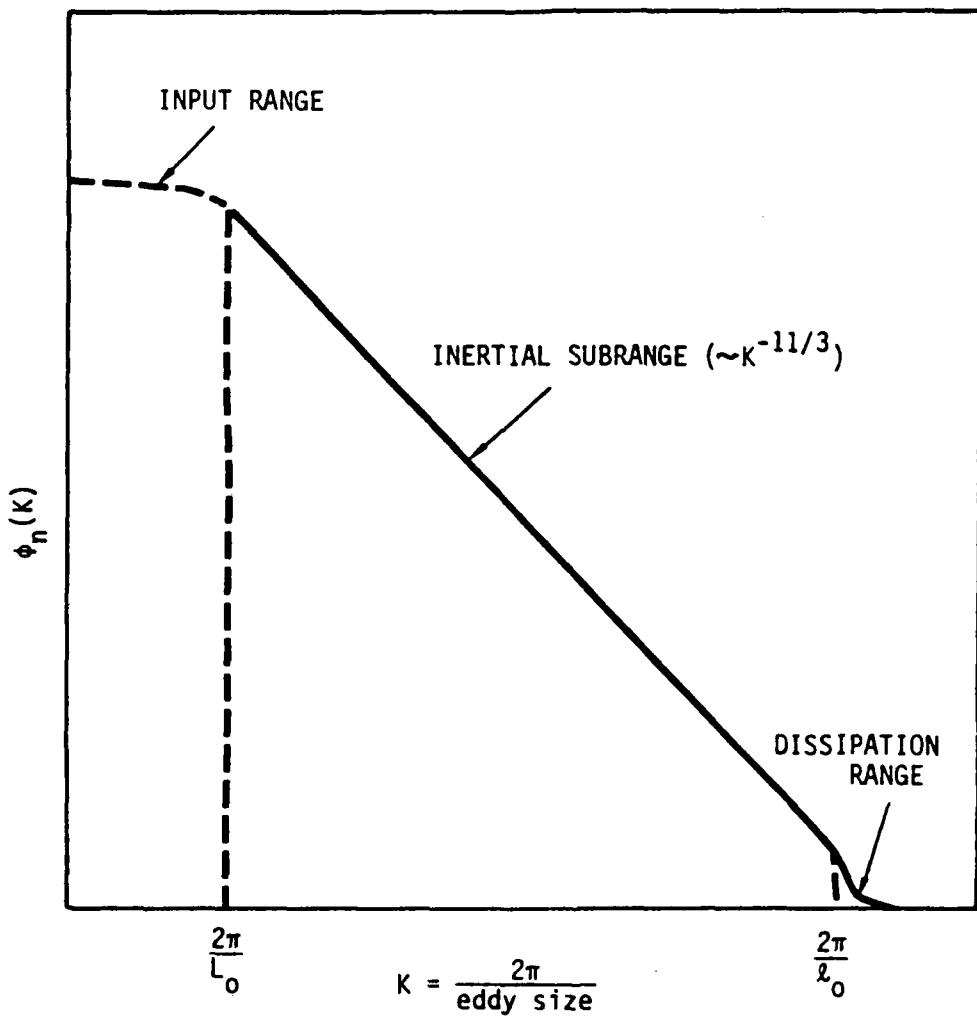
Figure 37. Kolmogorov index of refraction fluctuation spectrum.

$$\sigma_T(r) = 0.4(T(r) - T_a) \quad K \quad . \tag{73}$$

We then use the results of the previous subsection to calculate $\sigma_n^2(r)$ and then use Equation 72 to calculate $C_n^2(r)$. This method is appropriate to well mixed, well developed turbulence. We would expect this formalism to apply after the initial convective plume flow has decayed away and the flow has become dissipative (ie, Kolmogorov). This should apply in the higher altitude, weakly buoyant regions of the plume, provided there are no intermittency effects due to ambient turbulence interactions.

81

In the second method of calculating C_n^2, we relate the strength of the turbulence to the gradients of the mean plume parameters. Assuming the temperature is also essentially Kolmogorov in spectrum, we have an equation analogous to 72 for temperature

$$C_T^2 = \frac{1.91 \ \sigma_T^2}{L_o^{2/3}} \quad K^2 \ m^{-2/3} \qquad (74)$$

where C_T^2 is the structure constant for the temperature. The temperature structure constant for Kolmogorov fluctuations can be related to the mean temperature gradients by (References 13 and 11)

$$C_T^2 \cong b \ L_o^{4/3} \ |grad \ T|^2 \quad K^2 \ m^{-2/3} \qquad (75)$$

where T is the mean temperature and b is a constant which depends on the flow type. The exact magnitude of b is not well known. In ambient atmospheric flow b is estimated to be in the range 1.5 to 3.5 (References 14 and 15). Reference 15 recommends a value of 2.8. For non-well mixed plume flows we adopt the value

$$b = 3 \quad . \qquad (76)$$

In this gradient method we will also calculate the structure constant using a second, limiting value of b of

$$b_2 = 0.3 \quad . \qquad (77)$$

We expect this second value to be appropriate to well mixed flows. If we approximate

$$|grad \ T|^2 \approx \frac{\overline{T} - T_a}{L_o}$$

and assume for well mixed flows

$$\sigma_T \approx 0.4 \, (\overline{T} - T_a)$$

where $\overline{T}$ is an average mean temperature over the plume cross section, then using Equations 74 and 75 we find

$$b_2 \approx 1.91 \times (0.4)^2 = 0.3 \quad .$$

Combining Equations 74 and 75 we have in the general case

$$\sigma_T^2(r,z) = \frac{b \ L_o^2 |\text{grad } T(r,z)|^2}{1.91} \ K^2 \quad . \tag{78}$$

For the plume

$$|\text{grad } T(r,z)|^2 = \left(\frac{\partial T(r,z)}{\partial r}\right)^2 + \left(\frac{\partial T(r,z)}{\partial z}\right)^2 \tag{79}$$

and the radial and vertical gradients at a point are found from the plume model of Section 2. L_o is the outer scale of plume turbulence, the length of the temperature gradient region. For plumes

$$L_o \approx R \quad m \quad . \tag{80}$$

In this second method we assume non-well mixed flows and use Equations 69 and 70 to convert from the σ_T^2 of Equation 78 to σ_n^2. Equation 72 then gives C_n^2.

With C_n^2 defined, we next develop the propagation formulas. A primary measure of turbulence effects is the coherence length. The coherence length of a spherical wave after propagation from the screen to the laser is (References 15 and 16)

$$\rho_o = \left[1.46 \ k^2 x_s \int_0^1 d\xi (1 - \xi)^{5/3} \ C_n^2(\xi x_s)\right]^{-3/5} \quad m \tag{81}$$

where

ρ_o = coherence length (m)

x = distance from laser (m)

x_s = total distance from laser to screen (m)

k = $2\pi/\lambda_m$ (m^{-1})

λ_m = wavelength of laser (m)

$C_n^2(x)$ = structure constant of index of refraction fluctuations at point x $(m^{-2/3})$.

We assume that in the ambient atmosphere the turbulence is constant and equal to

$$(C_n^2)_A = \text{constant} = 10^{-14} \quad m^{-2/3} \quad ,$$

a value representative of relatively strong ambient turbulence. The ambient turbulence effects are generally negligible compared to the plume turbulence effects for relatively short path lengths (≤ 1000 m). We have written a computer program to solve Equation 81 for the Gaussian plume of Section 2. Far from the plume $C_n^2(x)$ is the atmospheric value; inside $C_n^2(x)$ is the plume value; at the fringes of the plume we take $C_n^2(x)$ as the maximum of the atmospheric or plume values.

Next consider the size and location of the beam spot size on the screen. The effect of turbulence will cause the beam to spread (in addition to the vacuum spread) and to move about from place to place on the screen (to "jitter"). Figure 38 shows a schematic of the spot geometry at the screen. At the screen the instantaneous spot, of average radius ρ_s, jitters from place to place on the screen with a time constant of the order of D/v, where D is the beam diameter and v is the rise velocity of the plume. The average distance of the centroid of the instantaneous spot from the center of the screen is ρ_c. For a long exposure time (average over many locations of the instantaneous spot) the average radius of the smeared spot is ρ_L.

First consider the propagation of the laser beam in free space. At the aperture ($x = 0$) we assume the amplitude distribution is Gaussian with a beam size (radius) of $D/2$ and the phase distribution is parabolic with a radius of curvature $-F_0$. This phase distribution will produce a beam focused at $x=F_0$. The free space beam radius, ρ_D, at the screen distance x_s from the laser is

$$\rho_D^2 = \frac{4x_s^2}{k^2 D^2} + \frac{D^2}{4}\left(1 - \frac{x_s}{F_0}\right)^2 \quad m \quad . \tag{82}$$

This is the diffraction limited behavior of a perfect laser beam. In our calculations we consider a collimated beam for which $F_0 = \infty$.
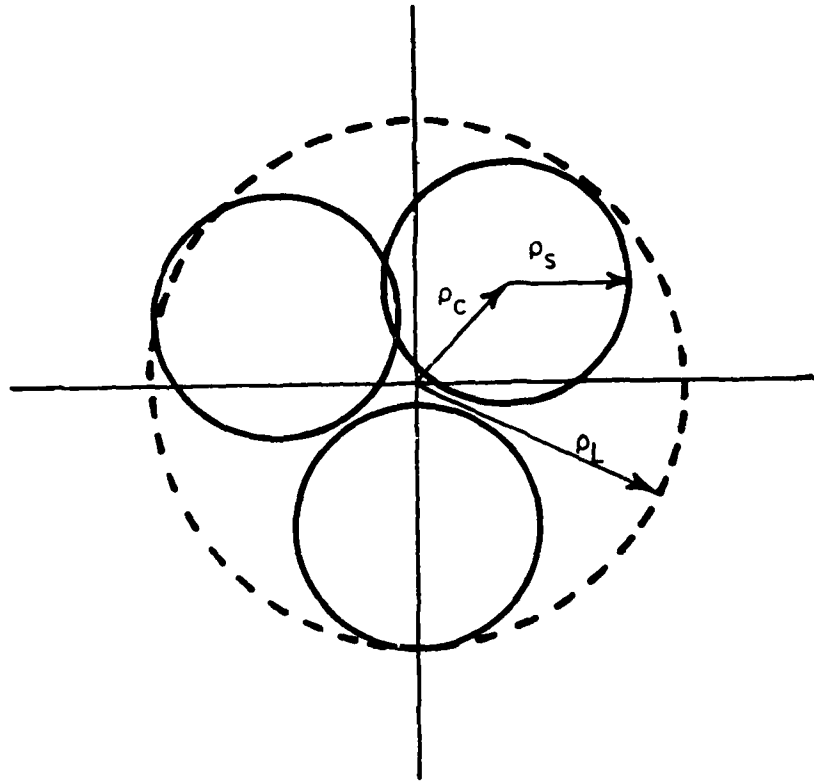
Figure 38. Spot geometry at screen.

The mean square of the long-term beam radius is usually defined by (Reference 16)

$$\left\langle \rho_L^2 \right\rangle = \frac{\displaystyle\iint_{-\infty}^{\infty} d^2\rho \ \rho^2 \Gamma_2(x_s,\vec{\rho},\vec{\rho})}{\displaystyle\iint_{-\infty}^{\infty} d^2\rho \ \Gamma_2(x_s,\vec{\rho},\vec{\rho})} \qquad m^2 \qquad (83)$$

where

$\vec{\rho}$ = radial vector lying in the plane of the screen (m)

85

$\Gamma_2(x,\vec{\rho}_1,\vec{\rho}_2)$ = second moment of the electric field

$$= \left\langle u(x,\vec{\rho}_1)u^*(x,\vec{\rho}_2)\right\rangle$$

u = electric field amplitude

$\langle\ \rangle$ indicates ensemble average.

Γ_2 is commonly called the mutual coherence function. For the Kolmogorov spectrum (Reference 16)

$$\left\langle\rho_L^2\right\rangle = \begin{cases} \rho_D^2 + \dfrac{4x_s^2}{k^2\rho_o^2} & 2R \ll x_L \\[20pt] \rho_D^2 + \dfrac{6.6x_s^3}{\ell_o^{1/3}}\displaystyle\int_0^1 d\xi(1-\xi)^2 C_n^2(\xi x_s) & 2R \gg x_L \end{cases}$$

where

$$\ell = [k^2 C_n^2 \ell_o^{5/3}]^{-1} \quad m$$

ℓ_o = inner scale of turbulent fluctuations (m).

In the atmosphere ℓ_o is of the order of a millimeter (10^{-3} m) and we assume this value for our calculations. The actual value of ℓ_o depends upon the rate at which the turbulent energy is being generated and dissipated. The computer routine which evaluates ρ_o, Equation 81, by numerical integration also evaluates the integral in the second part of Equation 84.

The mean square centroid location can be written

$$\left\langle\rho_c^2\right\rangle = \frac{\displaystyle\iint_{-\infty}^{\infty} d^2\rho_1 \iint_{-\infty}^{\infty} d^2\rho_2\ \vec{\rho}_1\cdot\vec{\rho}_2 \Gamma_4(x_s,\vec{\rho}_1,\vec{\rho}_1,\vec{\rho}_2,\vec{\rho}_2)}{\left[\displaystyle\iint_{-\infty}^{\infty} d^2\rho_1\ \Gamma_2(x_s,\vec{\rho}_1,\vec{\rho}_1)\right]^2} \tag{85}$$

where Γ_4 is the fourth moment of the field

$$\Gamma_4(x,\vec{\rho}_1,\vec{\rho}_2,\vec{\rho}_3,\vec{\rho}_4) = \left\langle u(x,\vec{\rho}_1)u^*(x,\vec{\rho}_2)u(x,\vec{\rho}_3)u^*(x,\vec{\rho}_4)\right\rangle \quad .$$

With $\left\langle\rho_L^2\right\rangle$ and $\left\langle\rho_c^2\right\rangle$ defined, the definition of $\left\langle\rho_s^2\right\rangle$ follows from the relation

$$\left\langle \rho_L^2 \right\rangle = \left\langle \rho_c^2 \right\rangle + \left\langle \rho_s^2 \right\rangle \quad . \tag{86}$$

A rigorous solution exists for the second moment Γ_2, so $\left\langle \rho_L^2 \right\rangle$ can be calculated directly. Unfortunately there is no rigorous solution for the fourth moment Γ_4, so $\left\langle \rho_c^2 \right\rangle$ and $\left\langle \rho_s^2 \right\rangle$ cannot be calculated directly. However, there are a number of approximations available for Γ_4, $\left\langle \rho_c^2 \right\rangle$, and $\left\langle \rho_s^2 \right\rangle$. We adopt the approximations given by Fante in Reference 16. Fante presents a number of separate cases depending on the strength of the turbulence and the path length. Define

$$x_{\rho D} = \text{minimum}[k\rho_D^2, kD^2] \quad m \quad .$$

Case 1:

$$\rho_o \ll D < L_o \text{ and } x_s \lesssim x_{\rho D} \quad .$$

Then approximately

$$\left\langle \rho_s^2 \right\rangle \approx \rho_D^2 + \frac{4x_s^2}{k^2\rho_o^2}\left[1 - 0.62\left(\frac{\rho_o}{D}\right)^{1/3}\right]^{6/5} \quad m^2 \tag{87}$$

$$\left\langle \rho_c^2 \right\rangle \approx \frac{2.97x_s^2}{k^2\rho_o^{5/3}D^{1/3}} \quad m^2 \quad . \tag{88}$$

For Case 1 we use Equation 86 to calculate $\left\langle \rho_L^2 \right\rangle$ instead of Equation 84. Case 2:

$$\rho_o \sim D \text{ and } x_s \lesssim x_{\rho D} \quad .$$

For this case there are no simple analytic expressions. Define

$$\beta^2 = \left(\frac{kD^2}{4x_s}\right)^2\left(1 - \frac{x_s}{F_o}\right)^2 \tag{89}$$

$$\mu = \left[\frac{\left\langle \rho_s^2 \right\rangle}{\left\langle \rho_L^2 \right\rangle}\right]^{1/2} \quad . \tag{90}$$

Then $\left\langle \rho_s^2 \right\rangle$ can be obtained from the numerical results plotted in Figure 39. Knowing $\left\langle \rho_L^2 \right\rangle$ and $\left\langle \rho_s^2 \right\rangle$, $\left\langle \rho_c^2 \right\rangle$ follows immediately from Equation 86.
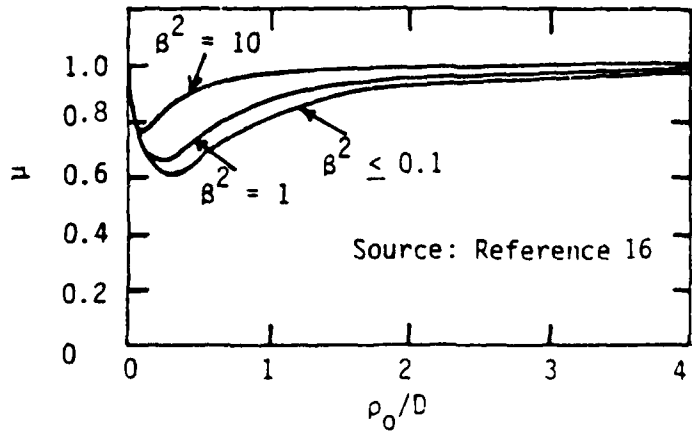
Figure 39. Ratio of the short- to long-term-averaged beam spread.

Case 3:

$$\rho_o \gg D \text{ and } x_s \lesssim x_{\rho D} \quad .$$

For this case there is very little beam jitter and

$$\left\langle \rho_s^2 \right\rangle \approx \left\langle \rho_L^2 \right\rangle$$

$$\left\langle \rho_c^2 \right\rangle \approx 0 \quad .$$

Case 4:

$$x_s \gg x_{\rho D} \quad .$$

Again for this case

$$\left\langle \rho_s^2 \right\rangle \approx \left\langle \rho_L^2 \right\rangle$$

and $\left\langle \rho_c^2 \right\rangle$ can be neglected. However case 3 was for weak turbulence. This case is due to strong turbulence. Here the beam has lost its coherence. The instantaneous picture on the screen no longer consists of a single spot but consists of a multiple number of smaller string-like spots at random locations within the ρ_L radius.

A computer routine has been written to solve these propagation equations. Results of some sample calculations are shown in Tables 3 through 11 and Figures 40 through 43. The tables show propagation results for a

Table 3 Laser beam propagation results for a plume with initial parameters $T_c-T_a=500$ K, $V_c=10$ m s^{-1}, $R=1$ m.

λ (μm)	D (m)	x_s (m)	Mixing Model	ρ_0 (m)	ρ_D (m)	$\sqrt{<\rho^2_L>}$ (m)	$\sqrt{<\rho^2_s>}$ (m)	$\sqrt{<\rho^2_c>}$ (m)
1	1.00E-03	5.00E+01	1	1.51E-03	9.56E-03	1.15E-02	1.04E-02	5.00E-03
			2	6.52E-04	9.56E-03	1.75E-02	1.26E-02	1.21E-02
		1.00E+02	1	1.51E-03	9.56E-03	1.94E-02	1.30E-02	1.49E-02
			2	6.52E-04	7.11E-02	3.85E-02	3.85E-02	0.
		1.00E+03	1	1.51E-03	3.11E-02	5.85E-02	5.83E-02	0.
			2	6.52E-04	3.1AE-01	6.59E-02	6.59E-02	0.
	1.00E-02	5.00E+01	1	1.51E-03	3.1AE-01	5.85E-01	3.84E-01	0.
			2	1.51E-03	3.1AE-01	6.59E-01	6.59E-01	0.
			3	6.52E-04	5.09E-03	A.19E-03	6.45E-03	5.07E-03
		1.00E+02	1	4.59E-04	5.09E-03	1.56E-02	1.33E-02	8.01E-03
			2	1.51E-03	5.09E-03	2.15E-02	1.86E-02	1.07E-02
		1.00E+03	1	6.52E-04	5.93E-03	2.22E-02	1.59E-02	1.55E-02
			2	4.59E-04	5.93E-03	4.95E-02	4.15E-02	2.67E-02
			3	1.51E-03	3.22E-02	2.17E-01	1.45E-01	1.65E-01
			1	6.52E-04	3.22E-02	4.91E-01	4.12E-01	2.67E-01
			2	4.59E-04	5.00E-02	6.96E-01	5.97E-01	3.54E-01
10.6	1.00E-03	5.00E+01	1	2.57E-02	5.00E-02	5.04E-02	5.03E-02	2.71E-03
			2	1.11E-02	5.00E-02	5.71E-02	5.1AE-02	5.44E-03
			3	7.57E-03	5.00E-02	5.45E-02	5.37E-02	7.51E-03
		1.00E+02	1	1.11E-02	5.00E-02	5.45E-02	5.35E-02	9.02E-03
			2	7.80E-03	5.00E-02	4.55E-02	6.75E-02	1.82E-03
			3	2.57E-02	5.01E-02	A.55E-02	8.20E-01	2.44E-02
		1.00E+03	1	7.80E-03	5.01E-02	2.17E-01	1.94E-01	7.04E-02
			2	1.11E-02	5.01E-02	4.91E-01	4.56E-01	1.82E-01
			3	7.80E-03	5.01E-02	6.52E-01	6.52E-01	0.
	1.00E-02	5.00E+01	1	2.57E-02	1.01E-01	1.01E-01	1.01E-01	0.
			2	1.11E-02	1.01E-01	1.02E-01	1.02E-01	0.
			3	7.57E-02	1.01E-01	3.84E-01	3.8AE-01	0.
		1.00E+02	1	2.57E-02	3.37E-01	3.39E-01	3.39E-01	0.
			2	1.11E-02	3.37E-01	3.40E-01	3.40E-01	0.
			3	7.80E-03	3.37E+00	3.38E+00	3.38E+00	0.
	1.00E-01	5.00E+01	1	2.57E-02	3.37E+00	3.39E+00	3.39E+00	0.
			2	7.80E-03	3.37E+00	3.40E+00	3.40E+00	0.
		1.00E+02	1	2.57E-02	1.15E-02	1.20E-02	1.15E-02	3.89E-03
			2	1.11E-02	1.15E-02	1.45E-02	1.25E-02	7.41E-03
			3	7.80E-03	3.41E-02	1.72E-02	1.37E-02	1.04E-02
		1.00E+03	1	2.57E-02	3.41E-02	3.66E-02	3.4AE-02	1.23E-02
			2	1.11E-02	3.41E-02	4.57E-02	3.79E-02	2.55E-02
			3	2.56E-02	5.37E-01	5.51E-02	5.36E-02	3.5CE-02
			1	1.11E-02	3.37E-01	3.62E-01	3.62E-01	0.
			2	2.57E-02	3.37E-01	3.84E-01	3.84E-01	0.
			3	1.11E-02	5.00E-02	5.09E-01	5.09E-01	0.
		3.00E+01	1	2.57E-02	5.00E-02	5.07E-02	4.1AE-01	2.A1E-02
		1.00E+02	1	1.11E-02	5.04E-02	5.17E-02	5.95E-02	3.22E-02
			2	2.57E-02	5.01E-02	5.1AE-02	9.29E-02	7.31E-01
		1.00E+03	1	7.80E-03	5.01E-02	5.A6E-02	9.29E-02	2.72E-02
			2	2.56E-02	6.03E-02	1.A3E-01	6.17E-02	1.01E-01
			1	1.11E-02	6.03E-02	1.10E-01	2.2AE-01	2.1AE-01
			3	7.80E-03	6.03E-02	9.3AE-01	3.65E-01	2.44E-01

Table 4. Laser beam propagation results for a plume with initial parameters
$T_c - T_a = 1000$ K, $V_c = 10$ m s^{-1}, R=1 m.

λ (μm)	D (m)	x_s (m)	Mixing Model	ρ_0 (m)	ρ_D (m)	$J_{v_1}^2$ (m)	$J_{\rho_s}^2$ (m)	$J_{\rho_c}^2$ (m)
1	1.00E-03	5.00E+01	1	1.30E-03	2.56E-03	1.20E-02	1.04E-02	6.07E-03
			2	9.76E-04	9.56E-03	2.22E-02	1.49E-02	1.66E-02
			3	5.98E-04	9.56E-03	2.17E-02	1.37E-02	1.69E-02
		1.00E+02	1	9.76E-04	5.11E-02	4.00E-02	4.00E-02	0.
			2	9.76E-04	5.18E-02	7.91E-02	7.41E-02	0.
			3	5.98E-04	5.18E-02	7.23E-02	9.01E-02	0.
		1.00E+03	1	1.29E-04	5.18E-01	7.91E-01	9.01E-01	0.
			2	9.76E-04	5.18E-01	7.23E-01	7.23E-01	0.
	1.00E-02	5.00E+01	1	1.30E-05	5.09E-03	8.89E-03	6.93E-03	5.56E-03
			2	9.76E-04	5.09E-03	2.00E-02	1.00E-02	1.04E-02
			3	5.98E-04	5.93E-03	2.96E-02	2.14E-02	1.21E-02
		1.00E+02	1	1.30E-03	5.93E-03	6.70E-02	1.77E-02	3.47E-02
			2	9.76E-04	5.95E-03	8.03E-02	9.95E-02	4.02E-02
			3	1.29E-05	3.22E-02	2.45E-01	1.66E-01	1.81E-01
		1.00E+03	1	1.76E-04	3.22E-02	6.72E-01	5.75E-01	3.47E-01
			2	1.29E-05	5.00E-02	8.05E-02	6.94E-01	3.02E-01
	1.00E-01	5.00E+01	1	1.30E-03	5.00E-02	5.05E-02	5.04E-02	7.10E-03
			2	9.76E-04	5.09E-02	5.59E-02	5.34E-02	1.25E-03
		1.00E+02	1	1.30E-05	5.00E-02	5.57E-02	9.01E-02	1.03E-02
			2	9.76E-04	5.00E-02	8.35E-02	9.01E-02	2.36E-02
		1.00E+03	1	1.29E-04	5.01E-02	9.51E-02	2.29E-01	2.74E-02
			2	1.76E-03	5.01E-02	2.51E-01	2.29E-01	1.03E-01
			3	9.98E-04	5.01E-02	6.71E-01	5.55E-01	2.36E-01
10.6	1.00E-03	5.00E+01	1	2.20E-02	1.01E-01	1.01E-01	1.01E-01	2.74E-01
			2	6.77E-01	1.01E-01	1.02E-01	1.02E-01	0.
		1.00E+02	1	2.20E-02	1.51E-01	1.02E-01		0.
			3	8.77E-03	3.37E-01	3.91E-01		0.
		1.00E+03	1	2.00E-01	3.37E-01	3.58E-01	3.38E-01	4.15E-03
			2	2.20E-01	1.57E+00	1.72E+00	3.41E+00	3.91E-03
	1.00E-02	5.00E+01	1	2.20E-01	1.15E-02	1.75E-02	1.34E-02	1.22E-02
			2	6.77E-01	1.15E-02	1.22E-02	1.49E-02	1.94E-02
		1.00E+02	1	2.00E-03	1.15E-01	1.72E-01	1.49E-01	3.15E-02
	1.00E-01	5.00E+01	1	6.77E-01	1.57E-01	1.72E-01	1.73E-01	4.12E-02
		1.00E+02	1	2.04E-02	1.57E-02		1.14E-02	3.10E-02
		1.00E+03	1	2.77E-02	2.04E-02	1.74E-01		2.79E-01

Table 5. Laser beam propagation results for a plume with initial parameters $T_c - T_a = 1500$ K, $V_c = 10$ m s^{-1}, R=1 m.

λ (μm)	U (m)	x_s (m)	Mixing Model	ρ_0 (m)	ρ_D (m)	$\sqrt{\langle\rho_1^2\rangle}$ (m)	$\sqrt{\langle\rho_s^2\rangle}$ (m)	$\sqrt{\langle\rho_c^2\rangle}$ (m)
1	1.00E-05	5.00E+01	1	1.25E-04	9.56E-03	1.22E-02	1.04E-02	6.32E-05
			2	3.15E-04	9.56E-03	2.11E-02	1.35E-02	1.65E-02
			3	3.74E-04	9.56E-03	2.26E-02	1.41E-02	1.77E-02
		1.00E+02	1	1.25E-03	3.1E-02	2.26E-02	4.05E-02	0.
			2	4.16E-04	3.1E-02	7.03E-02	7.03E-02	0.
			3	3.76E-04	3.18E-02	7.52E-02	7.52E-02	0.
		1.00E+03	1	1.25E-04	3.18E-01	4.05E-01	4.05E-01	0.
			2	3.15E-04	3.18E-01	7.05E-01	7.03E-01	0.
			3	3.74E-04	3.18E-01	7.52E-01	7.52E-01	0.
	1.00E-02	5.00E+01	1	1.25E-03	5.09E-03	9.08E-03	7.06E-03	5.71E-03
			2	4.15E-04	5.09E-03	2.36E-02	2.36E-02	1.17E-02
			3	3.76E-04	5.09E-03	2.60E-02	2.27E-02	1.77E-02
		1.00E+02	1	1.25E-03	5.93E-03	2.57E-02	1.86E-02	1.78E-02
			2	4.16E-04	5.93E-03	7.70E-02	6.65E-02	3.88E-02
			3	5.76E-04	5.93E-03	8.38E-02	7.38E-02	4.22E-02
		1.00E+03	1	1.25E-03	5.22E-02	2.55E-01	1.72E-01	1.85E-01
			2	4.15E-04	5.22E-02	7.69E-01	6.64E-01	3.89E-01
			3	3.76E-04	3.22E-02	8.49E-01	7.37E-01	4.22E-01
	1.00E-01	5.00E+01	1	1.25E-03	5.00E-02	5.50E-02	5.45E-02	7.94E-03
			2	4.15E-04	5.00E-02	5.61E-02	5.51E-02	8.63E-03
			3	1.25E-03	5.00E-02	9.15E-02	8.76E-02	1.06E-02
		1.00E+02	1	3.76E-04	5.00E-02	9.83E-02	9.00E-02	2.88E-02
			2	2.15E-04	5.01E-02	2.01E-01	2.38E-01	1.06E-01
			3	3.76E-04	5.01E-02	7.08E-01	7.21E-01	2.65E-01
		1.00E+03	1	2.12E-02	5.01E-01	8.08E-01	7.94E-01	2.88E-01
			2	6.06E-03	1.01E-01	1.01E-01	1.01E-01	0.
			3	7.06E-03	1.01E-01	1.02E-01	1.02E-01	0.
10.6	1.00E-03	5.00E+01	1	6.39E-03	1.37E-01	3.38E-01	3.38E-01	0.
			2	2.12E-02	1.37E-01	3.41E-01	3.41E-01	0.
			3	7.06E-03	1.37E-01	3.42E-01	3.42E-01	0.
		1.00E+02	1	6.39E-03	3.37E+00	3.38E+00	3.3E+00	4.21E-03
			2	2.12E-02	3.37E+00	3.41E+00	3.41E+00	7.94E-03
			3	7.06E-03	3.37E+00	3.42E+00	3.42E+00	4.54E-03
	1.00E-02	3.00E+01	1	1.15E-02	1.15E-02	1.23E-02	1.15E-02	3.11E-02
			2	7.06E-03	1.43E-02	1.43E-02	1.40E-02	1.29E-02
			3	6.39E-03	1.15E-02	1.94E-02	1.45E-02	1.36E-02
		1.00E+02	1	6.12E-02	1.41E-02	1.76E-02	3.51E-02	3.93E-02
			2	7.06E-03	5.41E-02	5.87E-02	4.36E-02	3.59E-02
			3	6.39E-02	5.37E-02	2.89E-01	3.73E-01	0.
		1.00E+03	1	2.12E-02	3.57E-01	3.75E-01	5.85E-01	2.97E-02
			2	7.06E-02	5.58E-01	6.26E-01	6.26E-01	7.94E-03
	1.00E-01	5.00E+01	1	2.12E-02	5.00E-02	5.02E-02	5.05E-02	6.54E-03
			2	7.06E-02	5.00E-02	5.25E-02	5.14E-02	6.45E-03
			3	6.39E-02	5.00E-02	5.26E-02	5.1E-02	3.11E-02
		1.00E+02	1	1.06E-03	5.01E-02	5.26E-02	5.24E-02	4.21E-02
			2	7.06E-03	5.01E-02	7.29E-02	6.70E-02	4.54E-02
			3	6.39E-03	6.01E-02	1.14E-01	1.20E-01	1.21E-01
		1.00E+03	1	2.12E-02	6.01E-02	8.45E-01	8.05E-01	7.94E-02
			2	7.06E-05	6.01E-02	5.51E-01	9.49E-01	2.88E-01

Table 6. Laser beam propagation results for a plume with initial parameters
$T_c - T_a = 500$ K, $V_c = 15$ m s^{-1}, R=5 m.

λ (μm)	D (m)	x_s (m)	Mixing Model	ρ_o (m)	ρ_D (m)	$\sqrt{\overline{v_L^2}}$ (m)	$\sqrt{\overline{v_{\rho_s}^2}}$ (m)	$\sqrt{\overline{v_{\rho_c}^2}}$ (m)
1	1.00E-03	5.00E+01	1	9.92E-04	9.56E-03	1.32E-02	1.07E-02	7.78E-03
			2	5.75E-04	9.56E-03	2.27E-02	1.42E-02	1.78E-02
			3	3.07E-04	9.56E-03	2.61E-02	1.57E-02	2.09E-02
		1.00E+02	1	9.90E-04	3.18E-02	4.34E-02	4.34E-02	0.
			2	5.80E-04	3.18E-02	7.47E-02	7.47E-02	0.
		1.00E+03	1	9.90E-04	3.18E-01	4.34E-01	4.34E-01	0.
			2	5.80E-04	3.18E-01	7.47E-01	7.47E-01	0.
	1.00E-02	5.00E+01	1	9.92E-04	5.09E-03	1.09E-02	9.37E-03	5.65E-03
			2	5.75E-04	5.09E-03	2.07E-02	2.27E-02	1.27E-02
			3	1.07E-04	5.09E-03	3.16E-02	2.78E-02	1.50E-02
		1.00E+02	1	9.99E-04	5.93E-03	3.26E-02	2.67E-02	1.87E-02
			2	5.80E-04	5.93E-03	8.43E-02	7.31E-02	4.19E-02
			3	3.00E-04	5.93E-03	1.03E-01	9.06E-02	4.97E-02
		1.00E+03	1	9.99E-04	3.22E-02	3.22E-01	2.62E-01	1.87E-01
			2	5.40E-04	3.22E-02	8.40E-01	7.29E-01	4.19E-01
			3	3.09E-04	3.22E-02	1.03E+00	9.04E-01	4.97E-01
	1.00E-01	5.00E+01	1	9.92E-04	5.03E-02	5.09E-02	5.04E-02	3.85E-02
			2	1.75E-04	5.00E-02	5.61E-02	5.54E-02	6.64E-03
			3	9.07E-04	5.00E-02	5.89E-02	5.79E-02	1.02E-02
		1.00E+02	1	7.80E-04	5.00E-02	9.34E-02	9.34E-02	1.27E-02
			2	1.09E-04	5.00E-02	1.15E-01	1.09E-01	2.85E-02
		1.00E+03	1	3.92E-04	5.01E-02	3.23E-01	2.97E-01	1.27E-01
			2	3.09E-04	5.01E-02	4.40E-01	4.74E-01	2.85E-01
			3	1.04E-04	5.01E-02	1.03E+00	9.74E-01	3.58E-01
10.6	1.00E-03	5.00E+01	1	1.69E-02	1.01E-01	1.01E-01	1.01E-01	0.
			2	6.18E-03	1.01E-01	1.02E-01	1.02E-01	0.
			3	1.27E-03	1.01E-01	1.04E-01	1.04E-01	0.
		1.00E+02	1	1.70E-02	1.37E-01	1.38E-01	1.38E-01	0.
			2	1.45E-03	1.37E-01	1.41E-01	1.41E-01	0.
		1.00E+03	1	1.25E-03	1.37E-01	5.04E-01	4.54E-01	0.
			2	1.70E-02	5.37E+00	5.34E+00	5.34E+00	9.00E-05
			3	1.26E-03	5.37E+00	3.41E+00	3.41E+00	2.94E-02
	1.00E-02	5.00E+01	1	3.34E-02	1.13E-02	1.24E-02	1.14E-02	1.57E-02
			2	5.22E-03	1.13E-02	1.95E-02	1.54E-02	1.62E-02
			3	1.70E-02	1.41E-02	2.04E-02	1.60E-02	3.55E-02

92

Table 7. Laser beam propagation results for a plume with initial parameters $T_c - T_d = 1000$ K, $V_c = 15$ m s^{-1}, R=5 m.

λ (μm)	τ (m)	x_s (m)	Mixing model	ρ_0 (m)	ρ_D (m)	$\sqrt{\langle\rho_L^2\rangle}$ (m)	$\sqrt{\langle\rho_s^2\rangle}$ (m)	$\sqrt{\langle\rho_c^2\rangle}$ (m)
1	1.00E-03	3.00E+01	1	9.50E-04	9.50E-05	1.36E-02	1.09E-02	8.10E-03
			2	2.86E-04	9.50E-05	2.75E-02	1.66E-02	2.20E-02
			3	2.76E-04	9.50E-05	2.82E-02	1.71E-02	2.25E-02
		1.00E+02	2	2.89E-04	3.18E-02	4.50E-02	4.50E-02	0.
			3	2.77E-04	3.18E-02	9.34E-02	9.06E-02	0.
		1.00E+03	1	9.38E-04	3.18E-01	9.50E-01	9.50E-01	0.
			2	2.89E-04	3.18E-01	4.05E-01	4.05E-01	0.
			3	2.78E-04	3.18E-01	4.33E-01	4.33E-01	0.
	1.00E-02	3.00E+01	1	9.30E-04	5.09E-03	1.15E-02	9.84E-03	5.95E-03
			2	2.86E-04	5.09E-03	3.38E-02	2.98E-02	1.59E-02
			3	2.76E-04	5.09E-03	3.50E-02	3.10E-02	1.64E-02
		1.00E+02	1	9.38E-04	5.93E-03	3.46E-02	2.45E-02	1.97E-02
			2	2.89E-04	5.93E-03	1.10E-01	9.72E-02	5.25E-02
			3	2.77E-04	5.93E-03	1.15E-01	1.01E-01	5.44E-02
		1.00E+03	1	9.38E-04	3.22E-02	3.43E-01	2.80E-01	1.97E-01
			2	2.89E-04	3.22E-02	1.10E+00	9.69E-01	5.75E-01
			3	2.77E-04	3.22E-02	1.15E+00	1.01E+00	5.44E-01
	1.00E-01	3.00E+01	1	9.30E-04	5.00E-02	5.10E-02	5.09E-02	5.95E-03
			2	2.86E-04	5.00E-02	6.01E-02	5.91E-02	1.04E-02
			3	2.76E-04	5.00E-02	6.04E-02	5.94E-02	1.12E-02
		1.00E+02	1	9.38E-04	5.00E-02	1.21E-01	1.16E-01	7.34E-02
			2	2.89E-04	5.00E-02	1.25E-01	1.20E-01	5.71E-02
			3	2.77E-04	5.01E-02	3.44E-01	3.16E-01	1.34E-01
		1.00E+03	1	9.38E-04	5.01E-02	1.10E+00	1.04E+00	3.58E-01
			2	2.89E-04	5.01E-02	1.15E+00	1.09E+00	3.70E-01
10.6	1.00E-03	3.00E+01	1	1.58E-02	1.01E-01	1.01E-01	1.01E-01	0.
			2	4.87E-03	1.01E-01	1.03E-01	1.03E-01	0.
			3	4.69E-03	1.37E-01	1.34E-01	1.03E-01	0.
		1.00E+02	2	1.59E-02	1.37E-01	1.38E-01	1.34E-01	0.
			3	4.92E-03	3.7E-01	1.44E-01	1.44E-01	0.
		1.00E+03	2	4.72E-03	3.7E-01	1.45E-01	1.45E-01	0.
			3	1.59E-02	3.37E+00	3.34E+00	3.34E+00	0.
			5	4.92E-03	3.37E+00	1.94E+00	1.94E+00	0.
				4.77E-03	3.37E+00	1.45E+00	1.45E+00	0.
	1.00E-02	3.00E+01	1	1.58E-02	1.13E-02	1.30E-02	1.19E-02	5.12E-03
			2	4.87E-03	1.13E-02	2.37E-02	1.66E-02	1.69E-02
			3	4.69E-03	1.11E-02	2.44E-02	1.64E-02	1.76E-02
		1.00E+02	1	1.59E-02	1.01E-02	3.01E-02	3.44E-02	1.70E-02
			2	4.92E-03	3.41E-02	7.67E-02	5.1E-02	5.65E-02
			3	4.72E-03	3.37E-01	7.93E-02	5.28E-02	5.91E-02
	1.00E-01	3.00E+01	1	1.58E-02	5.00E-02	5.04E-02	5.97E-02	5.11E-02
			2	4.87E-03	5.00E-02	5.42E-02	5.31E-02	1.04E-02
			3	4.69E-03	5.00E-02	5.45E-02	5.35E-02	1.12E-02
		1.00E+02	1	1.59E-02	5.01E-02	5.44E-02	4.29E-02	1.45E-02
			2	4.92E-03	5.01E-02	8.52E-02	7.75E-02	5.5E-02
			3	4.72E-03	5.01E-02	8.75E-02	7.95E-02	3.71E-02
		1.00E+03	1	1.59E-02	6.04E-02	2.70E-01	1.56E-01	3.54E-01
			2	4.92E-03	6.03E-02	6.91E-01	5.91E-01	3.54E-01
			5	4.72E-03	6.01E-02	7.20E-01	6.17E-01	3.70E-01

93

Table 8.   Laser beam propagation results for a plume with initial parameters
$T_c - T_a = 1500$ K, $V_c = 15$ m s^{-1}, R=5 m.

λ (μm)	D (m)	x_s (m)	Mixing Model	ρ_0 (m)	ρ_0 (m)	$\int r_a^2$ (m)	$\int r_s^2$ (m)	$\int r_c^2$ (m)

94

Table 9. Laser beam propagation results for a plume with initial parameters $T_c - T_d = 500$ K, $V_c = 20$ m s^{-1}, R=10 m.

λ (μm)	·	x_s (m)	Mixing Model	ρ_0 (m)	ρ_D (m)	$\sqrt{\rho_1^2}$ (m)	$\sqrt{\rho_s^2}$ (m)	$\sqrt{\rho_c^2}$ (m)
1	1.00E-03	5.00E+01	1	8.30E-04	9.56E-03	1.44E-02	1.15E-02	8.91E-03
			2	3.03E-04	9.56E-03	2.70E-02	1.62E-02	2.15E-02
			3	2.58E-04	9.56E-03	3.00E-02	1.85E-02	2.36E-02
		1.00E+02	1	8.55E-04	3.18E-02	4.69E-02	4.69E-02	0.
			2	3.17E-04	3.18E-02	8.50E-02	8.50E-02	0.
			3	2.65E-04	3.18E-02	9.66E-02	9.66E-02	0.
		1.00E+03	1	8.57E-04	3.18E-01	4.68E-01	4.68E-01	0.
			2	3.18E-04	3.18E-01	8.45E-01	8.45E-01	0.
			3	2.66E-04	3.18E-01	9.65E-01	9.65E-01	0.
	1.00E-02	5.00E+01	1	8.30E-04	5.09E-03	1.26E-02	1.04E-02	6.55E-03
			2	3.03E-04	5.09E-03	3.20E-02	2.82E-02	1.52E-02
			3	2.58E-04	5.09E-03	3.74E-02	3.31E-02	1.73E-02
		1.00E+02	1	8.55E-04	5.93E-03	3.7AE-02	3.15E-02	2.13E-02
			2	3.17E-04	5.93E-03	1.01E-01	8.83E-02	4.87E-02
			3	2.65E-04	5.93E-03	1.20E-01	1.06E-01	5.65E-02
		1.00E+03	1	8.14E-04	3.22E-02	3.74E-01	3.04E-01	2.12E-01
			2	3.14E-04	3.22E-02	1.00E+00	8.7HE-01	4.85E-01
	1.00E-01	5.00E+01	1	8.30E-04	3.72E-02	1.20E-02	1.06E-02	5.63E-01
			2	3.03E-04	3.72E-02	5.13E-02	5.11E-02	3.46E-03
			3	2.58E-04	5.00E-02	5.91E-02	5.42E-02	1.05E-02
		1.00E+02	1	2.58E-04	5.00E-02	6.22E-02	6.06E-02	1.1HE-02
			2	3.17E-04	5.00E-02	1.12E-01	1.07E-01	3.45E-02
			3	2.65E-04	5.00E-02	1.30E-01	1.24E-01	3.85E-02
		1.00E+03	1	8.57E-04	5.01E-02	3.75E-01	3.46E-01	1.45E-01
			2	3.18E-04	5.01E-02	1.00E+00	9.46E-01	5.30E-01
			3	7.66E-04	5.01E-02	1.20E+00	1.13E+00	5.84E-01
10.6	1.00E-03	5.00E+01	1	1.41E-02	1.01E-01	1.01E-01	1.01E-01	0.
			2	5.15E-03	1.01E-01	1.03E-01	1.05E-01	0.
			3	4.39E-03	1.01E-01	1.04E-01	1.04E-01	0.
		1.00E+02	1	1.05E-02	3.37E-01	3.38E-01	3.34E-01	0.
			2	5.39E-03	3.37E-01	3.43E-01	3.45E-01	0.
			3	4.51E-03	3.37E-01	3.46E-01	3.46E-01	0.
		1.00E+03	1	1.46E-02	3.37E+00	3.34E+00	3.34E+00	0.
			2	5.41E-03	3.37E+00	3.43E+00	3.43E+00	0.
			3	4.52E-03	3.37E+00	3.44E+00	3.46E+00	0.
	1.00E-02	5.00E+01	1	1.41E-02	1.13E-02	1.34E-02	1.21E-02	5.76E-03
			2	5.15E-03	1.13E-02	2.27E-02	1.61E-02	1.54E-02
			3	4.39E-03	1.13E-02	2.57E-02	1.73E-02	1.84E-02
		1.00E+02	1	1.45E-02	1.41E-02	4.13E-02	3.6HE-02	1.47E-02
			2	5.39E-03	1.41E-02	7.13E-02	5.91E-02	5.1HE-02
			3	4.51E-03	1.41E-02	4.09E-01	5.59E-02	6.21E-02
	1.00E-01	5.00E+01	1	1.46E-02	5.37E-01	9.09E-01	7.09E-01	0.
			2	5.28E-03	5.00E-02	5.05E-02	4.19E-01	0.
		1.00E+02	1	1.41E-02	5.00E-02	5.3HE-02	5.95E-02	3.15E-02
			2	1.45E-02	5.00E-02	5.52E-02	5.5HE-02	1.06E-02
			3	5.39E-03	5.01E-02	8.04E-02	7.32E-02	1.1HE-02
		1.00E+03	1	4.51E-03	6.03E-02	9.02E-02	8.16E-02	3.32E-02
			2	1.36E-02	6.03E-02	2.39E-01	1.70E-01	3.85E-01
			3	5.41E-03	6.05E-02	6.29E-01	5.55E-01	1.6HE-01
				4.52E-03	6.01E-02	7.51E-01	6.45E-01	5.84E-01

Table 10. Laser beam propagation results for a plume with initial parameters
$T_c - T_a = 1000$ K, $V_c = 20$ m s^{-1}, $R = 10$ m.

λ (μm)	D (m)	x_s (m)	Mixing Model	ρ_0 (m)	ρ_D (m)	$\sqrt{\langle \rho_L^2 \rangle}$ (m)	$\sqrt{\langle \rho_s^2 \rangle}$ (m)	$\sqrt{\langle \rho_c^2 \rangle}$ (m)
1	1.00E-03	3.00E+01	1	7.85E-04	9.56E-03	1.44E-02	1.15E-02	9.39E-03
			2	2.32E-04	9.56E-03	3.28E-02	2.02E-02	2.59E-02
			3	2.35E-04	9.56E-03	3.21E-02	1.97E-02	2.54E-02
		1.00E+02	1	8.11E-04	3.1AE-02	4.80E-02	4.80E-02	0.
			2	2.42E-04	3.1AE-02	1.04E-01	1.04E-01	0.
			3	2.40E-04	3.1AE-01	1.04E-01	1.04E-01	0.
		1.00E+03	1	8.13E-04	3.1AE-01	4.79E-01	9.79E-01	0.
			2	2.43E-04	3.1AE-01	1.05E+00	1.05E+00	0.
			3	2.41E-04	3.1AE-01	1.04E+00	1.04E+00	0.
	1.00E-02	3.00E+01	1	7.85E-04	5.09E-03	1.32E-02	1.15E-02	6.46E-03
			2	2.32E-04	5.09E-03	4.16E-02	3.70E-02	1.49E-02
			3	8.11E-04	5.93E-03	4.10E-02	3.65E-02	1.87E-02
		1.00E+02	1	8.42E-04	5.93E-03	1.32E-01	1.17E-01	2.22E-02
			2	2.40E-04	5.93E-03	1.35E-01	1.8E-01	6.10E-02
			3	8.43E-04	3.22E-02	2.94E-01	3.26E-01	6.14E-02
		1.00E+03	1	2.43E-04	3.72E-02	1.32E+00	1.77E+00	2.22E-01
			2	2.41E-04	3.72E-02	1.33E+00	1.1E+00	6.08E-01
			3	7.85E-04	5.00E-02	5.15E-02	5.12E-02	6.13E-01
	1.00E-01	3.00E+01	1	2.32E-04	5.00E-02	6.04E-02	6.35E-02	4.64E-03
			2	2.35E-04	5.00E-02	6.04E-02	6.32E-02	1.29E-02
			3	8.11E-04	5.00E-02	6.36E-02	6.17E-02	1.28E-02
		1.00E+02	1	2.42E-04	5.00E-02	1.41E-01	1.35E-01	1.52E-02
			2	2.40E-04	5.01E-02	1.42E-01	1.35E-01	4.16E-02
			3	8.13E-04	5.01E-02	9.95E-01	3.65E-01	4.1E-02
		1.00E+03	1	2.43E-04	5.01E-02	1.31E+00	1.25E+00	1.51E-01
			2	2.41E-04	1.01E-02	1.26E-01	1.26E+00	4.15E-01
			3	1.33E-02	1.01E-01	1.02E-01	1.02E-01	4.17E-01
10.6	1.00E-03	3.00E+01	1	1.94E-03	1.01E-01	1.04E-01	1.04E-01	0.
			2	3.99E-03	1.01E-01	1.04E-01	1.04E-01	0.
			3	3.11E-02	3.37E-01	3.3AF-01	3.3AE-01	0.
		1.00E+02	1	4.0AE-03	3.37E-01	3.47E-01	3.47E-01	0.
			2	1.3AE-02	3.37E+00	3.3AE+00	3.3E+00	0.
		1.00E+03	3	4.12E-03	3.37E+00	3.47E+00	3.47E+00	0.
	1.00E-02	3.00E+01	1	4.09E-03	3.37E+00	1.36E-02	1.21E-02	6.16E-03
			2	1.33E-02	1.13E-02	2.80E-02	1.42E-02	2.12E-02
			3	3.99E-03	1.1AE-02	2.77E-02	3.69E-02	2.09E-02
		1.00E+02	1	3.AE-03	3.41E-02	4.09E-02	3.65E-02	6.13E-02
			2	4.11E-03	3.37E-01	4.09E-01	5.67E-02	6.13E-02
			3	4.09E-03	3.37E-01	4.16E-01	3.16E-01	0.
	1.00E-01	3.00E+01	1	1.33E-02	5.00E-02	5.04E-02	5.94E-02	5.17E-02
			2	3.99E-03	5.00E-02	5.21E-02	5.2AE-02	1.21E-01
		1.00E+02	3	4.11E-03	5.01E-02	5.4E-02	6.21E-02	2.04E-02
			1	1.33E-02	5.01E-02	5.4AF-01	2.61E-02	2.61E-02
			2	3.99E-03	5.01E-02	5.47E-01	6.61E-02	6.67E-02
	1.00E-01	1.00E+03	3	4.11E-03	5.01E-02	5.31E-01	5.31E-01	4.15E-01
			1	1.3AF-02	6.01E-02	1.0AE-01	1.1E-01	4.17E-01

96

Table 11. Laser beam propagation results for a plume with initial parameters $T_c - T_a = 1500$ K, $V_c = 20$ m s^{-1}, $R = 10$ m.

| λ (μm)	D (m)	x_s (m)	Mixing Model	r_O (m)	r_D (m)	$\sqrt{\langle r^2_L \rangle}$ (m)	$\sqrt{\langle r^2_s \rangle}$ (m)	$\sqrt{\langle r^2_c \rangle}$ (m)
1	1.00E-03	3.00E+01	1	8.13E-04	9.56E-03	1.46E-02	1.14E-02	9.07E-03
			2	2.10E-04	9.56E-03	3.54E-02	2.19E-02	2.78E-02
		1.00E+02	1	2.29E-04	9.56E-03	3.27E-02	2.01E-02	2.58E-02
			2	8.41E-04	3.18E-02	4.72E-02	4.72E-02	0.
		1.00E+03	1	2.18E-04	3.18E-02	1.12E-01	1.12E-01	0.
			2	7.34E-04	3.14E-02	1.06E-01	1.06E-01	0.
	1.00E-02	3.00E+01	1	8.44E-04	3.14E-01	4.71E-01	4.71E-01	0.
			2	2.19E-04	3.18E-01	1.12E+00	1.12E+00	0.
			3	8.34E-04	3.18E-01	1.06E+00	1.06E+00	0.
		1.00E+02	1	8.13E-04	5.09E-03	1.28E-02	1.10E-02	6.60E-03
			2	2.10E-04	5.09E-03	4.59E-02	4.10E-02	2.04E-02
			3	2.29E-04	5.09E-03	4.20E-02	3.74E-02	1.91E-02
		1.00E+03	1	8.41E-04	5.93E-03	3.85E-02	3.14E-02	2.16E-02
			2	2.18E-04	5.93E-03	1.47E-01	1.31E-01	6.60E-02
			3	7.44E-04	5.93E-03	1.37E-01	1.21E-01	6.21E-02
	1.00E-01	3.00E+01	1	8.44E-04	3.22E-02	1.46E+00	1.30E+00	6.64E-01
			2	2.19E-04	3.22E-02	1.36E+00	1.21E+00	6.27E-01
			3	8.34E-04	3.22E-02	5.14E-02	5.12E-02	4.54E-03
		1.00E+02	1	2.10E-04	5.00E-02	6.76E-02	6.61E-02	1.40E-02
			2	2.29E-04	5.00E-02	6.51E-02	6.37E-02	1.30E-02
			3	8.41E-04	5.00E-02	6.27E-02	6.10E-02	1.47E-02
		1.00E+03	1	2.18E-04	5.00E-02	1.55E-01	1.39E-01	4.53E-02
			2	7.34E-04	5.01E-02	3.41E-01	3.52E-01	1.47E-01
			3	2.44E-04	5.01E-02	1.46E+00	1.39E+00	4.52E-01
			4	2.19E-04	5.01E-02	1.36E+00	1.29E+00	4.27E-01
10.6	1.00E-03	3.00E+01	1	1.34E-02	1.01E-01	1.01E-01	1.01E-01	0.
			2	1.57E-03	1.01E-01	1.05E-01	1.05E-01	0.
		1.00E+02	1	3.90E-03	1.01E-01	1.04E-01	1.04E-01	0.
			2	3.70E-03	3.37E-01	3.34E-01	3.34E-01	0.
		1.00E+03	1	1.97E-03	3.37E-01	3.50E-01	3.50E-01	0.
			2	1.43E-03	3.37E-01	3.48E-01	3.48E-01	0.
	1.00E-02	3.00E+01	1	1.37E-03	3.37E+00	3.38E+00	3.38E+00	0.
			2	3.37E-03	3.37E+00	3.49E+00	3.49E+00	0.
			3	3.09E-03	3.37E+00	3.48E+00	3.48E+00	0.
		1.00E+02	1	1.34E-02	1.13E-02	1.35E-02	1.21E-02	5.91E-03
			2	1.57E-03	1.13E-02	3.05E-02	1.97E-02	2.33E-02
			3	1.90E-03	1.15E-02	2.83E-02	1.85E-02	2.14E-02
		1.00E+03	1	1.43E-02	1.41E-02	6.15E-02	3.68E-02	1.91E-02
			2	3.70E-03	1.41E-02	9.73E-02	6.04E-02	7.63E-02
	1.00E-01	3.00E+01	1	1.43E-02	3.41E-02	9.15E-02	5.76E-02	7.11E-02
			2	1.71E-03	3.37E-02	9.11E-02	4.11E-02	0.
			3	5.94E-03	4.37E-02	9.69E-02	9.69E-02	0.

Figure 40. Propagation parameters as a function of altitude for mixing model 1.

98
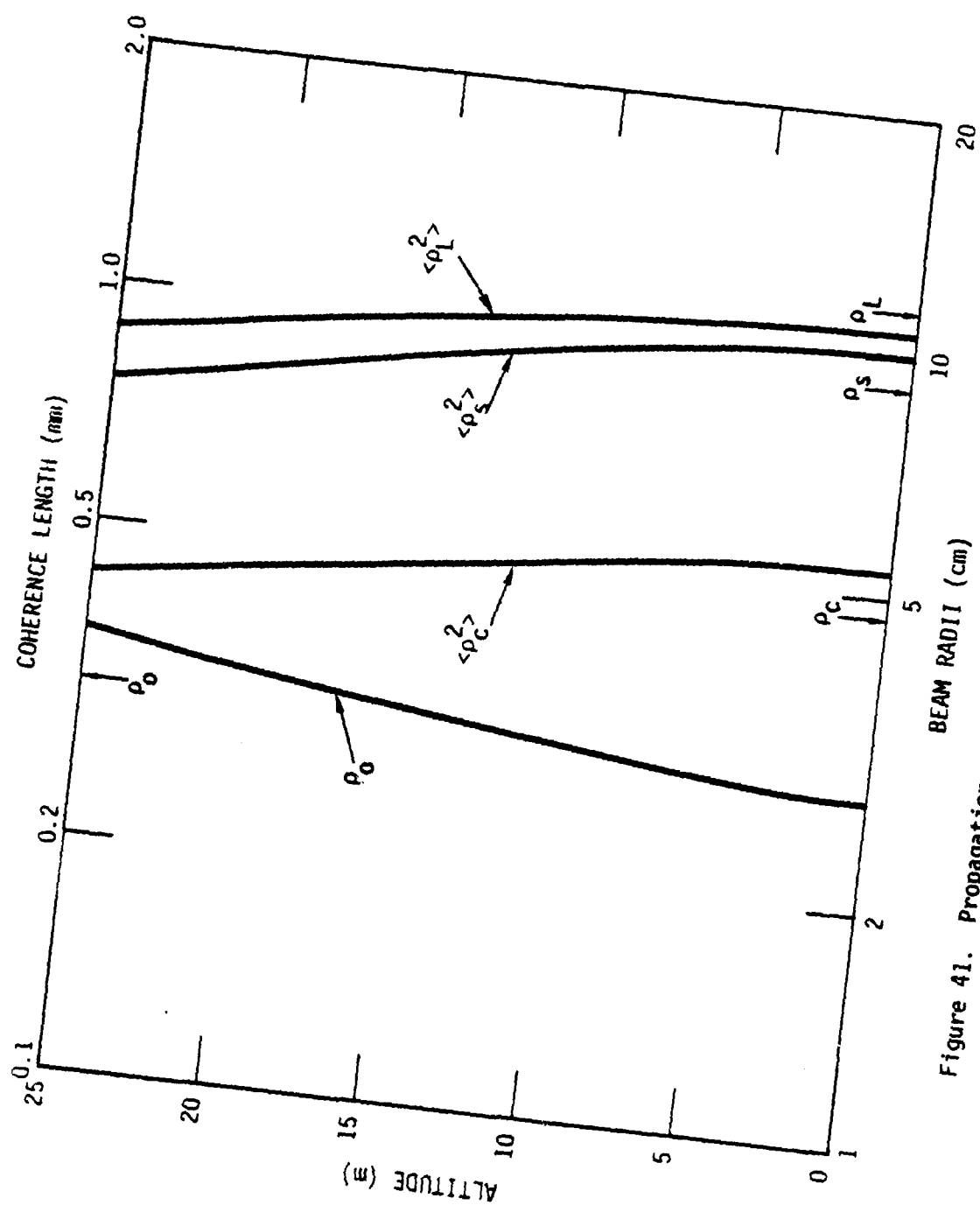
Figure 41. Propagation parameters as a function of altitude for mixing model 3.
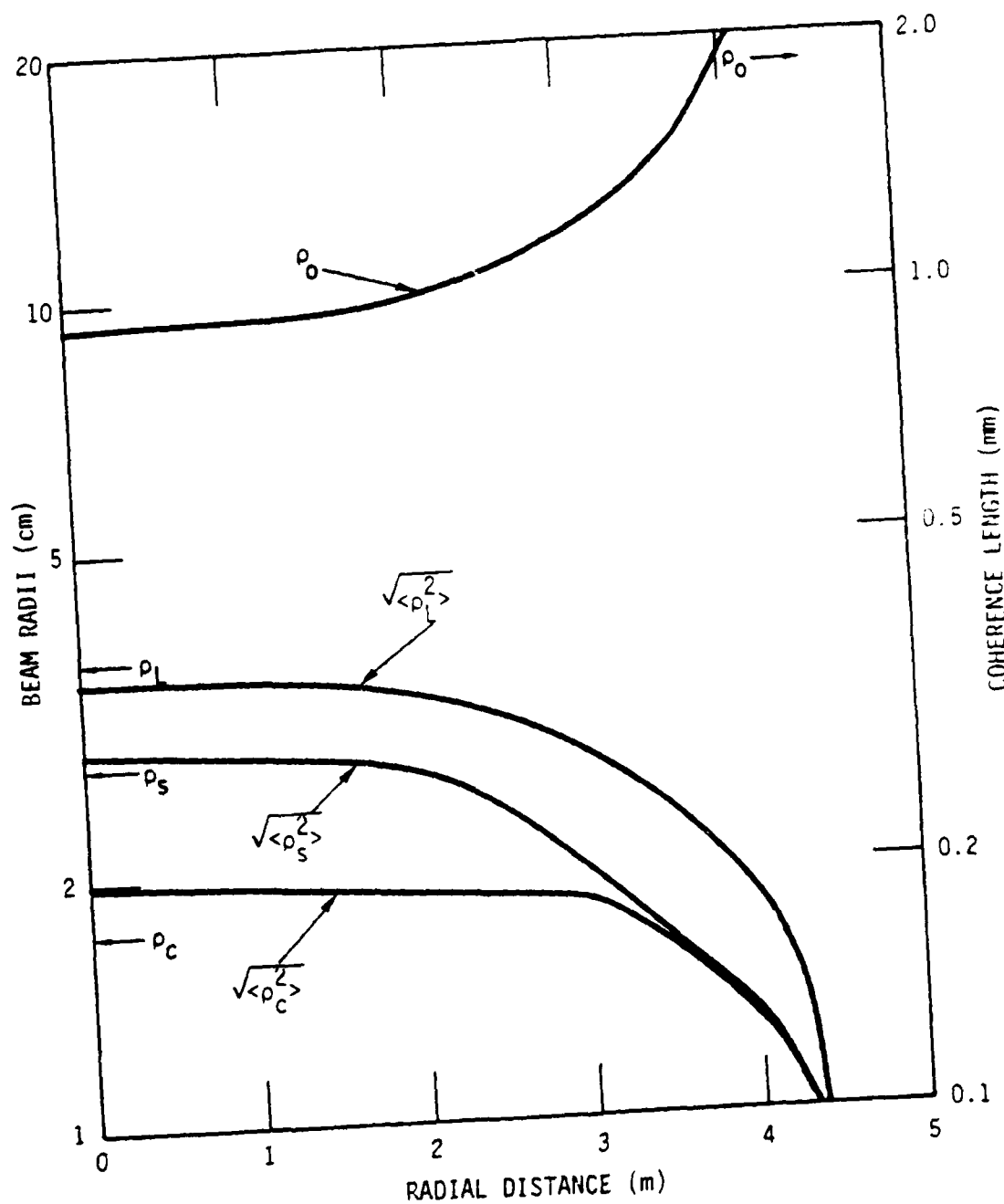
Figure 42. Propagation parameters as a function of radial offset for mixing model 1.
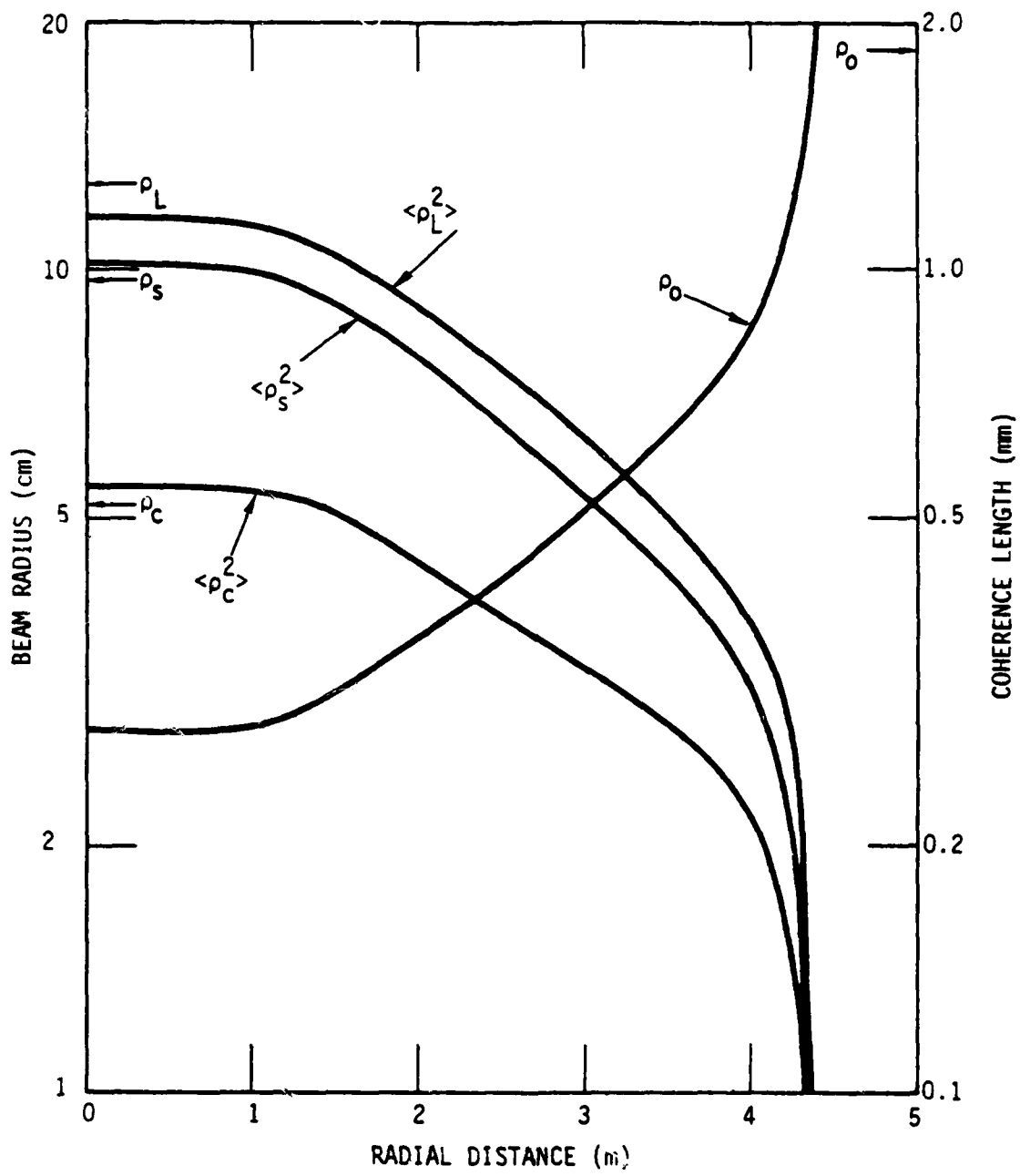
Figure 43. Propagation parameters as a function of radial offset for mixing model 3.

two meters above the plume reference plane (flame tips) which intersects
the plume centerline. Initial plume radii were 1, 5, and 10 meters with
initial rise velocities of 10, 15, and 20 m s^{-1}, respectively. For each
plume, three initial excess centerline temperatures of 500, 1000, and
1500 K were taken. These cases correspond to the plumes shown in Figures
4, 7, 10, 13, 16, 19, 22, 25, and 28. Laser wavelengths were chosen at
1 and 10.6 μm; the beam was taken as collimated with initial beam diam-
eters of 1 mm, 1 cm, and 10 cm. The two-order magnitude variation in
beam diameter was chosen for two reasons:

1. to illustrate the sensitivity of the results to beam
   diameter, and
2. to cover the expected diameter range of laboratory,
   experimental, and battlefield lasers.

Total path lengths chosen were 30, 100, and 1000 meters, with the plume
centered at the midpoint of the path. The path length range was chosen
to cover the typical shorter paths of an experimental test and the longer
paths of the battlefield.

Results are given for the three mixing models where for

Mixing model 1: $\sigma_T = 0.4(T - T_a)$

2: $\sigma_T^2 = \dfrac{b \, l_o^2 |grad \, T|^2}{1.91}$, $b = 0.3$

3: $b = 3$.

Mixing model 1 is the well-mixed, Gaussian fluctuation case. Mixing
models 2 and 3 are the non-well mixed discrete bimodal temperature
fluctuations. The turbulent propagation results tabulated are the
coherence length, and root mean square values for long- and short-term
beam spread, and beam centroid offset. Also given for comparison pur-
poses is the vacuum spread of the beam, ρ_D; the difference between the
total and vacuum spread is due to turbulence effects.

Figures 40 through 43 illustrate the variation with altitude and radial offset. For the plume of Figure 16, initial conditions $T_c-T_a =$ 1000 K, V = 15 m s^{-1}, R = 5 m, the propagation parameters were calculated as a function of altitude for the 100-m path length for the 1-μm wavelength, and the 1-cm beam diameter. All paths intersect the plume centerline. Results are shown in Figures 40 and 41 for mixing models 1 and 3. To illustrate the radial offset effect, the path at 2-meters altitude was progressively offset from the plume centerline. The offset results are shown in Figures 42 and 43, again for mixing models 1 and 3. The dotted segments in Figure 40 is the region of transition from one propagation approximation to the next (from case 1 to case 2, Equations 87 to 90). The long- and short-term radii are relatively continuous, but the centroid offset is slightly discontinuous. Over the first 25 meters of this plume there is a relatively small change in the propagation parameters with altitude. The excess centerline temperature has fallen from 1000 K at the reference plane to only about 200 K at 25 meters. As shown in Figure 35, 200 K is still near the peak of the index of refraction fluctuations. The turbulence effects will diminish rapidly with temperature as the temperature drops below about 100 K. The turbulent effects for the non-well mixed flows, mixing model 3, are about a factor of 3 larger than the well-mixed Gaussian model 1. This is about the range of effects to be expected between the convective and dissipative regions of the plume.

As expected the turbulence effects decrease rapidly as the ray path approaches the plume edge (Figures 42 and 43). Not only is the plume temperature decreasing, but the total path length through the plume turbulence is also decreasing. Again the difference in mixing models is about a factor of 3 in propagation effects.

103

SECTION 4
CONCLUSIONS AND RECOMMENDATIONS

In this report we have developed models for

1. the mean plume parameters including radius, temperature, and velocity as a function of altitude,

2. the turbulence associated with the plume mean parameters, and

3. the effects on optical beams propagating through the plumes including both mean bending and turbulence effects.

Some of the models have been verified by previous experimental evidence, but verification of the remaining models must await the planned plume test series.

The models for the mean radius, temperature, and velocity of the plume as a function of altitude have a solid theoretical base, and have been verified by experimental measurements. We expect the results predicted by the mean plume models to be fairly accurate when compared to experimental data on essentially ideal plumes. An ideal plume is a plume generated under controlled conditions with negligible intermittency effects. An ideal plume can be readily generated under laboratory conditions, but may be difficult to generate under field conditions. As mentioned previously, interactions of the plume flow fields with the ambient flow fields may introduce significant intermittency. The plume may move about in space or may even break up. If the plume merely moves about, then the model predictions can be used, noting that the predictions apply at the instantaneous location of the plume. But if the plume breaks up or the ambient interactions introduce significant additional mixing, then the model predictions would no longer apply.

In contrast to the fairly solidly based models for the mean plume parameters, the models for the plume temperature fluctuations are primarily theoretical with little experimental verification. For well developed plume turbulence, experimental data verify the well mixed formulation model, Equation 61; see, for example, Reference 10. But the non-well mixed models are purely theoretical with no experimental verification. Moreover, for both the well and the non-well mixed models, there is no experimental verification for the assumption that the index of refraction fluctuations have a Kolmogorov spectrum. We can reasonably expect the well developed, well mixed flow to be Kolmogorov. But until the initial convective flow decays into a dissipative flow, we do not expect the spectrum to be Kolmogorov. Hopefully the planned test series will measure the spectrum.

For small total bending angles, the ray tracing models for the mean bending are solidly based in both theory and experiment. The problem lies in defining the mean thermal environment of the plume; the tracing of a ray through this environment is straightforward.

Given that the turbulence spectrum is Kolmogorov, the propagation models have been derived theoretically and verified experimentally (see Reference 16). However the experimental verification has been primarily for propagation in ambient atmospheric turbulence. We also expect the models to apply to propagation through the localized highly intense plume turbulence, but experimental verification awaits the upcoming test series.

An experimental test series on fire plumes will be conducted at the White Sands Missile Range in the near future. This test series should eliminate many of the current uncertainties in the plume models. The present plume and propagation models can be used for test planning. For field test propagation predictions, we recommend mixing model 3, the non-well mixed flow model. The initial plume flow is convective, which is non-well mixed. As the altitude increases the convective flow decays into a dissipative flow. If fully established with no intermittancy, the dissipative flow should be well mixed, corresponding to

mixing model 1. But for the field tests, we expect the ambient inter-
actions to introduce intermittances, tending to produce non-well mixed
flows. Thus for field tests, mixing model 3 is recommended for all
altitudes for planning purposes.

The specific details of the forthcoming plume test series will be
determined by the available test equipment and budget considerations,
but some general recommendations can be made. A variety of fire sizes
and burning rates should be employed if time and budget allow. However
it is more important to take data at a number of altitudes in a single
plume than to take data at a single altitude in a number of different
plumes. To eliminate the complicating effects of particulates, the
fires should be clean, i.e., essentially smokeless.

Ideally, over the data collection period for a given plume, the
intrinsic parameters of the plume should be time independent. The
burning rate of the fire should be constant. The ambient conditions
should be chosen as calm as possible to minimize ambient interactions.
If there is significant lateral motion of the plume, then measurements
should be recorded relative to the instantaneous plume centerline.
This relative measurement requires that the probe or laser beam posi-
tion and the plume position be recorded at each measurement time.

To characterize the mean plume parameters, the plume diameter and
mean centerline temperature and rise velocity should be measured at a
number of altitudes. At selected altitudes the temperature and velocity
should be measured as a function of horizontal distance from the plume
centerline.

Since the ultimate purpose of the plume modeling effort is to pre-
dict propagation effects, measurements of various propagation effects
are a must. For direct comparison with model predictions, measurements
should include short- and long-term beam spread and jitter (centroid
location). Measurement of the short-term beam spread and jitter re-
quires that the response time of the measuring system be fast enough to
measure the instantaneous beam spot as it flits from point to point on

the receiving screen. The time it takes the spot to move from one point
to the next is approximately

$$\Delta t \approx \frac{D}{v}$$

where D is the diameter of the beam at the plume location and v is the
plume rise velocity.

The diameter of the beam when it passes through the plume should be
small compared to the diameter of the plume. This will minimize the
effects of inhomogenities in the turbulence strength and spectrum over
the cross sectional dimension of the beam. Optical beams should have
no problem meeting this smallness criterion. However if microwave
beams are fielded as an adjunct to the optical tests, some care may be
required in the relative placement of transmitter, plume, and screen
(receiver).

The temperature is the controlling system parameter for plume
turbulence and propagation effects. At optical frequencies the tempera-
ture fluctuations determine the index of refraction fluctuations; the
contributions due to pressure and water vapor fluctuations are negligible.
The quantity required for turbulence propagation calculations is the
spectrum of the index of refraction fluctuations, which in turn follows
directly from the spectrum of temperature fluctuations. If the instru-
mentation is available, measurements of the plume temperature spectrum
would be extremely valuable. A series of measurements at increasing
altitudes would determine the decay of the initial convective flow into
the dissipative flow. The measurements will determine if or when the
index of refraction fluctuations approach the presently assumed Kolmogorov
spectrum.

REFERENCES

1. Zel'dovich, Ya. B., "Limiting Laws for Turbulent Flows in Free Convection," *Zh. Eksp. Teoret.*, Fiz. 7 (12), 1463 (1937).

2. Schmidt, W.Z., "Turbulent Propagation of a Stream of Heated Air," *Z. Angew. Math. Mech.*, 21, 265-351 (1941).

3. Taylor, G.I., *Dynamics of a Mass of Hot Gas Rising in Air*, U.S. Atomic Energy Commission, MDDC, 919, LADC 276 (1945).

4. Rouse, H., C.S. Yih, H.W. Humphreys, "Gravitational Convection from a Boundary Source," *Tellus 4*, 201 (1952).

5. Batchelor, G.K., "Heat Convection and Buoyancy Effects in Fluids," *Q. Jl. R. Met. Soc.*, 80, 339-358 (1954).

6. Morton, B.R., G.I. Taylor, J.S. Turner, "Turbulent Gravitational Convection from Maintained and Instantaneous Sources," *Proc. R. Soc.*, 234A, 1-23 (1956).

7. Morton, B.R., *Modeling Fire Plumes*, Tenth Symposium (International) on Combustion, 973-982 (1965).

8. Gilmore, F.R., *Equilibrium Composition and Thermodynamic Properties of Air to 24,000°K*, RAND Corp., Santa Monica, California, Research Memorandum RM-1543, 24 August 1955.

9. Kumer, J.B., et al, *Low Altitude Phenomenology for Optical Systems, Volume 1—Basic Analysis*, DNA 3527T-1, Lockheed Palo Alto Research Laboratory, 25 September 1975.

10. George, W.K., R.L. Alpert, F. Tamanini, "Turbulence Measurements in an Axisymmetric Buoyant Plume," *Int. J. Heat Mass Transfer.*, Vol. 20, 1145-1154 (1977).

11. Strohbehn, J.W., editor, *Topics in Applied Physics, Volume 25—Laser Beam Propagation in the Atmosphere*, Springer-Verlag, 1978.

12. Bean, B.R., and E.J. Dutton, *Radio Meteorology*, National Bureau of Standards Monograph 92, March 1966.

13. Tatarski, V.I., *The Effects of the Turbulent Atmosphere on Wave Propagation*, U.S. Department of Commerce, 1971.

14. Ishimaru, A., *Wave Propagation and Scattering in Random Media, Volume 2—Multiple Scattering, Turbulence, Rough Surfaces, and Remote Sensing*, Academic Press, 1978.

15. Monin, A.S., A.M. Yaglom, *Statistical Fluid Mechanics*, MIT Press, Cambridge, MA, 1971.

16. Fante, R.L., "Electromagnetic Beam Propagation in Turbulent Media," *Proc. IEEE*, Vol. 63, No. 12, 1669-1692, December 1975.

DATE
ILMED

-8